NISTIR 5701

PROCEEDINGS

METROLOGY ISSUES IN TERAHERTZ PHYSICS AND TECHNOLOGY

National Institute of Standards and Technology
Gaithersburg, MD
December 13, 1994

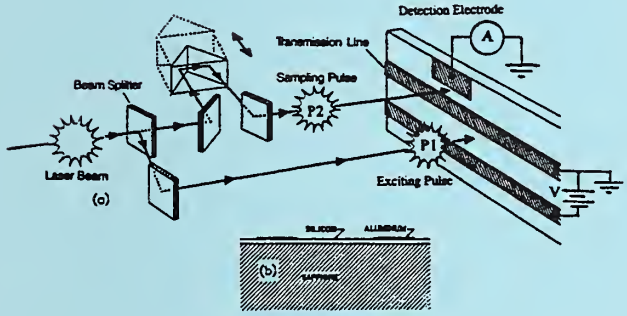

Prepared and Edited by:

Raju Datla[1], Erich Grossman[2]
National Institute of Standards and Technology,
[1]Gaithersburg, MD 20899-0001; [2]Boulder, CO 80303

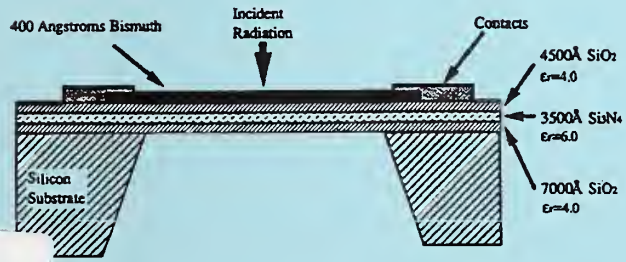

and

Mitchell K. Hobish
5606 Rockspring Road
Baltimore, MD 21209-4318

NISTIR 5701

PROCEEDINGS

METROLOGY ISSUES IN TERAHERTZ PHYSICS AND TECHNOLOGY

National Institute of Standards and Technology
Gaithersburg, MD
December 13, 1994

Prepared and Edited by:

Raju Datla[1], Erich Grossman[2]
National Institute of Standards and Technology,
[1]Gaithersburg, MD 20899-0001; [2]Boulder, CO 80303

and

Mitchell K. Hobish
5606 Rockspring Road
Baltimore, MD 21209-4318

U.S. DEPARTMENT OF COMMERCE
Ronald H. Brown, Secretary

TECHNOLOGY ADMINISTRATION
Mary L. Good, Under Secretary for Technology

NATIONAL INSTITUTE OF STANDARDS
AND TECHNOLOGY
Arati Prabhakar, Director

Table of Contents

PROCEEDINGS

METROLOGY ISSUES IN TERAHERTZ PHYSICS AND TECHNOLOGY

Gaithersburg, MD
December 13, 1994

Prepared and Edited by:
Raju Datla[1], Erich Grossman[2]
National Institute of Standards and Technology,
[1]Gaithersburg, MD 20899-0001; [2]Boulder, CO 80303
and
Mitchell K. Hobish
5606 Rockspring Road
Baltimore, MD 21209-4318

Executive Summary

Introduction

Tremendous progress has been made in recent years in the development of new sources, detectors, antennas, and materials for the terahertz (THz) spectral region, i.e., from 100 GHz (3 mm wavelength) to 10 THz (30 μm wavelength). Similarly, dramatic improvements have been made in workhorse technologies, such as terahertz Schottky diodes and molecular gas lasers. This progress in device development opens the door to many exciting applications in remote sensing of the Earth's atmosphere, automotive and military radar, molecular spectroscopy, materials characterization for process control, and astronomy. However, very little attention has been paid to questions of accurate measurement techniques, calibration, and standards at THz frequencies.

In order to discuss metrology issues and the role NIST might play in the rapidly advancing field of THz technology, the staff in various divisions of NIST's Physics Laboratory, in collaboration with the staff in the Electronics and Electrical Engineering Laboratory (EEEL), convened a Workshop on *Metrology Issues in THz Physics and Technology*. The workshop was held at NIST on December 13, 1994, and was attended by 50 representatives from industry, academia, and federal agencies.

The speakers for the morning session addressed the general topic of THz applications, with specific reference to applications in remote and atmospheric sensing, commercial applications of THz technology using both coherent and non-coherent sources, and THz applications in microelectronics. The afternoon session's

speakers addressed specific measurement issues, including both coherent and incoherent absolute power measurement, antenna efficiency, spatial beam measurement, and measurement of material properties. Following the afternoon's presentations, an open discussion addressed the specific areas that NIST should target to support research and development work in the THz region, and the role(s) NIST could play in support of these activities. Many speakers lamented the lack of data on optical properties--emittance, reflectance, and transmittance--of materials in the THz region. Equal concern was expressed at the lack of standards for absolute power measurements in the THz region. ***For rapid progress in THz physics and technology the consensus and recommendation was that NIST should address: (1) the measurement, validation, and dissemination of optical properties of materials; and (2) the development of standards for absolute power measurements from both single mode and multimode sources.***

The organizing committee, the Workshop program, and a list of attendees are provided in Appendices I-III.

Opening Remarks

After an initial welcome by Raju Datla, of the Infrared Radiometry Group at NIST (Gaithersburg), Erich Grossman, Cryoelectronic Metrology Group, NIST (Boulder) discussed prior NIST work at THz frequencies. This work has addressed frequency-related measurements, detector development, and lower frequency (but still THz-capable) techniques. Of particular note was the work done in 1972 by Evenson, *et al.*determining the speed-of-light by measuring both the frequency and the wavelength of the methane stabilized HeNe laser line at ~3.4 μm (88 THz) with a relative standard uncertainty of about 1 x 10^{-9}. For the frequency measurement they had to build a frequency synthesis chain starting from the existing frequency standard, which is the cesium atomic clock at ~10 GHz, all the way to the HeNe line at 88 THz. This measurement was performed with high speed, high bandwidth, nonlinear metal-insulator-metal (MIM) diodes, which were used extensively for harmonic generation and heterodyne mixing. These diodes were largely developed at NIST/Boulder. As a result of the accuracy achieved in these measurements, metrologists decided to change the definition for the meter.

Other techniques and instrumentation developed by NIST include the laser magnetic resonance (LMR) spectrometer, and the tuned far infrared (TuFIR) spectrometer, which were used to measure the transition frequencies of lines from atomic, molecular, and ionic species. Recent work by NIST in this area has been to measure arbitrary lines in the visible spectrum that are separated by THz frequencies from very accurately known visible lines. GaAs Schottky photodiodes are being used as optical photomixers and THz harmonic generators. Also, Josephson junctions with THz characteristic frequencies have been developed, which are useful as heterodyne mixers and harmonic generators when placed at antenna feed points, and as voltage-tunable GHz and THz oscillators when deployed as phase-locked, two-dimensional arrays.

In the area of power measurements, emphasis was placed on development of low-noise, cryogenic detectors. The high T_c

transition edge bolometer developed at NIST/Boulder measured a noise-equivalent power (NEP) of 9 pW/√Hz which, until recently, was a world record for this kind of measurement.

Grossman concluded with a discussion of THz metrology issues that he hoped would prompt discussion throughout the workshop. These included:

- absolute power measurements, especially for calibration of calorimeters;
- spatial measurement to determine beam quality and to characterize antennas;
- frequency-related measurements for reference frequencies and frequency synthesis, and to determine spectral purity;
- optical measurements to determine optical constants for bulk materials;
- the emittance/reflectance (diffuse and specular) of surfaces; and,
- performance measurements on devices.

Session I: Applications Overviews

The morning session was chaired by Charles Clark, Chief, Electron and Optical Physics Division, NIST (Gaithersburg), who introduced Peter Siegel, from the Jet Propulsion Laboratory. Siegel addressed the use of THz techniques and devices in remote Earth-sensing applications in his presentation on *Heterodyne Radiometry for Millimeter and Submillimeter-Wave Earth Remote Sensing*. This work, prepared in cooperation with Joe Waters, described the science drivers for microwave remote sensing of the Earth, with specific reference to NASA's Upper Atmosphere Research Satellite (UARS). This satellite, launched in 1991, has provided valuable data on the distribution of gaseous constituents of our atmosphere, using an instrument called the Microwave Limb Sounder (MLS). The MLS has been used to address details of stratospheric ozone chemistry, upper tropospheric and stratospheric greenhouse gases, measurement of volcanic pollutants in the lower stratosphere, and measurements through ice clouds and aerosols. A general introduction to limb sounding demonstrated the utility of the technique to measure atmospheric constituents. One of the advantages of this technique is that one can measure the vertical distribution of the species with much finer resolution than is available through nadir based column measurements. Heterodyne limb sounding also allows high spectral resolution, has excellent sensitivity, provides simultaneous measurements in many channels, and allows the use of long-life millimeter wave detectors that operate at room temperature.

Siegel addressed the receiver requirements for Earth remote sensing, and noted ways in which they differ from requirements for astrophysical measurements. Generally, the constraints on Earth remote sensing are not as stringent as those for astrophysics, as the signals are stronger and the spectra of Earth's atmospheric constituents are well known. There are constraints, however: (1) the observation time window is on the order of 1 s, as the satellite is moving very quickly in its orbit; (2) there is a limit on power consumption, so the number of radiometers needed to cover spectra of different frequencies cannot be arbitrarily large, and

all radiometers that are used must be turned on at the same time to record the spectra of different species simultaneously; and, (3) absolute calibration of the radiometers, especially beam characteristics, must be known a priori with very high accuracy. However, the implementation of suitable technologies in the UARS-MLS resulted in data acquisition within 2 days of its deployment, with continuous data having been received for over 39 months.

Siegel then addressed the follow-on to UARS-MLS, the Earth Observing System (EOS) MLS, scheduled for flight as part of NASA's EOS mission, with specific attention paid to the differences in technology between the two instruments, and the measurement benefits that would accrue. He enumerated the need for data and standards for the scientific experiments planned in the new mission. For radiance calculations some of the needs are: (1) high accuracy emissivity data for materials used in the calibration loads for the frequency range of 100 GHz to 2.5 THz; (2) absolute filter transmittance data; (3) absolute radiometric sideband calibration; and, (4) antenna beam patterns across all RF bands up to 2.5 THz. For instrument calibrations, some of the needs at submillimeter wavelengths are: (1) standards for absolute power measurements; (2) standards for absolute frequency measurements; (3) characterized blackbody-emissivity equivalent-load temperatures; (4) standards for spot noise temperature measurements; and, (5) relative sideband response measurements.

The use of THz techniques in remote sensing was further explored by Kelly Chance, Harvard-Smithsonian Center for Astrophysics, who described *THz Applications in Atmospheric Sensing*. Most of his work has been on stratospheric sensing of profiles of trace gases involved in ozone chemistry as a function of altitude, based on balloon-borne, Fourier transform spectrometry. These techniques give unique measurements of H_2O_2 as well as HO_2, OH, and favorable measurements of HOCl, ClO, HCl, and HF. These emission measurements yield diurnal behavior. These methods are particularly suitable for stratospheric measurements, where as tropospheric lines are too broad and too obscured by H_2O to be measured by THz techniques, except in special cases. Chance described the Smithsonian Astrophysical Observatory FIRS-2 instrument, which uses a double-beam Fourier transform spectrometer (FTS), covering the ranges 80 cm^{-1} to 210 cm^{-1} to (2.4 THz to 6.2 THz) and 350 cm^{-1} to 700 cm^{-1} with a resolution of 0.004 cm^{-1} . The fine rotational and vibrational spectral patterns of several species are collected in the Smithsonian Astrophysical Observatory Database, which is available via file transfer protocol (ftp). Given the role(s) of OH in atmospheric chemistry, Chance and his colleagues are developing the OH Interferometer Observations (OHIO) concept for satellite-based measurements of stratospheric OH. This is an option for the generalized far infrared (FIR) Fabry-Perot instrument, optimized for satellite use, and is a collaborative effort of the Smithsonian Astrophysical Observatory, the National Air and Space Museum, the Naval Research Laboratory, and with scientists in The Netherlands and Germany.

The application of THz techniques to characterization of electronic semiconductor materials was described by Larry Carr of the R&D Center/Electronic Materials Labora-

tory, Grumman Aerospace and Electronics. His presentation on *Applications of Synchrotron Far-IR to Studies of Electronic Materials* described the properties of FIR beams from synchrotrons, and applications. Carr first described the basics of how synchrotron radiation is generated, and then went on to address the features of such radiation. Key to its use is its continuous spectral coverage from microwaves through X-rays; that it is two to three orders of magnitude brighter than thermal sources; that it is pulsed (due to electron bunching); and that it is spatially coherent, with small beam divergence. The electrons in a synchrotron storage ring are made to travel in bunches because of the location of an RF cavity in one part of the ring, which provides energy to the electrons to make up for losses, and to prolong their lifetime in orbit. The radiation exits the port as pulses with duration and separation based on the spatial extent of the electron bunch and the separation between bunches. In the case of a single bunch, the pulse repeats each revolution. The radiation exits as a highly collimated beam with a small divergence angle because of the relativistic speeds of the electrons. This latter feature is very useful for IR microspectroscopy. The pulse characteristic is used to determine response times for high-speed FIR detectors such as quantum well infrared photodiodes (QWIP) and high T_c superconductors. As an example, Carr showed results of a study of the responsivity of an AT&T quantum well infrared detector, with a measured response time of less than 500 ps. The IR radiation pulse has also been used as a probe for pump-probe spectroscopy of detector materials, such as GaAs and HgCdTe. Examples of this work were shown for undoped GaAs, which revealed the scattering rates and time dependence for electrons and holes.

Material characterization was also addressed by Jim Allen, from the Center for Free-Electron Laser (FEL) Studies, University of California, Santa Barbara (UCSB), who spoke on the *Applications of Free-Electron Lasers as Terahertz Sources*. Allen described some details of the FEL facilities at UCSB, and characteristics of the radiation they produce: The radiation is tunable over the range 120 GHz to 4.8 THz; it is quasi-cw, in 1 μs to 20 μs pulses with a fractional frequency instability of approximately 10^{-6}; its power output is from 500 W to 5 kW. These characteristics make such radiation ideal for examining materials properties in the gap between electronic and photonic regions, and enable its use to examine nonlinear quantum transport in semiconductor nanostructures. Allen described two applications: definition of high frequency limits in resonant tunneling diodes, and photon-assisted tunneling in semiconductor structures. The potential impact of this technique on technology will be to define the high frequency limits of conventional electronics and to enable new electronics at THz frequencies.

A fascinating new concept in THz beam generation was described by Daniel Grischkowsky, Oklahoma State University, School of Electrical and Computer Engineering, in his presentation on *Femtosecond THz Beam Generation and Applications*. This optoelectronic approach uses a charged coplanar transmission line circuit irradiated by a laser. With a potential across the gap the line generates a current pulse when hit by a laser pulse at the gap. The current pulse drives a dipole antenna and radiates at THz frequencies. The semiconductor is fabricated to give a response of less than 1 ps. The same principles are used with a similar

semiconductor chip to detect the THz radiation. This technique can give a THz signal-to-noise ratio (SNR) of 1000:1. Grischkowsky showed the results of an optimized optoelectronic system radiating THz radiation with pulse widths on the order of femtoseconds, with an SNR on the order of 10 000:1. Perfect synchronization between the transmitter and receiver is possible. The combination of an ultrafast source and detector can then be used to do time-domain spectroscopy to examine the dynamics of several gas species, e.g., N_2O and H_2O, to perform non-contact characterization of materials such as N- and P-type GaAs, to perform ranging measurements, and to examine temperature distributions in flames.

Session II: Specific Measurement Areas

Having discussed several application areas, the Workshop next focussed on metrology issues in a session chaired by Kenneth Evenson, Time and Frequency Division, NIST/Boulder. Evenson introduced Neal Erickson, from Millitech, who gave a presentation on *Power Standards for the Near Millimeter and Submm Region.* In an incisive talk, Erickson described the state of the art with respect to power standards in the GHz range, stating that standards are poorly established above 90 GHz, and nearly completely absent above 140 GHz, to the point where the manufacturers of devices cannot state with complete certainty the accuracy and precision of their instruments in these regions. This lack of standardization makes it difficult to verify theories or to confirm expectations, leading to uncertainties in local oscillator power for mixers, efficiencies of multipliers, laser output power, and more. Erickson went on to describe power measurement problems in the submillimeter region, where available power is small from most sources, and accurate calorimeters are not sufficiently sensitive. Unknown harmonic content, spurious oscillations, and contaminating lines make it difficult to verify purity. Erickson described the advantages and disadvantages of several types of power sensors including waveguide-mounted sensors (waveguide calorimeters, waveguide thermistors or thermocouples, and diode detectors), and quasi-optical devices, such as quasi-optical laser power meters (thermopiles), acoustic wave sensors, pyroelectric sensors, and thin-film bolometers, all of which have possible non-uniform absorption characteristics. Based on these deficiencies, Erickson described the parameters necessary for an improved waveguide calorimeter design, which could be an excellent general-purpose sensor throughout the submillimeter region if speed and drift could be improved. It requires two matched sensors, as it is a differential measurement device; the lower limit to measurable temperature is set by the thermal isolation of the elements and the match in the drift of the two sensors. It should be feasible to achieve a 10 μW measurement level and a time constant of less than 10 s an uncertainty of a few percent. He described a prototype device that he has constructed based on a WR-10 waveguide input, intended for use between 80 GHz to 1 THz. It has a responsivity of 100 K/W and a time constant of 7 s. The root means square drift is 7 μW, which could be improved by better insulation. He expressed the view that NIST involvement could help produce a better device.

An excellent example of the need for well-characterized, standardized, and calibrated measurement tools was provided by

John Mather, NASA Goddard Space Flight Center, who described the important results obtained with the *Far Infrared Absolute Spectrophotometer (FIRAS)* instrument flown on the Cosmic Background Explorer (COBE) satellite. The purpose of this measurement was to compare the cosmic microwave background to an accurate blackbody in an effort to provide information about the earliest epochs in the history of the observable universe as a test of the Big Bang Theory of cosmology. FIRAS is intrinsically a differential device, matching observation against a perfect blackbody. This ordinary differential interferometer has two inputs and two outputs, which are used to generate an interferogram. The blackbody is isothermal (to within 1 mK), operating at liquid He temperatures (1.5 K), and can be heated to change the temperature of the device over the range from 2 K to 20 K. The detector is a bolometer, using a diamond substrate blackened with chromium gold alloy, and a heavily doped silicon chip thermister. Painstaking calibration produced measurements that demonstrate that there is no deviation between the temperature of the observed cosmos and that of a blackbody curve at 2.726 K; there was no deviation found at <0.03 % of peak from 0.5 mm to 5 mm, thereby confirming the Big Bang Theory.

Astrophysical measurements provide one of several motivations for *Laboratory Spectroscopy in the THz Region*, as discussed by Geoff Blake, California Institute of Technology. By exploring this region with a widely tunable system, Blake and his coworkers are able to obtain high spectral resolution and sensitivity near the quantum limit. This provides a tool for rotational spectroscopy for astronomy and atmospheric remote sensing. Linewidth requirements are very stringent in these applications. Heterodyne receivers up to the 1.5 THz region are needed to cover *ortho-* and *para-* H_2O lines. Similarly, in the laboratory, THz measurements are needed to examine diatomic molecules by measuring rotational and vibrational eigenstates to get potentials. These parameters are necessary to fully understand molecular interactions in chemistry and biochemistry, where bonds vibrate in the mid-IR ($400cm^{-1}$ to $4000cm^{-1}$). FIR measurements would allow characterization of weaker bonds or heavier molecules, such as found within and between proteins. Such interactions are key to the pharmaceutical industry, where quantitative structure modeling is used in the rational design of new drugs. Blake spoke about laboratory spectroscopy measurements on molecules using FIR lasers modulated by microwaves using semiconductor mixers. New applications are becoming available using heterodyne sources obtained by photomixing of optical lasers using optoelectronic devices built with GaAs to provide pulse widths on the order of 150 fs. Several such devices have been built, and will be flown on the Kuiper Airborne Observatory in April 1995 to do submillimeter astronomy, looking for ground-state $^{18}O^{16}O$ isotomer of the oxygen molecule in natural abundance at near-THz frequencies. In addition, a miniaturized device is being designed to fly on the Perseus remotely piloted vehicle and ER2 platforms to take stratospheric measurements on small scales, on the order of 100 m, on the order of cloud sizes. These optical photomixers are broadband, have no mechanical tuners over the full bandwidth range from DC to 1.5 THz, and, in principle, can be interfaced to computers to allow complete control of instrument operation and data acquisition.

A similar THz source has been developed by Alan Pine and Richard Suenram of the Molecular Physics Division at NIST/Gaithersburg, in collaboration with Elliott Brown and coworkers at MIT Lincoln Laboratory who have fabricated a new, low-temperature-grown, GaAs device that acts as an ultrafast photomixer. Pine has incorporated this device into a broad-band THz spectrometer using two narrow-linewidth (1 MHz) dye lasers. The spectrometer operates by focusing the output of the two dye lasers onto the ultrafast photomixer; the output of the photomixer is the difference frequency between the two dye lasers. Holding one dye laser frequency fixed, and tuning the frequency of the second, results in broad-band, tunable output in the far infrared region. The output is passed through an absorption cell containing the compound of interest, and the radiation is detected by a helium-cooled bolometer. This spectrometer has been used to obtain high-resolution spectral data from 150 GHz to 1 THz; Lincoln Laboratory has fabricated newer devices that should operate to 4 THz. In support of this work, NIST is working on implementing solid-state diode lasers as pump sources for the ultrafast photomixers. Once the linewidths of the diode laser sources have been reduced to <1 MHz and suitable locking schemes developed, computer control to make the new instrument "user-friendly" will be implemented.

Extending the utility of THz measurements into the realm of materials science and technology, Robert Giles, from the Submil-limeter Technology Laboratory, University of Massachusetts, Lowell, described the *Characterization of Material Properties at Terahertz Frequencies*. The main goal of this work is to acquire millimeter wave radar cross-section signatures of hard bodies, such as tanks in a battlefield, using submillimeter-wave model measurements. This requires the knowledge of optical properties of materials at submillimeter wavelengths in order to develop realistic models for scaling, etc. To support these goals, they must produce high-fidelity, scale replicas of complex metallic structures, design a wide range of optical properties measurement systems using current submillimeter wave source/detector technology, establish precise calibration standards, and scale millimeter wave dielectric properties of composite materials at submillimeter wave frequencies. Four techniques have been explored: submillimeter ellipsometric measurement, high-precision submillimeter wave reflectometry, laser-based Brewster's angle measurements, and FIR Fourier transform spectroscopy. Giles showed details of design and development of suitable instrumentation, and the use of these techniques in their laboratory specifically for evaluating the optical properties of materials at THz frequencies. They have established calibration standards for performing reflectivity measurements to a repeatability of $\pm 0.1\%$. Also, they have developed a variety of artificial dielectric materials for bulk and thin film applications, and have tailored their optical properties for the fabrication of frequency-selective absorbing structures.

Continuing in the vein of calibration-related activities, Gabriel M. Rebeiz, Electrical Engineering/Computer Science Department, University of Michigan, Ann Arbor, described his work in the area of *Planar Antennas, Power Meters, and Calibration Techniques at Terahertz Frequencies*. Rebeiz showed some photomicrographs of beautifully etched antennas,

clearly demonstrating the state of the art in design and fabrication of planar antennas. He showed their normalized antenna patterns and compared them with theoretical predictions. In most cases there was good quantitative fit; even where experimental values differed from theory, the qualitative fit was excellent. His group's designs for reflector antennas integrated with detectors show extremely high gain (>30 dB) with very small size and good coupling efficiency (84 %) to Gaussian beams, making them suitable for radiometric and communications applications. Using similar principles, they have been able to construct easy-to-build, monolithic THz power meters that are accurate to within ±5 %, and can be arrayed for spatial sampling. Rebeiz went on to describe several methods to calibrate antenna gain. The two-antenna method, the radiometric method, and the plane wave method were discussed. He showed the areas of applicability and problems associated with each method.

Harold Fetterman, Electrical Engineering Department, University of California, Los Angeles, addressed issues of *Optoelectronic Measurement Techniques*. He described measurements performed in his laboratory using picosecond lasers and optical switches. His group was able to measure the current gain and the optical response of an AlInAs/GaInAs high electron mobility transistor (HEMT), and similar characteristics of an AlGaAs/GaAs heterojunction bipolar transistor (HBT) up to 100 GHz. He concluded that for frequencies above 100 GHz, no measurement techniques are available. Fetterman expressed the view that NIST should address measurement techniques for high frequencies and develop standards for, e.g., testing repeatability. Several electro-optical sampling techniques were discussed, including frontside probing of microstrip transmission lines, and backside probing of coplanar transmission lines. Coplanar photoconductive switches have been designed and implemented, as has a pulsed millimeter wave radiation experiment, used to measure radiation from 45 GHz to 75 GHz in real time using heterodyne detection. Using microfabrication techniques, Fetterman and his group have been able to design repetition rate multipliers, power splitters, and optical delay lines suitable for use in optoelectronic applications, as well as integrated optical waveguide-HBT structures, which they have characterized. Fetterman expressed the view that it would be a real breakthrough to put THz signals on optical signals and use the enormous bandwidth that is available, for example 2000 GHz at 1.3 μm, for communications. Such implementation is a real possibility, as he outlined how optical techniques could be used to generate, detect, and transmit THz radiation. He recommended that NIST develop standards and techniques which would make THz technology commercially viable for communications.

Round-Table Discussion

As a lead-in to the round-table discussion, Neal Erickson was asked to provide some information about the market for millimeter and submillimeter components and full systems, based on his company's data. Major volume applications consist of imaging systems for aircraft landing and contraband detection, and short-range radar for automobile collision avoidance. Smaller markets are expected for submillimeter wave systems. Based on his perspective from the commercial sector, Erickson offered the following as examples of what NIST could offer industry:

- calibration of power from sources;
- characterization of absorbers for radiometer calibration and antenna measurements;
- waveguide standards at frequencies above 325 GHz; and
- quasi-optics and antennas, standard gain horns, and low-gain probes for near-field scanning.

Using these suggestions as a jumping-off point, the Discussions chairman, Richard Harris, Chief, Cryoelectronic Metrology Division, NIST/Boulder, opened the floor for discussion by requesting that members of the three major participating groups—industry, academia, and government—tabulate what they each felt were suitable areas for NIST to address. Much discussion ensued, with key points recorded for later analysis. Topics raised included:

- THz modulation of optical communication;
- FTIR systems;
- industrial applications, including imaging for aircraft landing, volcanic SO_2, collision avoidance, and contraband detection;
- frequency measurements and phase noise;
- tools for high frequency measurements, (e.g., sampling, vector network analyzers);
- calibration round-robins;
- spatial measurements of antenna characteristics;
- provision of standard reference materials;
- source comparisons;
- standard attenuators;
- environmental monitoring;
- phased arrays for mapping;
- generation of standards for absolute power;
- calibrated sources;
- optical properties of materials; and
- instruments to support process monitoring in several industries.

After discussion of the relative merits of each of these suggestions, and some extended debate over NIST's proper role with specific reference to its charter, a vote was taken to determine which of the above areas should most properly be addressed by NIST. The attendees at the workshop (excluding NIST staff) were asked to vote. The most votes (in descending order) were for NIST to:

- ***take an active role in the measurement, evaluation, and dissemination of optical properties of materials (16);***
- ***provide absolute power standards (9 for single mode, 6 for multimode);***
- ***provide tools for frequency measurements (5);***

- *provide standard reference materials (4); and*

- *provide calibrated sources (4).*

Several other topics received less than four votes. NIST's participation in collaborative efforts was discussed, as was its potential role in forming the nucleus of such efforts.

The attendees expressed great pleasure in the format and outcome of the workshop, and look forward to further meetings of this sort as industry, academia, and government organizations move further into the THz realm.

PROCEEDINGS

NIST's Historical Activities in THz Metrology

Erich Grossman A1-A5
Cryoelectronic Metrology Group
NIST (Boulder)

NIST has a long heritage of work in the area of THz metrology. This work has addressed frequency-related measurements, detector development, and lower frequency (but still THz-capable) techniques. Of particular note was the work done in 1972 by Evenson *et al.* on a frequency synthesis-based speed-of-light measurement. This measurement chain amply demonstrated a basic principle of THz research, that one should "...not do such measurements unless absolutely necessary, as the experiments are too complex." Basically, this work simultaneously measured the frequency and wavelength of a stabilized HeNe laser line; the results changed the definition of the standard meter from one of physical distance (length) to a time-based measurement. The relative standard uncertainty of this measurement was 1×10^{-9}, limited only by the existing standard of length, based on the krypton 86 transition. As noted in Figure 1, Evenson started with a cesium frequency standard and built a frequency synthesis chain up to 88 THz. Each mixer in the chain was used for harmonic generation and mixing. They were point-contact MIM diodes, developed in Evenson's laboratory. Relative to other mixers these devices were high bandwidth, low-conversion-gain, barely nonlinear components, whose speed was unsurpassed. The mixing was done from the 10 GHz klystron to 150 GHz with a servo loop, and then from the 150 GHz klystron to an HCN laser. The process took advantage of an "accident of nature" in that the twelfth harmonic of the HCN laser falls on the 10.8 THz water vapor line, which raises the frequency to input to a CO_2 laser line. They then filled the 2.7 THz gap to a second CO_2 laser line by mixing with the third harmonic of the HCN laser. The second CO_2 line was tripled to beat against the HeNe laser, which was locked to the CH_4 transition.

One technique that took advantage of the ability to accurately measure transition lines resulted in development of the FIR optically pumped laser magnetic resonance (LMR) spectrometer (shown in Figure 2), used to do molecular spectroscopy to characterize transition frequencies of various atomic, molecular, and ionic species. These transitions may be thought of as reference frequencies in the THz frequency range. LMR works on paramagnetic species, and works by magnetically tuning a transition of the species of interest into resonance with a FIR laser.

The tunable far infrared (TuFIR) spectrometer is useful for absorption spectroscopy and laser frequency measurements. The technique is similar to the frequency synthesis experiment described earlier for the speed of light measurements, and is described in the caption to Figure 3. The reradiated beam is then used for ordinary absorption spectroscopy, directly detected by, for example, a bolometer. If a high-pressure waveguide laser is used in place of one of the CO_2 lasers, extra tuning, up to several hundred MHZ, is possible. This

technique may be used to measure the frequency of unknown lasers, or for non-paramagnetic species.

Additional work has been done to transfer the accuracy of few accurately known atomic transition frequencies to arbitrary lines in the visible region. These arbitrary lines are separated from the known lines by THz frequencies. Using GaAs Schottky diodes as optical photo mixers and THz harmonic genearators, Hollberg and Waltman were able to perform these measurements up to 1 THz of frequency separation.

In frequency synthesis using higher order harmonic generation, one issue that commonly arises is that of the spectral purity of the fundamental, because the phase noise of an oscillator increases with the square of the harmonic order, thereby producing a noise pedestal that swamps out the narrow frequency component of interest. NIST has a group that makes careful measurements of spectral purity (i.e., phase and amplitude noise of oscillators), and looks at the effects of harmonic generation in frequency synthesis.

The development of new detectors for power measurements emphasizes low noise; therefore, development of cryogenically cooled detectors has been of importance. Low-noise detector work at NIST has recently focussed on high T_c super-conductors. Of note are the development of YBCO Josephson junctions, which have the world record for characteristic frequency, which is the product of the critical current and the normal state resistance of the junction. These antenna-coupled structures are fabricated by deposition of YBCO across a step in the substrate. The Josephson junction is at that break, with normal metal in between superconductors; these are the *S-N-S* junctions. The characteristic frequencies for structures shown in Figure 4 are on the order of 1 THz to 4 THz; the structures can be used as mixers up to the order of the characteristic frequency. There is still some irreproducibility in the fabrication process, but the best samples have current equivalent noise levels on the order of 9K.

Other work using YBCO/YSZ devices employs high T_c transition edge bolometers fabricated on silicon, which is opaque at THz frequencies. With special buffering, high quality YBCO can be deposited on the substrate. Air bridge isolation is provided by simple silicon micromachining at the feed of the antenna, as shown in Figure 5, and is responsible for the excellent performance. These devices demonstrate a noise equivalent power (NEP) of 9 pW/√Hz, better by a factor of two than other devices available at the time. The electrical NEP, with 20% optical efficiency, was 2 pW/√Hz, with a time constant that was less than or equal to 10 μsec.

Another use of Josephson junctions that has been examined at NIST is in building 2-D array oscillators. The arrays allow cumulative addition of their internal oscillations to produce high power levels. These oscillators are voltage-tuned to GHz and THz frequencies; they have very narrow bandwidth.

With these investigations as a basis for further discussion, some THz metrology issues that might be examined by this workshop are shown in Figure 6. A key issue, as seen under the heading of Spatial Measurement, is *beam quality*. Any kind of

spatial measurement (antenna pattern, etc.) must conform to an ISO-9000 standard for beam quality, known as M^2, as defined in Figure 7. This is not the same as mode content, but is rather the number of modes in the beam. Based on a Gaussian beam geometry, M^2 is the product of the angular and spatial width, normalized to wavelength. This definition is satisfactory where spot size is the ultimate criterion. However, there is some question as to whether this is the appropriate standard to use for beam quality, particularly at THz frequencies. Here, coupling efficiency is more important, and is usually the parameter of interest.

Heterodyne Radiometry for Millimeter and Submillimeter-Wave Earth Remote Sensing

Peter Siegel & Joe Waters **A6-A11**
Jet Propulsion Laboratory

The science priorities that are addressed by millimeter and submillimeter wave Earth remote sensing are shown in Figure 1; of particular interest is the study of ozone chemistry. Specifically, in the millimeter and submillimeter bands there are signals from many species of interest in ozone chemistry. The abundance of these species can be derived across the entire earth's atmosphere, from stratosphere to tropopause; the lines become optically thick in the tropopause.

One of the most well-known atmospheric phenomena in recent years is the so-called "ozone hole" over Antarctica, which appears yearly during the Antarctic winter. An example of the observational data is found in Figure 2, which shows the "depth" and areal extent of a typical ozone hole. Evidence for a diminution of ozone over the Antarctic extends back to the late 1970s, when ground- and satellite-based data showed a severe drop in ozone concentration, followed by a rise in ozone levels as atmospheric temperatures in the region increase with the onset of the austral spring. Subsequent research has tied the formation of the hole to the use of fluorocarbons, an industrial by-product, coupled with the peculiarities of temperature, ultraviolet radiation, and wind and cloud patterns over Antarctica.

In an effort to more fully understand the mechanisms responsible for the formation of the hole, and to better understand the dynamics of Earth's upper atmosphere generally, the Upper Atmosphere Research Satellite (UARS) was launched from the Space Shuttle in 1991. An instrument key to understanding the vertical distribution of gases in the atmosphere was the Microwave Limb Sounder (MLS). The MLS was used to address details of stratospheric ozone chemistry, upper tropospheric and stratospheric greenhouse gases, measurement of volcanic pollutants in the lower stratosphere, and measurements through ice clouds and aerosols.

Column measurements of atmospheric constituents give total levels, but not their vertical distribution. Heterodyne microwave limb scanning, as diagramed in Figure 3, measures molecular thermal emission spectra through the atmospheric limb at all altitudes using a mechanically scanning reflector. All spectral lines are fully resolved at all altitudes, thereby allowing weak lines to be measured in the presence of strong nearby lines. Heterodyning gives the highest possible spectral resolution, continuous measurements in all channels, excellent sensitivity, and the allows for the use of long-life, robust detectors that operate at

room temperature. Further, millimeter-wave measurements are unaffected by ice, clouds, or aerosols, thereby allowing monitoring under conditions where other techniques would not be effective.

The hardware required for Earth remote sensing is similar to that required for astrophysical investigations, but generally the constraints on Earth remote sensing are not as stringent as those for astrophysics. Because the brightness temperature of most molecular species in the Earth's atmosphere is >10 K, signals are strong enough at submillimeter wavelengths such that quantum-limited detectors are not required. However, with more sensitivity available, faster scanning can be done, and more horizontal resolution can be obtained. Astrophysical lines are typically < 0.1 K, so much higher sensitivity detectors are required. In Earth remote sensing, the primary collecting area is filled by the signal beam, so there is no sensitivity advantage in going to larger antennas. Astrophysical sources usually do not fill the beam unless very high resolution (large diameter) antennas are used. Finally, spectral lines in the Earth's atmosphere are fully mapped in millimeter and submillimeter regions in the laboratory for all species of interest, with 100 MHz resolution, so line confusion is readily avoided. In astronomy, there are many more species in space, much larger temperature differences to span, and there are still many unidentified radicals which may cause line overlap and concomitant confusion.

This is not to say that there are no constraints on heterodyne technology for Earth remote sensing. Satellite orbital motion and requirements on vertical scanning limit integration time to <1 s per profile. Fixed frequency receivers require wide IF bandwidth and double sideband operation to cover the required spectral lines in an efficient manner. There is also a need to make simultaneous observations at all frequencies and at all times to interpret the data in terms of atmospheric composition as a function of time. The satellite orbits the Earth some 20 times a day; interpretation gets complicated if the data are not available in all channels simultaneously. Finally, extremely tight constraints on beam efficiency, baseline flatness, and absolute calibration are required for proper molecular line retrieval at all vertical layers. The line shape as a function of pressure must be known very accurately.

The MLS on UARS has three, fix-tuned, whisker-contacted, GaAs Schottky diode heterodyne radiometers that were state-of-the-art for the 1980s. These radiometers are used with six, 15-channel filter banks as follows:

Frequency (GHz)	Molecular species
205	ClO, H_2O_2, O_3
183	H_2O, O_3
63	O_2 (pressure/temperature)

An example of the spectral coverage afforded by the MLS design is shown in Figure 4.

The primary antenna is a 1.6 x 0.8 m ellipsoid, with 3.5 km vertical and 10 km horizontal resolution. The scan range is 0 km to 120 km in 0.05° steps, with 1.8 s dwell time. The robust design implemented in this instrument resulted in data acquisition within two days of its deployment, with

continuous data having been received for 39 months. The limiting factor at present appears to be degradation of the mechanical scanning assembly; the electronics are still functioning well.

Often, the public asks, "Of what concern is the Antarctic ozone hole to those of us in more temperate climes?" Data from UARS-MLS show distributions of some species known to be involved in ozone destruction over mid-latitude regions similar to those found in the Antarctic. The juxtaposition of ClO and O_3 during the winter of 1993 shows that there is at least the potential for O_3 reduction over these regions, in a manner similar to that over Antarctica, as shown in Figure 5. To further address this and other phenomena, a follow-on to the UARS-MLS is being readied as part of NASA's Earth Observing System (EOS) suite of missions. The EOS-MLS, scheduled for launch in 2000, will have five millimeter and submillimeter-wave radiometer bands (at 215 GHz, 310 GHz, 640 GHz, and two-2520 GHz), and will measure radicals, reservoirs and source gases in all four ozone-depleting cycles: oxygen, chlorine, hydrogen, and nitrogen. In addition, hydroxyl, volcanic pollutants (such as SO_2), and stratospheric and upper tropospheric water and ozone will be measured. Specifically, the spectral bands and associated measurements are as shown in Table 1.

The EOS MLS signal flow block diagram is shown in Figure 6, and the simplified EOS-MLS beam path is shown in Figure 7. Comparisons between the UARS-MLS and EOS-MLS are shown in Figure 8. Additional technology for 2.5 THz channel for measuring hydroxyl includes an open structure mixer and an integrated submicron diode, and a local oscillator consisting of an RF-excited CO_2 laser pumping an FIR methanol gas laser.

The EOS-MLS front-end development is being conducted by a collaborative team with personnel from JPL, the University of Virginia Semiconductor Device Laboratory, the University of Michigan Center for Space THz Technology, the University of Massachusetts Department of Astronomy, Martin Marietta Laboratories, and the Rutherford Appleton Laboratories, UK.

In an effort to ensure a long-term, validated and calibrated data set, EOS is paying close attention to calibration needs for its instruments. The needed standards for EOS-MLS are listed in Figure 9.

Table 1. EOS–MLS Spectral Bands and Measurements

Radiometer Center Freq.	I.F. Band Center	Primary Measurement	Secondary Measurement	Required Sensitivity 0.6" Integ., SSB
216.29	-10.16 -11.94 +17.66	O_3 (UARS) Upper troposph. H_2O pressure/temp, $O^{18}O$	^{35}ClO (UARS), SO_2	$T_{sys} < 3000$ K
310.5	-3.70 +4.70 +6.70 -12.02 +14.65	HNO_3 Tropopause H_2O Upper troposph. O_3 pressure/temp. $O^{18}O$ Stratospheric H_2O	Stratospheric O_3	$T_{sys} < 4500$ K
642.87	±6.60 +7.33 +9.98 -16.93 -17.48	^{35}ClO N_2O $H^{35}Cl$ Stratospheric O_3	HOCl, HO_2 BrO HO_2	$T_{sys} < 10,000$ K
2522.78 (2 channels)	-8.41 -12.78	OH OH		$T_{sys} < 15,000$ K

Mixers: Planar balanced or subharmonically pumped antiparallel-pair planar-Schottky-diode to 640 GHz Planar integrated antenna/Schottky diode for 2.5 THz (whiskered waveguide or corner-cube backup)
IF: 5 broadband HEMT amplifiers (MMIC proposed, discrete narrow-band if necessary)
LO: InP Gunn osc. for 216/310 channels, InP Gunn osc. and planar-diode varactor multiplier for 640 channel CO_2 pumped methanol laser at 2522 GHz
Back End: 17 filter banks, 1.3 GHz, 25 channels 6-96 MHz baselined, stacked AOS's proposed
Integration Time: 0.6 sec Field of View: 1.5 km at limb 640/2.5 THz, 3 km for 310 GHz, 4 km for 215 GHz
Orbit: Sun synchronous, 705 km, 98° inc., forward looking Mission Life: 6 years continuous operation
Delta Launch in late 2002, Mass: 500 kg Power: 625W Data Rate: 100 kbps

THz Applications in Atmospheric Sensing

Kelly Chance A12-A20
Harvard Smithsonian Institution

The major chemistry of ozone depletion in the stratosphere falls into three basic families: odd-hydrogen, odd-nitrogen, and odd-halogen. As shown in Figure 1, each family is exemplified by a catalytic cycle of odd oxygen (O_3 + O) destruction mediated by a free radi-cal pair, steps of radical production and chain termination, and side reactions involving the sequestering of active species and coupling of the different chemical families (more recent understanding of ozone depletion chemistry indicates the importance of bromine chemistry, which is not included in the figure). Many of the species involved in this chemistry can be measured well and, in some cases uniquely, in the atmosphere using spectroscopy in the THz region. The hydroxyl radical (OH) is of parti-cular interest because of its central role in the ozone-related photochemistry, and because remote sensing measurements of stratospheric OH are limited to the THz region. Figure 2 shows portions of far infrared (i.e., THz region) spectra obtained from a stratospheric balloon platform using the Smithsonian Astrophysical Observatory (SAO) FIRS-2 Fourier transform spectrometer. The region is chosen to high-light the specific OH emission lines that are the best for remote sensing measurement of OH anywhere in the atmospheric spectrum. The different spectra correspond to different sampling heights in the atmosphere.

As a complement to the satellite-based heterodyne remote sensing measurements discussed by Siegel earlier in this volume, non-coherent techniques such as balloon-borne Fourier transform emission spectroscopy in the far infrared/submillimeter spectral region can also be used for measurement of altitude profiles in the stratosphere of a number of trace gases involved in ozone photochemistry. Use of these techniques in the 0.6-6 Thz range gives unique measurements of OH, HO_2, and H_2O_2 and favorable measurements of HOCl, ClO, Hcl, and HF. Figure 3 shows an example of the distributions of most of these species, plus others measured simultaneously, from a balloon flight of the FIRS-2 instrument in September 1989. Because the measure-ments are made in emission, the diurnal behavior of the concentration profiles of reactive species can be monitored. Thz techniques are parti-cularly suitable for stratospheric measure-ments; tropospheric lines are too broad and too obscured by H_2O to be measured well in the Thz region except in special cases. There is also potential for the use of Thz techniques in mesospheric and thermospheric physics and chemistry. In support of the atmospheric measurement programs, laboratory spectro-scopic measurements using a number of techni-ques, coherent and incoherent, provide spectro-scopic details necessary for the identification and quantitative analysis of spectral features. The TuFIR technique, developed in the NIST Boulder Laboratory, is worth of particular mention here.

The SAO FIRS-2 balloon instrument is a sensitive, high-resolution (0.004 cm^{-1} unapodized) Fourier transform spectro-meter, plus limb-sounding telescope and gyroscope- and accelerometer-stabilized pointing system. It measures the spectral ranges 70 cm^{-1} - 210 cm^{-1}, using a Ga-doped germanium photo-conductor detector, and 350 cm^{-1} - 700 cm^{-1}, using a Cu-doped germanium photoconductor detector. The far infrared channel includes complete coverage of the 2-6 THz region.

An example of the ratospeheric spectrum for this region is given in Figure 4. The spectrum is dominated by strong H_2O lines that are apparent throughout the region and, particularly below 3 THz, a forest of weaker O_3 lines. The major lines used for measurement of trace species are identified on the spectrum and also listed in Table 1. The atmospheric spectrum at these frequencies, other than contributions from H_2O and O_3 is dominated by lines from small, polar molecules (diatomics and nearly-symmetric prolate tops) that have hydrogenic moments of inertia and thus large rotational partition functions. This class of molecules includes many of the most important trace stratospheric species, explaining why THz measurements are particularly important to determination of ozone layer photochemistry. For example, several small features in the 3 THz region, each of less than 1% emissivity, provide the only measurements of H_2O_2 in the stratosphere.

The SAO maintains a molecular line database for analysis of atmospheric spectra from 10 cm^{-1} - 800 cm^{-1} (0.3 THz - 24 THz). This database combines the best currently available line parameters from various measurements and calculations as well as the HITRAN and JPLSMM databases. It is currently available electronically to the general scientific public via *ftp*. An example of recent results from a TuFIR study made to improve the analysis of atmospheric spectra is the set of HO_2 transitions and term energies shown in Figure 5. The SAO database itself is described in more detail in Figure 6.

Given the central importance of OH in stratospheric chemistry, it is important to develop a technique for global monitoring of OH from space. The OH Interferometer Observations (OHIO) concept for satellite-based monitoring of OH is being developed in a joint effort by the SAO, the National Air and Space Museum, NASA Goddard Space Flight Center, the Space Research Organization of the Netherlands, and several other collaborators. OHIO would measure the F_1, $7/2^+ \rightarrow F_1$, $5/2^-$ OH transition at 3.551 THz, using a simple Fabry-perot/grating instrument. The key technology that permits the technique to work is the development of high-T_c YBCO transition-edge bolometers operation at greater than 80 K. Figure 8 shows a synthetic stratospheric spectrum, based upon FIRS-2 measurements, with a possible configuration for the Fabry-Perot and grating transmission functions. Such syntheses and associated retrieval studies show that OHIO should be able to perform global mapping of stratospheric OH using currently-available technology.

A summary of some of the key points of this presentation is given in Figure 9.

Table 1. Line Locations for THz Measurements of Trace Stratospheric Species

OH		H_2O_2		ClO	
THz	cm^{-1}	THz	cm^{-1}	THz	cm^{-1}
2.51433	83.869	2.81734	93.976	0.64945	21.663
3.03627	101.279	3.36279	112.171		
3.03664	101.291			HBr	
3.54379	118.208	HF			
3.55119	118.455			1.50055	50.053
4.21230	140.507	4.91468	163.936	1.50102	50.069
5.35823	178.731	6.13197	204.540	2.99536	99.914
5.36387	178.920			3.48976	116.406
5.65034	188.475	HCl		3.49084	116.442
5.66351	188.914				
		3.12199	104.138	NO_2	
HO_2		3.74222	124.827		
		4.35367	145.223	2.98374	99.527
0.62566	20.780	4.36018	145.440	3.10196	103.470
4.25849	142.048	4.96809	165.718	3.12317	104.178
4.30681	143.660	4.97551	165.965	3.17440	105.886
4.32432	144.244	5.58783	186.390	3.20348	106.856
4.37126	145.810			3.25435	108.554
4.39032	146.445	HOCl		3.48401	116.214
4.56198	152.171			3.48492	116.244
4.58797	153.038	2.98378	99.528		
4.65355	155.226	4.28628	142.975		
4.71896	157.407	4.28668	142.988		
		4.31549	143.949		
		4.31641	143.980		
		4.40547	146.951		
		4.67133	155.819		
		4.75945	158.758		

Applications of Synchrotron Far-IR to Studies of Electronic Materials

Larry Carr A21-A26
R&D Center - Electronic Materials Laboratory
Grumman Aerospace and Electronics
Bethpage, NY

Synchrotron radiation is the light emitted by electrons circulating in and confined to a large ring. Bending magnets along the orbit keep the electrons circulating. As a result of the acceleration along curved paths the electrons reaching relativistic speeds emit light in a narrow solid angle, accessible via several access ports in a beam tangential to the orbit. In the case of the National Synchrotron Light Source (NSLS) at the Brookhaven National Laboratory, an additional, large-aperture port has been added to allow for the extraction of long-wavelength infrared radiation.

Synchrotron storage rings produce radiation output from the microwave region to X-rays; indeed, most storage rings are designed for X-ray investigations. The features of NSLS are shown in Figure 1. The total IR power per bandwidth emitted by synchrotron could be less than that of conventional thermal source (like Globar) especially at near-IR and mid-IR wavelengths. Most thermal sources emit radiation in 2π steradians. Only a portion of such radiation can be captured for experiments, whereas synchrotron radiation is emitted as a beam with very small divergence because of the relativistic acceleration of electrons, so most of it can be captured for experiments. For this reason, synchrotron IR emission is two to three orders of magnitude brighter than that from thermal sources along the line of sight. At longer wavelengths ($\omega < 100$ cm^{-1}), how-ever, the synchrotron begins to have significant power compared to thermal sources because the rate of fall-off of the synchrotron power is on the order of $\omega^{1/3}$ (which is slow), while blackbody (thermal) sources fall off on the order of ω^2 in this spectral range.

The light from the synchrotron is spatially coherent. The source size is few hundred microns across, which is typical of the cross section of the electron beam. As it is emitted in a narrow angle, it is possible to focus this light into a very small spot to do microscopic investigations. Most of the work underway in the facility at NSLS is for microspectroscopy. However, there are pulse timing applications which take advantage of the pulsed nature of the beam. The pulses occur because of electron bunching in the synchrotron, as opposed to a continuous stream. The bunching is the result of acceleration of electrons in an RF cavity in one part of the beam; they have to synchronize with the RF excitement as they pass through the cavity. The bunches result in pulse duration on the order of tens to hundreds of picoseconds, and time separa-tions of similar magnitude, based on the separation between electron bunches. As mentioned earlier, the light is spatially coherent, making it easy to split the beam and use the two paths as an interferometer. The light is also polarized, but this has not been exploited to any degree in our experiments. Typical power in the range $0 < \omega < 300$ cm^{-1} is on the order of 10 mW peak power for 0.5 ns pulse duration, with 70 μW of average power. Comparison of some features of several available synchrotron sources are shown in Figure 2. The SRC-Aladdin synchrotron is in Wisconsin; the NSLS's are in Brookhaven, New York, the CAMD is in Baton Rouge, Lousiana, the ALS is in Berkley, California, and the APL is in Illinois.

The minimum separation in time is based on the minimum feasible separation between bunches in space; this is unique for each machine. Maximum separation may be found when all the electrons are made into one bunch and the period is the time required for the bunch to complete one orbit around the ring. For example, the APS would have very high energy photons, which may make it impossible to extract IR out of background. The ALS may be more suited for future experiments because of the short pulse width.

The unique characteristics of such IR beams from synchrotrons make them eminently suitable for characterization of optoelectronic device materials such as would be used in photon detectors and photon sources, for characterization of photo-excitation dynamics by measuring transient electrical photoresponse, and in pump-probe spectro-scopy. In the first case, this amounts to measuring the electrical output that results from the input of a light pulse. In the case of pump-probe (two-photon) spectroscopy, a light pulse stimulates the material, and a second pulse is then injected and spectro-scopic measurements are made.

Transient electrical photoresponse measurements are performed to determine the response speed of photodetector devices or materials that make up these devices. In one case, the quality of the material that constitutes the detector can be determined by measuring the photocarrier life time. Knowing the carrier lifetime of the material allows determination of the response time of the device and its relationship with the carrier lifetime of the detector material; typically, very long lifetime gives high responsivity. Another class of experiments is to determine the response time of a device. An example of this kind of study is shown in Figure 3, which shows the responsivity of an AT&T quantum well infrared photodetector (QWIP), and some associated measurement parameters. These measurements gave an upper bound on the response time of quantum wells. The response time is fast, i.e., less than 500 ps. Theoretically, response time can be as fast as 50 ps because of the fast recombination times in these materials.

Another major use of infrared synchrotron radiation (IR-SR) is for time-resolved (pump-probe) measurements, as shown in Figure 4. The basic technique begins by application of a laser pulse to a sample, which creates photoexcitation. After a chosen time interval (Δt), an infrared pulse is made incident to probe the excitations. The output infrared pulse is then detected and spectroscopically analyzed. The process is then repeated for various Δts to extract time-dependence of spectral features. Based on a system originally developed at NSLS by Dave Ederer of NIST, a pump probe system was setup for IR as shown in Figure 5. A pulsed laser diode is driven by an electrical pulse system synchronized to the synchrotron's RF, and thereby automatically locked to the RF of the ring. The laser pulse is fed directly to the sample's cryostat assembly via fiber optic cable, terminating within a few millimeters of the sample's surface; no other optics are required for the exciting pulse. The probe pulse goes through an FTIR system which covers 20 cm^{-1} to 2000 cm^{-1}; the detector is typically a silicon bolometer.

In pump-probe spectroscopy, which is essentially photospectroscopy, the measured quantity is the negative change in transmission of the IR through the sample; an

experimental scenario is presented in Figure 6. The magnitude of typical ($-\Delta T/T$) signals is on the order of 10^{-3}, requiring high-performance spectroscopy. Sample penetration is often no more than approximately 1 μm, which simplifies analysis. For undoped GaAs semiconductors at long wavelengths, the sample is prepared by creating a thin conducting layer on a transparent surface. As a result, the negative of the change in transmittance is directly proportional to the surface conductance of the film on the surface.

An example of such an analysis is found in Figure 7, which shows time-resolved FIR spectroscopy of undoped GaAs. The majority of the signal was quasi-static, with a relaxation time of more than 100 ns. There are two components to the relaxation. The fast component decays in 10 ns, whereas the slow component decays over a much longer time. The scattering rate for the slow component is similar to that for holes in such material. The fast component has a different shape, indicating a slower scattering rate, and may be due to electrons. For ease of interpretation, the fast component data have been magnified by a factor of ten. This technique, then, provides a way to distinguish between electrons and holes in a semiconductor in a time-dependent fashion.

Another analysis, of HgCdTe, shown in Figure 8, shows the time-dependent signals and a thermal signal. The thermal signal is obtained by warming the sample by about 1K. It is significant, and must be subtracted from the time-dependent signal to obtain proper characterization of the sample. The figure shows the photocarrier density that was extracted, and its decay as a function of time at different temperatures. A summary of, and conclusions from this work are shown in Figure 9.

Applications of Free-Electron Lasers as Terahertz Sources

S. James Allen **A27-A34**
Center for Free-electron Laser Studies
University of California, Santa Barbara

There is a technology gap between applications of electronics and photonics. Electronics technology is well established, and goes up to several hundred GHz. Similarly, photonics typically extend from 10 THz and above. There is roughly a two order of magnitude gap between electronic (up to several hundred GHz) and photonic (down to 30 μm) regions, as shown in Figure 1. Exploring this gap is important, and free-electron lasers (FELs) have significant utility in this area.

The FEL facility at UCSB generates radiation which is tunable over the range 120 GHz to 4.8 THz. Unlike most other FELs, which are driven by RF linear accelerators and produce pulsed radiation on the order of picoseconds, the lasers at the Center are driven by an electrostatic generator. As a result, the radiation is quasi-cw, in 1 μs - 20 μs pulses with a frequency stability of approximately 10^{-6} while the pulse is on; there is pulse-to-pulse jitter of about 10^{-3}, which could limit the kinds of experiments performed using this facility. Power output is from 500 W to 5 kW.

One of the scientific thrusts at UCSB is to examine nonlinear quantum transport in semiconductor nanostructures in THz electric fields. The other area is to investigate novel phenomena in semiconductor nanostructures. Two examples of application of these FELs

are discussed here: definition of high-frequency limits in resonant tunneling diodes RTDs), and photon-assisted tunneling in semiconductor nanostructures.

RTDs are two-terminal devices that pass current through a quantum well structure if the quantum states are in resonance with an emitter. Specifically, we examined the InGaAs/AlAs system to address state-of-the-art materials that have the capacity to produce the highest frequency responses possible. This work was done in collaboration with researchers at Hughes Research Laboratory. The collaborators and the project definition are shown in Figure 2.

The approach is to measure the I-V characteristics at high frequencies to understand what controls the fundamental processes and the speed of these devices. While difficult to do, a useful approach is to measure the second derivative of the I-V response by making the RTD a detector and measuring the detectivity of the RTD as a function of frequency, as diagramed in Figure 3. The frequency response of InGaAs/AlAs is shown in Figure 4. It shows a roll-off in rectified response at about 700 GHz, corresponding to a relaxation time on the order of 220 fs. The interpretation is that this experiment measured something about the intrinsic relaxation of the RTD, which controls its high frequency performance. However, theorists would say this experiment should not have worked at all. The experiment clearly worked and it is therefore necessary to understand the physics underlying this phenomenon. Here, the FEL provided the power to couple into the micro-device in a crude way. Its tunability has provided temporal dynamics as a result of measurements done in the frequency domain. This kind of experiment clearly shows the capabilities of the FEL in this domain.

With regard to investigating new phenomena, our interest is in photon-assisted tunneling in resonant tunneling diodes. RTDs provide gain by taking advantage of differential negative resistance, and have gain from DC up to extremely high frequencies. However, it does not seem likely one can push RTDs to perform at optical frequencies in a conventional way. One approach to overcoming this limitation is provided by photon-assisted tunneling, i.e., using the RTD as a narrow-band device by biasing it in the voltage region, as shown with an arrow on the I-V curve in Figure 5. There would be real gain in the form of a population inversion between the emitter state and the quantum well state. This application will take technology from the electronic realm to the photonic, and so we explored the issue of photon assisted tunneling. Although we would have preferred to work with RTDs, which had not been done previously, we approached it in a complicated—but neat—manner, as shown in Figure 6.

We examined a sequential resonant tunneling superlattice, which is nothing but a series of coherently coupled RTDs. The I-V characteristic may be thought of as follows: At very low voltage the curves are dominated by simple transport through the lower quantum well states. By applying a voltage to align a ground state with an excited state, the current steps up. The current steps up further as we sequentially step up through excited states. We took this superlattice and buried it in a bow-shaped antenna, and examined the photon-assisted tunneling, as shown in Figure 7. The black curve is the previously shown I-V curve. Irradiation with, in this case, 3.4

THz radiation causes a change in the shape of the I-V curve, with different kind of steps, as shown by the light curve. The new set of steps corresponds to tunneling into 0-photon, and 1-photon and 2-photon sidebands of quantum well states. This phenomenon is usually associated with quasi-particle tunneling in superconductor- insulator-superconductor structures. However, we were able to show this kind of phenomena with FELs on semiconductor structures. The next step is to translate the physics of this phenomenon to RTDs to do narrow band gain physics, and to realize photonic-like gain media at THz frequencies.

FELs have come a long way since their introduction. We have been able to look at nonlinear quantum transport in semiconductor nanostructures, and at some novel physical phenomena. Areas of potential technology impact are the definition and understanding of high frequency limits of conventional electronics, and to enable new electronics at THz frequencies.

Femtosecond THz Beam Generation and Applications

Daniel Grischkowsky A35-A44
School of Electrical and Computer Engineering
Oklahoma State University

Examination of physical and chemical phenomena, characterization of materials, and ranging studies will likely be facilitated by the generation of very bright, ultrashort pulses of radiation at terahertz frequencies, driven by laser light. The optoelectronic approach described here uses a charged coplanar transmission line circuit irradiated by a laser as shown in Figure 1.

The photoconductive switch (typically silicon on sapphire) is hit with short (50 fs) pulses of laser light, shown as an initial pulse in Figure 1, at a repetition rate on the order of 10^8. With a 10 V potential across the 10 μm gap, the line generates two sub-picosecond current pulses, each traveling in opposite directions on the coplanar transmission line for each optical pulse hitting the semiconductor. These transient electrical pulses cannot be measured electronically, so techniques similar to those used to generate the pulses are used to measure them. By splitting the incident laser beam, one path can be delayed, thereby producing a sampling pulse different from the initial pulse (Figure 1). When the guided electrical current pulse on the transmission line goes by the PAD as shown in the Figure 1, a transient voltage develops across the gap. With a voltage applied, irradiation with a sampling laser pulse at the gap generates a current which can be measured by the ammeter, A, as shown in Figure 1. The measurement is a measure of current as a function of time delay between the initial and sampling pulses. The setup is diagrammed in Figure 2, and an example of the sample current detected is shown in Figure 3.

What is most interesting for our purposes at this meeting is that the initial current pulse generated by the initial laser pulse produces a pulse of THz radiation. It acts like a dipole "supernova" as shown in Figure 4. In other words, the laser pulse of 50 fs generates the current surge which produces THz radiation. Due to boundary considerations the radiation is emitted as a cone into the sapphire substrate in contact with the thin semiconductor surface that was hit by the laser. Figure 5 shows the sapphire lens which collimates the THz radiation; the detector for

measuring it is shown in Figure 6. The detection mechanism is similar to the mechanism for generating the radiation. Early configurations used sapphire lenses for collimation; later approaches use high-resistivity silicon. A typical transient current pulse is shown in Figure 7; Figures 8 and 9 show the pulses detected after a propagation of 10cm and 100cm respectively through air. The numerical Fourier transform of the 10 cm propagated pulse (Fig. 8) is shown in Figure 10, demonstrating useful energy out to 1.2 THz. Oscillations on the shoulders shown in Figure 9 were a mystery at one time, but they turned out to be the absorption lines of water vapor in the THz beam path. They are identified as shown in Figure 11, which is the Fourier transform of Figure 9, including the oscillations in the shoulder.

With careful attention to geometry, the optoelectronic system has been improved, as shown in Figure 12. It has been used as an ultrafast dipole antenna, providing pulse widths on the order of femtoseconds, with a signal-to-noise ratio (SNR) on the order of 10 000:1. We have excellent synchronization between the transmitter and receiver, with no jitter. Calculated CW power in a typical beam is on the order of 10 nW, which has been verified by measurement with an Infrared Laboratories bolometer. This coherent system is again gated by the photoconductive switch, and the noise is inversely proportional to resistance.

Quiescent resistance when the switch is off is about 10 MΩ , rapidly dropping to 400Ω when the switch is gated on. The system is limited by the ballistic acceleration of the electrons; the consequent performance agrees with Drude theory in the time domain. In addition, there is significant absorption in the silicon-on-sapphire substrate, resulting in attenuation of higher frequency components. To overcome some of these limitations a faster system was designed with smaller dimensions using polysilicon over thermal oxide on a high-resistivity silicon substrate to eliminate absorption by the sapphire substrate. This "ultra" system has a unity transfer function, and produces a 200 fs pulse. The numerical Fourier transform demonstrates useful power out to 6 THz. The combination of an ultrafast source and detector can be used for several applications, including antenna characterization, time-domain spectroscopy, non-contact characterization of materials, ranging measurements; and to examine the temperature distributions in flames.

The system was used to perform time-domain spectroscopy on H_2O in a N_2 environment, using MgO lenses. Measurements are taken with and without the sample, and the pulse output is then compared. Examples of results are shown in Figure 13, with acquisition of the strongest water lines out to 1.4 THz, as shown in Figure 14. Because amplitude was measured, it is possible to derive phase information, as well. The results agree with an assumption of Lorentzian lines, with 1:1 correspondence between line strength and phase shift. The results shown in Table 1 give strong indication that this technique can produce better SNR laboratory results than Fourier spectroscopic analysis, from low frequencies up to 4 THz; spectral resolution, however, is comparable.

In an effort to examine more exotic samples, the system was used to investigate spectral lines in a flame. The expectation was that new lines would be evident; this was not

found to be the case. Water lines were found throughout the spectrum, and so were used to do thermometry as a function of location in the flame. Data were obtained by comparing line strength differences (cool water vapor vs. water lines in the flame, which increase due to their temperature).

Semiconductor wafers can be characterized with reasonably good spectral amplitude out to 4 THz. *P*-type GaAs data are shown in Figure 15. The relative phase measure goes up to 60 radians across the frequency range. Experimentally, the greatest problem is the stability of the reference pulse, as measurements can take in excess of 5 minutes. "Good" amplitude results (±5%) have been obtained (and phase stability of ±0.05 radians), but better performance is needed. Absorption results and index of refraction data are shown in Figure 16, where the solid line is a fit to Drude theory. The fit is quite good, but not exact. The reasons for this have to do with absorption at surfaces, phase changes, and Fabry-Perot effects if the sample is sufficiently thick. Early analysis assumed that surface transmission functions were real; these measurements, taken with absorption coefficients as high as 500 cm^{-1}, show that this assumption is flawed. Inserting a phase correction as the imaginary part of the equation accounts for the differences, and demonstrates again that Drude theory accurately describes the system. A complete analysis for *n*- and *p*-type GaAs is shown in Figure 17.

Impact excitation and coherent effects were investigated in a system consisting of a molecular vapor cell filled with methyl chloride vapor. Irradiating with a short THz pulse produces a spectrum that covers the vibrational ground state rotational band. After the initial excitation, vapor itself emits pulses on its own. From examination of the response the molecule can be fully characterized, with excellent agreement between theory and experiment.

Table 1. Comparison of our experimental results with theoretical predictions for the indicated lines in THz

WATER VAPOR							
line	Exp. α_o	(10)	(11)	(12)	(13)*	(14)*	(15)*
0.557	9.4(2)	9.6	9.9	8.6	4.6	10.8	
0.752	6.9(4)	6.8	6.9	5.9	5.1	7.1	
0.988	5.0(4)	5.0	5.1	4.3	2.2	5.3	5.1
1.097	32.0(10)	33.8	34.3		33.8	33.8	33.8
1.113	10.1(7)	10.2	10.5		1.5	10.3	10.1
1.163	37.9(14)	38.2	39.1		36.7	38.6	35.9
1.208	9.8(7)	12.9			14.7	12.1	11.2
1.229	8.5(7)	10.0			7.1	10.5	9.7
1.410	23.1(30)	30.5			45.9	31.6	29.4

Power Standards for the Near Millimeter and Submm Region

Neal Erickson A45-A46
Millitech Corporation

Given the increasing interest in performing measurements at THz frequencies, it is unfortunate that power standards are poorly established in the 90 GHz range, and nearly completely absent above 140 GHz. Typical spreads in measured power are found in Table 1. The manufacturers of devices can not state with complete certainty the accuracy of their instruments in these regions. The users of these devices are forced to accept the claims of the manufacturer: there is no cross-checking, as there is no standard to compare with, and the device with the greatest claim tends to stand as the "best". This lack of accuracy makes it difficult to verify theories or to confirm expectations, leading to uncertainties in, for example, local oscillator power for mixers, efficiencies of multipliers, laser output power, and various other conversion processes, such as photomixing. Further, the submillimeter field is maturing to a state where customers expect better standards than any one company can provide. While the market is currently small, it is growing, and practical applications for THz technology are increasing. Some of the power measurement problems in the submillimeter region are summarized in Figure 1.

Table 1. Spread in Measured Power as a Function of Frequency

Frequency (GHz)	Measurement Spread (dB)
94	±0.5
200	±1
300	±2
500	±3-4

The inability to measure voltage standing wave ratios (VSWR) is particularly difficult because of the mismatch on the source and the detector. It is the biggest and most prevelant reason why power in the submm region is not measured accurately. The inability to make swept measurements is the main reason for this, because problems would clearly be seen with the ripple in the measurements. Very narrow-band spot measurements done with lasers do not give enough information. The frequency range is very large, and it is very hard to imagine a power sensor that would work well over more than a decade. The load sensitivity of particular laser sources is also a problem, as tiny reflections can cause widely fluctuating coupled output power. Reflections on the order of as little as 1% back into the beam can cause changes in output power by a factor of two. The situation with other output sources is not as bad, but even in the case of frequency multipliers the output match can be quite poor. Without isolators, it is going to be hard to get much accuracy unless the sensor is perfect.

There are advantages and disadvantages to several types of power sensors, including waveguide-mounted sensors (waveguide calorimeters, waveguide thermistors or thermocouples, and diode detectors), and quasi-optical devices, such as quasi-optical laser power meters (thermopiles), acoustic wave sensors, pyroelectric sensors, and thin-film bolometers, all of which have possible nonuniform absorption characteristics. These are summarized in Table 2. Based on these advantages and disadvantages, it is just a matter of choice to pick one and improve it to make it as standard device.

Table 2. Characteristics of Available Power Sensors

Waveguide-mounted Devices	Advantages	Disadvantages
Waveguide calorimeter	• can be extremely well-matched (with careful design) • fairly easy to calibrate with DC heating	• tends to be slow (30 sec time constant) • tends to be insensitive (>50 μW reliably detectable power)
Waveguide thermistor or thermocouple	• fairly sensitive (5μW)	• narrow bandwidth (some are quite wide, but only by "accident") • rapidly varying VSWR (not often well-matched)
Diode detector	• very sensitive, with slowly varying VSWR	• not very linear • difficult to calibrate
Quasi-optical Devices		
Quasi-optical laser power meter (thermopile)	• no modulation needed	• slow and very insensitive (>0.5 mW) • uses optical black absorber, poor in submm region
Acoustic wave sensor	• fairly sensitive (5μW) • large area (3 cm square)	• requires modulation • thin-film absorber with inherently poor match
Pyroelectric sensor	• extremely sensitive (nW)	• requires modulation, thin-film absorber • small area (3-5 mm diameter)
Thin-film bolometer	• fairly sensitive • small area (1 cm sq, max)	• requires modulation, thin-film absorber

NOTE: All quasi-optical devices have possible nonuniform absorption.

The waveguide calorimeter has potential as an ideal general purpose sensor throughout the submillimeter region. The main problems of speed and drift can be improved by careful design if some of the accuracy inherent in calorimeters can be sacrificed. It is more important to get down to a 10 μW measurement level and a time constant of less than 10 s at an uncertainty of few percent, than to try to achieve an almost impossible dream of 0.5% uncertainty at these low power levels. Several characteristics of such an improved calorimeter can be defined.

- Drift level should be < 2 μW

- Time constant should be < 10 sec

- As the time constant is proportional to the product of sensor mass, C_v, and thermal resistance, a low mass sensor is to be preferred to minimize the time constant.

- As the responsivity ($\Delta T/\Delta P$) is proportional to the thermal resistance, it should be easy to make the responsivity high by increasing the thermal resistance of the sensor to the thermal ground.

- Two matched sensors are required to make a well balanced device. If one is the sensor the other one is a dummy which is mechanically and thermally identical. If one gets heated, the other one is used to track the drift in the system. A null measurement can be made to improve the accuracy.

- The lower limit to measurable temperature is set by the thermal isolation of the elements and the match in the drift of the two sensors.

- The VSWR must be very low for accurate measurements of poorly matched sources. With a source VSWR of at least 3:1 and a sensor VSWR of 1.1:1, the measurement uncertainty would be on the order of 4%.

We have built a prototype calorimeter, intended for use from 80 GHz - 1 THz. Its characteristics are as follows:

- It is based on a WR-10 waveguide input.

- It uses platinum resistance thermometer sensors because they are linear and available in small sizes.

- The absorber is made of thin-slab of ferrite, 0.5 mm thick, which has high absorption and low mass.

- It uses a thin-wall (75 μm) stainless steel waveguide, fabricated by chemical etching,

- The design, diagramed in Figure 2, has a measured VSWR of < 1.1:1 at 80 GHz, with about a fraction of a percent reflection coefficient. Presumably, it gets better at higher frequencies, but there is no way of knowing its behavior at THz frequencies.

- The noise and drift between sensors is about 0.7 mK rms.

- It has a responsivity of 100 K/W, and the drift is 7 μW rms.

- The drift can be reduced with better insulation; a 2 μW goal seems achievable.

- The time constant is 7 s, and a and fully settled measurement is possible in 20 s, or about 3 time constants.

The problem of coupling to quasi-optical sources exists. Not that many of modes of a quasi-optical source will couple into a single mode waveguide of WR-10 size. Therefore, for quasi-optical sources the waveguide losses are uncertain. One could use feed

horns. But they are reflective unless they are tapered slowly and loss gets higher if tapered too slowly.

This is a modest attempt to build a standard sensor, but NIST involvement could result in production of a much better device.

Shortly after this conference, Erickson reported the completion of a second calorimeter. Its drift level was 0.1 mK, with responsivity of 380 K/W, resulting in a power drift of approximately 0.3 μW rms. The time constant was 20 s. The general construction was identical to the first version, except more refined.

Far Infrared Absolute Spectrophotometer (FIRAS)

John Mather A47-A51
NASA Goddard Space Flight Center

An excellent example of the development of well-characterized, standardized, and calibrated measurement tools is provided by the FIRAS instrument, flown on the Cosmic Background Explorer (COBE) satellite. The FIRAS instrument was designed to compare the cosmic microwave background to an accurate blackbody to provide information about the earliest epochs in the history of the observable universe as a test of the Big Bang Theory of cosmology.

FIRAS is a polarizing Michelson interferometer, as diagramed in Figure 1. It is intrinsically a differential device, matching observation against a blackbody. Radiation enters the sky horn and is focused by a collimating concentrator (a Winston cone, or a compound paraboloid concentrator). The instrument is calibrated by an essentially perfect blackbody, which can be pivoted to fill the sky horn's full field of view. Measurements demonstrate that the blackbody has at least a -45 dB reflection coefficient. This is a multi-mode quasi-optical device at millimeter wavelengths. The aperture diameter of the horn is 30 cm. After collimation, the radiation is fed to two wire grid polarizing beam splitters (with concomitant delay), and then recombined to obtain an interference pattern. A separate input reference blackbody allows operation in differential fashion. The result of the beam splitting and polarization is that the device acts as an ordinary differential interferometer, with two inputs and two outputs.

The blackbody calibrator is diagramed in Figure 2. The cone angle of the re-entrant cone is about 25°. From a quasi-optical standpoint, this means that the receiver sees multiple bounces. It takes 7 bounces for specular light (which is negligible) to get out. The calibrator is made of iron-loaded epoxy (Ecosorb CR-110), kept isothermal to within 1 mK, operating at liquid He temperatures (1.5 K). Heating elements allow the temperature of the device to be varied over the range 2 K to over 20 K.

The mirror transport mechanism is based on a parallelogram linkage, as shown in Figure 3. The flex pivots are leaf springs in a barrel, and are available from Bendix. They are excellent substitutes for ball bearings at low temperatures, require no lubrication, and do not wear out. The carriage moves smoothly in an arc, driven by a magnet in a coil driven by a power amplifier; there is a feedback loop from the velocity sensor. In order to determine when to take an interferogram and monitor the mirror positions, there is a 20 μm pitch grating anchored to the mirror translation bar, with a fiber optic light pipes on one side and a spherical mirror on the other. Light is

sent through the fiber optic cables to the top mirror; the reflected light is detected after passing through the grating in each direction. A sinusoidal signal is seen as the grating moves back and forth; there is a mark on the grating to indicate when to start taking data.

We use a bolometer detector, using a 7.8 mm diameter diamond blackened by chromium-gold alloy; it suspended on two tensioned Kevlar threads. Diamond is used for its low heat capacity (C_v). A heavily doped silicon chip is used as a thermometer; at low temperatures the chip acts as a temperature-sensitive resistor. The device can detect 10^{-14} W in one second. While the reflection coefficient is not low, compensation is possible because the device is embedded in the larger spectrometer, and may be dealt with as part of the calibration process.

A sample interferogram is shown in Figure 4. In order to null the sky signal, the temperature of the internal reference body was tuned to establish this null, as shown in the top curve. To start the calibration process, the temperature of the internal reference body was raised by 12 mK, with results as shown in the middle curve where a negative-going signal is found. The external calibrator was then substituted for the sky, generating the bottom curve. Based on these three interferograms alone, we were able to conclude that the sky has a black body spectrum to within 1%.

The four orders of magnitude sensitivity and exacting accuracy that we were able to obtain derives from painstaking calibration of the instrument, as outlined in Figure 5. Many calibration-related effects had to be addressed, including:

- bolometer gain (9 parameters, $< 1\%$)
- instrument emission (6 sources)
- coherent vibrations (< 1 μm)
- frequency scale shift ($<0.5\%$) (from C^+ emission line at 157 μm)
- thermometer drift (5 mK, 60 days)
- multipass harmonics (2X, 3X, $< 1\%$)
- random thermometer errors (0.25 mK @ 2.7 K)
- general temperature shift (7 mK)
- random peak position shift (< 1 µm)
- decaying smooth spectrum offset (<0.1%, 60 days)
- additional drifts from sky data (<0.1%)
- comparison of detectors and modes (<0.1%)

These procedures produced measurements that demonstrated that no deviation between the observed cosmos and a blackbody curve at 2.726 ± 0.01 K, as shown in Figure 6. There is no deviation found at <0.03% of peak from 0.5 mm to 5 mm, thereby confirming the Big Bang Theory.

Generalizing the technique, we conclude that with a quasi-optical system, where one can ignore waveguide effects and coherent phenomena, one can make averages over spectral bands and multiple modes, and thereby achieve greater accuracy than is possible with single-mode systems. While this is not surprising, our results show that such techniques are indeed practicable.

Laboratory Spectroscopy in the THz Region

Geoff Blake A52-A65
California Institute of Technology

Far infrared applications in chemistry, biology, and astrophysics require widely tunable instruments with high spectral resolution and very high sensitivity, close to the quantum limit. For example, the need for rotational and vibrational spectroscopy in atmospheric chemistry and astrophysics is demonstrated in Figure 1, showing the 30 K blackbody spectrum, with several lines superimposed. Both line width and line shape are important for such measurements. Line width requirements for heterodyne sources are very stringent in these applications. Space-qualified heterodyne receivers and oscillators up to 1.5 THz region are needed to cover ground-state *ortho* and *para* H_2O lines. THz measurements over a wider range are needed to examine diatomic molecules, and to measure rotational and vibrational eigenstates to get parameters necessary to fully understand molecular interactions in chemistry and biochemistry, where bonds vibrate in the mid-IR (400 cm^{-1} - 4000 cm^{-1}). FIR measurements would allow characterization of heavier molecules or weaker bonds, such as are found within and between proteins. Such interactions are key to the pharmaceutical industry, where quantitative structure modeling is used in the rational design of new drugs. Given the dependence of such modeling on input energies for interactions, it becomes of paramount importance that reliable values be made available. For example, instruments that cover the range from 40 cm^{-1} to 400 cm^{-1} are necessary to characterize the energies generated in the interaction between H_2O and CO.

Fourier transform spectrometers that can address such requirements exist, but their very design leads to some operational problems. As diagramed in Figure 2, an input supersonic jet with random three-dimensional motion is converted into a uniform flow by expansion through a slit; the average translational temperature in the bulk frame is only a few Kelvin, so collisions are soft, and molecules tend to cluster. We use argon as the base gas where as many others use helium. Laser irradiation orthogonal to the slit examines molecules that show little or no Doppler broadening due to the expansion. Line widths are well under 1 MHz even at 30 cm^{-1} - 40 cm^{-1}, as shown in Figure 3, for a measurement at 456 GHz for two HCl molecules. The power-to-noise ratio is about 1 part in 10^6 for 10 μW of light. A summary of the laser power necessary to obtain a minimum detectable fractional absorption of 1 part in 10^8 as a function of frequency is shown in Figure 4.

A practical demonstration of this technique is found in Figure 5. The CO_2 laser pumps an FIR laser, resulting in 10 - 100 mW output power, used as input to a rooftop GaAs diode mixer. The fixed-frequency FIR laser light is mixed with a tunable microwave source. Based on a simple Beer's Law relationship, power transmitted from the planar jet cell is measured at a liquid-helium-cooled detector as a function of microwave frequency. The challenge is to remove unwanted, fixed-frequency FIR light. This is accomplished through use of a silicon etalon.

This system can be used to describe the interaction between three H_2O molecules. The geometry of this system is shown in Figure 6, which represents the ground-state

of the trimer, with two protons up and one proton down. The protons can flip, but there are energetic barriers to such a process; the size of the spectral splitting in the spectrum indicates the height of that barrier. A sample spectrum is shown in Figure 7 for D_2O (which has the same molecular geometry as for the H_2O trimer, but is a slightly heavier molecule). The flipping motion of the unbonded proton is found at 41 cm^{-1}; each of the individual lines is split into a quartet. The scale bar in Figure 7 is 5 MHz. The noise scale with a 300 ms time constant is 2×10^{-6}, which includes 1 ppm of shot noise for 10 μW of power. Phase lockable controlled oscillators with 1 MHz line widths are necessary for these measurements. Figure 8 shows the spectra. The lowest mode is at $\Delta K = \pm 1$ as shown earlier. The next one, at $\Delta K = 0$ occurs at 250 cm^{-1} and has also been seen by researchers at Berkeley. These optically pumped FIR lasers put out 10 to 100 mW of power up to 150 cm^{-1}; the spectrometers give complete coverage from DC to 150 cm^{-1}. However, these clusters have lines above that. Photomixing allows access to those lines. Alan Pine and Rick Suenram at NIST and our group at Caltech have been working with Elliot Brown of MIT/Lincoln Laboratory to produce and use these devices. Brown's best devices have lifetimes of 150 fs, as shown in Figure 9. These are provided by low temperature GaAs which is grown at 200°C instead of growth at 600°C to 700°C. By constructing a somewhat more complicated structure than a simple dipole, i.e., by fabricating fingers on a substrate, biasing them, and irradiating with two lasers, electrons will flow to the terminals, and may be coupled to an antenna, as shown in Figure 10. A more recent version is shown in Figure 11; a typical measurement setup is shown diagrammatically in Figure 12, with a typical frequency response shown in Figure 13. The slower fall-off with frequency for the Spiral 2 (8 μm) device is clear. At the longest wavelengths, 25 mW of optical power produces 30 μW from the waveguide structure. There is something of an issue as to the actual power being produced by these devices. For spectroscopic purposes, 1 μW of power gives 1 part per million sensitivity, and these devices are good enough for that.

It is now even possible to replace the titanium-sapphire lasers with commercially available distributed Bragg reflector laser diodes, operating at 852 nm, which put out 100 mW for trapping studies (Figure 14). By keeping the size down, it is possible to build devices that can be flown in satellites and airplanes. In April 1995, these photomixers are scheduled to be flown on the Kuiper Airborne Observatory to do submillimeter astronomy, looking for ground-state oxygen at near-THz frequencies. In addition, a more miniaturized device is being designed to fly on the Perseus remotely piloted vehicle (Figure 15) and ER2 platforms to take stratospheric measurements on small scales (on the order of few hundred meters), to examine distributions of between ClO, HCl, H_2O, and HNO_3 These optical photomixers are broadband, have no mechanical tuners over the full bandwidth range from DC to 1.5 THz, and, in principle, can be interfaced to computers to allow complete control of instrument operation and data acquisition.

In line with the work reported by Geoff Blake for the generation of the THz radiation, there have been developments at NIST and in Germany. Richard Suenram, acting chief of the Molecular Physics

Division at NIST provided the following synopsis of that work.

A new technique for the generation of THz radiation has been developed by Alan Pine and coworkers at NIST, Gaithersburg in collaboration with Elliott Brown and coworkers at MIT's Lincoln Laboratory, in Boston. Lincoln Laboratory has fabricated a new low-temperature grown GaAs device which acts as an ultrafast photomixer. Alan Pine has incorporated this device into a new broad-banded, THz spectrometer using two narrow linewidth (1 MHz) dye lasers. The spectrometer operates by focusing the output of the two dye lasers onto the ultrafast photomixer. The output of the photomixer is the difference frequency between the two dye lasers. Thus by holding one dye laser fixed in frequency and tuning the frequency of the second, a broad-banded, tunable output in the far infrared spectral region is obtained. The output power is passed through an absorption cell containing the compound of interest and the radiation detected by a helium cooled bolometer. At the present time this new spectrometer has been used to obtain high resolution spectral data from 150 GHz to 1 THz.

Elliott Brown and coworkers have fabricated newer devices that should operate to 4 THz. Current work at NIST is focusing on implementing solid state diode lasers as pump sources for the ultrafast photomixer devices. Once the line widths of the diode laser sources have been reduced to <1MHz and suitable locking schemes developed, efforts toward computerizing and making the new instrument "user friendly" will be implemented.

A second type of THz spectrometer has been developed by scientists in Germany in collaboration with scientists in Russia. During the cold war, the USSR had a large program in the development of backward wave oscillator (BWO) technology. Recently these tubes have been made available commercially on the Western markets. These electron tubes produce milliwatts of radiation in the spectral region from below 100 GHz to over 1.5 THz. These two groups of scientists working together have developed a phase-locked BWO system that is capable of computerized scanning over frequency windows up to approximately 1 GHz bandwidth. In these systems the high frequency tube is phase locked to a lower frequency synthesizer-driven BWO. This synthesizer driven system is computer controlled so that precise high-resolution scans can be obtained. Typically the THz radiation passes through an absorption cell containing the gas of interest and the radiation is then detected by a fast InSb cryogenically cooled detector.

Characterization of Material Properties at Terahertz Frequencies

Robert H. Giles A66-A71
Submillimeter Technology Laboratory
University of Massachusetts, Lowell

In the realm of material science, terahertz frequency measurement systems provide significant utility in the characterization of material properties. With support primarily from the U.S. Army National Ground Intelligence Center (NGIC), Submillimeter Technology Laboratory (STL) researchers have been advancing the field of terahertz

technology to the application of modeling millimeter-wave and microwave radar for more than a decade [1]. Research in modeling radar requires design of a wide range of measurements systems using current sub-millimeter-wave source/detector technology, establishment of precise calibration standards, production of high-fidelity scale replicas of complex metallic structures, and scaling of millimeter-wave dielectric properties of composites at submillimeter-wave frequencies. This paper explores four measurement techniques typically employed by STL to perform the characterization of materials:

(1) laser-based submillimeter-wave ellipsometry;
(2) high-precision reflectometry;
(3) laser-based Brewster's angle measurements; and
(4) FIR Fourier transform spectroscopy (FTS).

While trade-offs exist between precision and ease of implementation, each technique provides unique capabilities. As the most precise method of measuring a material's submillimeter-wave optical properties, laser-based ellipsometry can measure the extinction coefficient to a precision of a few percent and has the advantage of being able to evaluate opaque as well as transparent materials. High-precision submillimeter-wave reflectometry allows reflectivity measurements to an uncertainty of 0.1%. Laser-based Brewster's angle measurements, while not highly precise, allow rapid determination of dielectric constants for lossy materials based solely on front-surface reflectivity; and FIR Fourier transform spectro-scopy (FTS) allows one to characterize the optical properties of materials as a function of frequency.

Laser-Based Submillimeter-Wave Ellipsometry

Ellipsometry determines material optical properties by measuring a change in the reflected polarization state from the sample. By knowing the incident polarization state and measuring the reflected polarization state as a function of several incident angles, it is possible to derive a material's refractive index (n) and extinction coefficient (k) [2]. Using a mathemat-ical representation developed by D.A. Holmes [3], the STL research team designed six quartz quarter-wave retardation plates (QWPs) to analyze the reflected polarization state at six specific frequencies covering 500 GHz to 2.5 THz.

Shown schematically in Figure 1, the submillimeter-wave ellipsometry technique implemented by STL [4] relies on a QWP analyzer whose incident angle is adjusted until its relative phase shift is $\pi/2$. As originally suggested by Oldham [5], the tilted QWP analyzer can then transform the sample's reflected radiation from some unknown elliptical state, χ_{ref}, to a linear state. The orientation of the linear state is made known via the high-speed rotating linear polarizer. The data on the angular orientation of the QWP and the linear state are reduced via equations 1, and the reflected polarization state from the material is inferred. [1]

$$\chi_{ref} = \frac{E_s}{E_p} = f(\alpha, \theta, t_r) \text{ where } |\chi_{ref}| = \frac{1 + t_r^2 \tan^2\alpha \tan^2(\alpha+\theta)}{\tan^2\alpha + t^2 \tan^2(\alpha+\theta)}$$

$$\text{and } \phi_{ref} = \phi_p - \phi_s = -t_r(\cot\alpha + \tan\alpha)\tan(\alpha+\theta)$$

The reflected state also depends upon the transmissivity ratio of the ordinary (s) and extraordinary (p) components in the birefringent QWP. Taking this ratio and using the fundamental equation of ellipsometry [2], equa. 2, one can determine the amplitude and phase ratio between the s and p components. The automated system is shown in Figure 2. Since the radiation is modulated via the rotating linear polarizer, a two-phase lock-in amplifier is used to demodulate the signal to determine the orientation of the linearly polarized state created between the QWP and the linear polarizer.

[2]

$$\frac{\chi_{inc}}{\chi_{ref}} = \frac{E_{s_i}}{E_{p_i}} \times \frac{E_{p_r}}{E_s} = \frac{R_p}{R_s} = \rho = \tan\psi e^{i\Delta}$$

Depicted in Figure 3 is calibration data from the ellipsometer, obtained using vertically polarized radiation. On the left is the demod-ulated intensity as a function of rotation of the QWP through 360°. The peaks with higher and lower amplitudes correspond to the ordinary and extra-ordinary axes of the QWP. The ratio between peaks is the transmissivity ratio for the QWP(t_r), which is dependent on the bire-fringence of the quartz QWP. By determining the orientation of the QWP for each peak (α) and measuring the phase using the two-phase lock-in amplifier (θ, see right hand graph of Figure 3), the unknown reflected polarization state from the sample can be calculated, equation 1.

As exemplified by Figure 4, STL's A.J. Gatesman was able to establish the submillimeter-wave optical properties of high-purity silicon by obtaining experimental data for a sample over a range of incident angles.[6] The refractive index and extinction coefficient of a material is determined by using them as variables in the Fresnel equations, and finding the best fit between experimental data and theoretical prediction (the continuous line in Figure 4). As shown in Table 1, the optical properties are obtained with very high precision and accuracy with the extinction and absorption coefficients given for a one cm sample thickness. Maximum uncertainities are $\Delta n \approx \pm 0.002$ and $\Delta k \approx \pm 0.0001$, however, the thickness and incident angle of the plate must be known to within ± 1 μm and $\pm 0.5°$, respectively.

Since the ellipsometric measurement technique relies only on the relative

Table 1. The SMW Ellipsometrically measured Optical Properties of Silicon

λ (μm)	ν (THz)	refractive index	extinction coeff	absorption coeff
117.72748	2.55	3.4162±0.0002	0.00007 ±0.00002	0.07±0.02
191.84803	1.56	3.4160±0.0002	0.00006±0.00003	0.04±0.02
236.6008	1.27	3.4164±0.002	0.00007±0.00004	0.04±0.02
513.0157	0.58	3.4164±0.002	$0.000004^{+0.00008}_{-0.00004}$	$0.01^{+0.02}_{-0.01}$

amplitude between the reflected s and p components and not the absolute reflectivity of the sample material, the variation in intensity of the incident laser radiation does not cause loss of accuracy. Silicon etalons could then be established as calibration reflection standards, based on the small uncertainties achieved in measuring their optical properties and by exploiting the low loss nature of the material. [7,8]

High-Precision Reflectometry

A.J. Gatesman used the silicon etalons as reflection standards when developing his high-precision submillimeter-wave reflectometer. [6,9] As STL's second method of characterizing materials, reflectometry was used to evaluate the high frequency performance of metals.[9] A block diagram of the optics and measurement components of the reflectometer are shown in Figure 5. To minimize standing wave problems as well as feedback to the laser, attenuators are inserted in the beam since the system's signal-to-noise ratio is sufficient to allow this. In staring mode, this system achieves reflectivity uncertainties on the order of $\pm 0.1\%$.

The largest difficulty in performing precise reflection measurements is maintaining alignment to the incident beam when samples and standards are interchanged. The sample fixture is designed to have spring-loaded samples and standards mounted against a precision ground flat surface to minimize alignment uncertainties. The sample stage is rotated with a 4 inch diameter air bearing to obtain interchangeability on the order of $\pm 0.03°$. As shown in Table 2, STL's submillimeter-wave reflectometer allows one to measure the differences in reflectivity of metals with $\pm 0.1\%$ uncertainty.

Table 2. The Submillimeter-Wave Reflectivity of Metals

Metal	R (0.58 THz)	R (2.55 THz)
Copper	0.997	*
Silver	0.994	0.995
Gold	0.994	0.994
Aluminum	0.995	0.994
Nickel	0.994	0.991
Chromium	0.993	0.974

Laser-Based Brewster's Angle Measurement Technique

For rapid determination of the submillimeter-wave optical properties of lossy materials, STL's researchers implemented a third measurement method which exploits the relationship between Brewster's angle, θ_B, and a material's refractive index (i.e., $n = \tan \theta_B$).[10] Shown in Figure 6, this optical arrangement measures a material's reflectivity from 0° to 85° incidence, monostatically. The transmitter and receiver remain fixed while rotating the dihedral sample mount. One face of the dihedral is a gold first surface mirror while the second surface is a vacuum chuck for quickly securing a sample.

The measured reflectivity data provides Brewster's angle, θ_B, to a precision of $\pm 0.1°$. While the accuracy of this system is no where near comparable to the two previously discussed systems, its optical configuration is simple to setup and measurements can be made rapidly. The

measured reflectivity of glass, acrylic, and polycarbonate are displayed in Figure 7. To evaluate the refractive index values given below, a curve fitting technique using the Fresnel reflection coefficient (p-wave) was applied to the reflectivity measurements. This technique is a relatively insensitive measure of a material's extinction coefficient, k.

Far-Infrared Fourier Transform Spectroscopy

As the fourth technique for measuring optical properties of materials, far-infrared Fourier transform spectroscopy (FIR FTS) enables one to characterize materials as a function of frequency. [11,12] As shown in Figure 8, transmission (and/or reflection) measure-ments are performed for a sample over the submillimeter wavelength region and the frequency dependent complex refractive index is ascertained using the Fresnel coefficient multiple reflection theory of etalons. Ultimately, determination of the refractive index, n, to an uncertainty of ± 0.01 is possible by either knowing the order of a fringe, m, using the expression: $n = m/(2 \cdot t \cdot \nu)$, or by the difference between the orders of two fringes, m_1 and m_2,

[3]

where $2 \cdot t \cdot n \cdot \nu_1 = m_1$ and $2 \cdot t \cdot n \cdot \nu_2 = m_2$
therefore $n = \Delta m/(2 \cdot t \cdot \Delta \nu)$.

The uncertainty in determining a material's refractive index by this technique is a function of the sample thickness, t, as well as the material's index of refraction.

Applications

STL's interest in materials research revolves about an effort in tailoring the dielectric properties of composite structures, or finding materials with optical properties at THz frequencies that simulate materials at milli-meter-wave or microwave frequencies. Based on measurements using the four characterization techniques, STL has developed a variety of artificial dielectric materials for bulk and thin film applications, and have tailored their optical properties for the fabrication of frequency-selective absorbing structures.[13] A variety of binders such as vinyl acetate, silicone, polyethylene, and epoxy resins have been loaded with powdered agents such as carbon, silicon, and stainless steel flake, in order to achieve the desired submillimeter-wave optical properties.

The optical properties of these powder loaded binders proved ideal for creating an anechoic layer on metal surfaces. As shown in Figure 9, a thin film provides the vehicle for which phase and amplitude matching of the incident electric field can occur. Calculation of the structure's optical behavior can be performed using the Fresnel equations. With a reflectivity of ≈ 1 for aluminum, the resonant structure's theoretical reflectivity is approximated as

$$R \sim \left| \frac{r + e^{-2i\beta}}{1 + re^{-2i\beta}} \right| \qquad [4]$$

$$\text{where } r = \frac{N-1}{N+1} \quad \text{and} \quad \beta = 2\pi t N / \lambda$$

are the thin film's front surface reflectivity and phase thickness, respectively.

As evident by equation 4, a phase thickness of a quarter wavelength will cause

destructive interference. If the amplitude of the electric field reflected from the quarter-wavelength thin film's front surface equals that of the back surface which suffers absorption, all the incident electric field is reflected back into the material and complete resonant absorption is estab-lished. A reflectivty null at the frequency of choice can be achieved by the proper choice of materials. STL's realization of the resonant structure using a vinyl acetate film loaded with stainless steel flake is illustrated in Figure 10.

Summary

In summary, the Submillimeter Technology Laboratory research staff has developed a complement of precision measurement systems specifically for evaluating the optical properties of materials at THz frequencies. STL has established the calibration standards for performing reflectivity measurements to a precision of $\pm 0.1\%$, developed a variety of artificial dielectric materials for bulk and thin film applications, and tailored their optical properties for the fabrication of frequency selective absorbing structures. All these techniques should prove eminently useful for further investigations of materials properties in the terahertz frequency regime.

Acknowledgements

Several colleagues at the University of Massachusetts Lowell's Submillimeter Technology Laboratory have made significant contributions to this work. In the early '80s, Dr. Jerry Waldman, while working at MIT Lincoln Laboratory, developed techniques for scaling millimeter-wave radar at submillimeter-wave frequencies. He moved the laboratory to Lowell in 1982 and developed a research group for designing measurement systems to acquire scaled radar data at terahertz frequencies. As the performance of these measurement systems improved, the fidelity of scaled replicas became a driving issue along with modeling the dielectric properties of composite materials. By the direction of W.E. Nixon, support to STL from the U.S. Army National Ground Intelligence Center diversified to encompass a wide range of materials research. Under support for this program the author received his Ph.D. for the design and fabrication of a submillimeter-wave ellipsometer and A.J. Gatesman received a Ph.D. for developing the high-precision reflectometer.

References

1. J. Waldman, H.R. Fetterman, W.D. Goodhue, T.G. Bryant, D.H. Temme; "Submillimeter Modeling of Millimeter Radar Systems," SPIE Proceedings on Millimeter Optics, Vol. 259, p.152 (1980).

2. R.J. Archer, "Determination of Properties of Films on Silicon by Method of Ellipsometry," Bell Sys. Tech. J., 1962.

3. D.A. Holmes, "Exact Theory of Retardation Plates," J. Opt. Soc. Am., Vol. 54, No. 9, September 1964, pgs. 1115-1120.

4. R.H. Giles, "Design of a Submillimeter Ellipsometer and Application to the Measurement of the Complex Indices of Refraction of Materials," Ph.D. Thesis,

University of Lowell, Lowell, Massachusetts, 1986.

5. W.G. Oldham, "Ellipsometry Using a Retardation Plate as Compensator," JOSA, Vol. 57, No. 5, 617, 1967.

6. A.J. Gatesman, "A High Precision Reflectometer for the Study of Optical Properties of Materials in the Submillimeter," Ph.D. Thesis University of Lowell, Lowell, Massachusetts, 1993.

7. D. Grischkowsky, et.al., "Far-Infrared Time-Domain Spectroscopy with Terahertz Beams of Dielectrics and Semiconductors," J. Opt. Soc., Am. B, Vol. 7, No. 10, October 1990.

8. T. Ohba and S. Ikawa, "Far-Infrared Absorption of Silicon Crystals," J. Appl. Phys., Vol. 64, No. 8, 15 October 1988, pgs. 4141-4143.

9. A.J. Gatesman, R.H. Giles and J. Waldman, "A High Precision Reflectometer for Submillimeter Wavelengths," JOSA B, Feb. 1995.

10. R.H. Giles, A.P. Ferdinand, J. Waldman, ULRF and W.E. Nixon, and W. Reinhold AFSTC: "Submillimeter Wavelength Modeling of Dielectric Materials in Polarimetric Radar Approaches," Proceedings of the NATO Advanced Research Workshop on Direct and Inverse Methods in Radar Polarimetry, Bad Windsheim, Federal Republic of Germany, September 1988.

11. A.J. Gatesman, R.H. Giles, G. Phillips, J. Waldman, University of Lowell, and L.P. Bourget, R.S. Post, ASTEX: "Far Infrared Spectroscopic Study of Diamond Films," Proc. of MRS Society, 162, 185 (1989).

12. R.H. Giles, A.J. Gatesman, and J. Waldman, "A Study of the Far-Infrared Optical Properties of Rexolite™," International Journal of Infrared and Millimeter Waves, 11, 1299 (1990).

13. R.H. Giles, A.J. Gatesman, J. Fitz-Gerald, S. Fisk and J. Waldman, "Tailoring Artificial Dielectric Materials at Terahertz Frequencies," The Fourth International Symposium on Space Terahertz Technology, April 1993, Los Angeles, CA.

Planar Antennas, Power Meters, and Calibration Techniques at Terahertz Frequencies

Gabriel M. Rebeiz **A72-A83**
Electrical Engineering/Computer Science Department
University of Michigan, Ann Arbor

The technology for the design and fabrication of planar antennas has matured considerably in recent years. However, techniques for planar antenna calibration at THz frequencies are still not easy to implement. Prediction of normalized antenna patterns, that is, patterns in different directions relative to one another, can be done very accurately. Because the metals used to fabricate these antennas do not change their conductivity to any significant degree with frequency, it is possible to design, calculate and model patterns at, for example, 40 GHz, and measure at 500 GHz and find good agreement.

Several planar antennas have been designed and built based on mature technologies, one of which is shown in Figure 1. This 256 channel array was built at the University of Michigan. The match between measured characteristics and theoretical performance, shown in Figure 2, is quite good. In most cases there is good quantitative fit; even where experimental values differ from theory, the qualitative fit is excellent. Designs for THz integrated reflector antennas, as shown in Figure 3, show extremely high gain (>30 dB) with very small size and show good coupling efficiency to Gaussian beams (84%), making them suitable for radiometric and communications applications. The match at 2.56 THz between measured and theoretical patterns is excellent, as shown in Figure 4, demonstrating the maturity of this technology. Several antenna types have been fabricated, including log periodic, double slot, double dipole, integrated horns, corner cubes, and more. In the realm of receiver technology, it is even possible to build an antenna integrated with a submicron Schottky diode, as shown in Figure 5; it was designed by the University of Michigan and built by the University of Virginia. Other examples are the dual slot antenna with an integrated Schottky diode fabricated at the University of Michigan, shown in Figure 6, and the 2.5 THz horn that was fabricated at the Appleton-Rutherford Laboratory, shown in Figure 7. The latter is a corrugated horn with a waveguide 25 μm to 50 μm in diameter, as shown in Figure 8.

To calibrate antenna gain, one must first determine antenna directivity, that is, how much *enhancement* is there in one direction *vs.* another direction. This is obtainable from the normalized pattern alone. It is important to have a good linear detector and to reduce the standing waves and losses in the measurement system. However, the following caveats should be noted: Full two-dimensional measurements should be performed, and radiation must be measured in the cross-polarization direction, since many antennas have as much as 10% of their power radiated in the cross-polarization direction. To fully characterize antennas with, e.g., 12 dB - 20 dB directivity, it is necessary to measure all side lobes and down to -30 dB; reflector-type antennas require measurements down to -40 dB or -50 dB. The measurements are easier with reflector-type antennas because there is a wider aperture, more available power, and more gain, thereby producing greater signal to be measured. Our laboratory finds agreement between theory and measure-ments at -30 dB at THz frequencies with no difficulty.

With a good analysis of directivity, it is now possible to address gain calibration. In its simplest form, gain is the product of losses and directivity. Losses have three origins: (1) mismatch losses (which can be severe), (2) mode losses on dielectric substrates because of field trapping inside the subshak; and, (3) resistive losses (usually small) in the antenna itself.

The most common approach calibration at low frequencies are the so-called the two-antenna and three-antenna methods, as shown in Figure 9. However, this does not work well at THz frequencies, for the reasons outlined in the Figure.

Another method is called the radio-metric method, with possibilities as diagramed in Figure 10. While it is difficult to calibrate the antenna alone this way, it is easy to

calibrate the antenna and mixer system, because the power at the load is well-known (but limited by the emissivity of the absorber) and the power in the calibrated IF chain is also well-known. However, using this method, one cannot distinguish, for a 10 dB loss, whether the loss is, for example, 1 dB in the antenna and 9 dB in the mixer, or 5 dB in the antenna and 5 dB in the mixer, etc. This works well in receiver applications, as all that is required is to characterize the system conversion loss between the RF source and the IF port.

Figure 11 shows another method, called the plane wave method, that can be used with a calibrated plane wave power density from the source and a calibrated planar (bolometer) detector. However, in the case of detector calibration, impedance mismatches make it difficult to separate the antenna response from that of the power detector. In good design, the mismatch losses are typically less than 10%.

To calibrate power density, several years ago we constructed a THz power meter, as shown in Figure 12. The silicon nitride film is very thin. The total thickness of the silicon nitride film with silicon dioxide on either side is less than 1.4 microns. The key factor for its excellent performance is that the absorbing layer is many wavelengths (λ) long (in this case, $>2\lambda$), and therefore the system can be represented by a transmission line equivalent circuit, as shown. Its performance can be modeled and calibrated in reference to standards. This worked well from 500 GHz to 2.5 THz. Beyond 3 THz the transmittance of the bismuth layer is not well known; therefore, it could not be used as a calibrated detector.

In summary, the art of designing and fabricating planar antennas has advanced well, and their normalized patterns can be predicted with reasonable accuracy. In principle, it is possible to characterize (calibrate) the gain of planar antennas at THz frequencies. However, different calibration methods present different problems, and have different areas of usefulness.

Optoelectronic Measurement Techniques

Harold Fetterman **A84-A98**
Electrical Engineering Department
University of California, Los Angeles

The focus of this presentation is first to address picosecond measurements, and second, what NIST could do in regards to problems people are encountering in performing such measurements. The outline of the presentation is shown in Figure 1. Superconductivity will be mentioned as one of the application areas. The presentation will address the importance of mixing and mode locked systems. Finally the presentation will focus on how this field should link up with optics. It is not merely a question of using optics to create THz frequencies; it is more important to put THz signals on optical frequencies and transmit them. If you look at the dispersion at 1.3 μm, which is the fiber optic communications channel, it is flat over 2 THz. Therefore, THz signals can be put on optical signals and make use of the bandwidth to package information. Developing standards and techniques for this to happen will be very important to make this field commercially viable.

Regarding picosecond pulse measurements, our approach is to put picosecond pulses on devices for testing purposes; we do this at extremely high frequencies. The basic tools for our approach, diagramed in Figure 2, allow us to put an electrical pulse into a device and examine its impulse response by sampling the output. The instrumentation and tools necessary to such measurements include a beam generation device (based on a coupled Nd:YAG mode-locked frequency-doubled laser), whose output is fed to a picosecond dye laser. After suitable beam splits to provide input to, e.g., autocorrelators and choppers, the sampling beam and generation beam are fed through lenses to a closed-cycle helium refrigerator containing the device under test and Austin type optical switches, allowing measurements as a function of temperature. The switches used are simply damaged silicon, and show useful frequency response to 250 GHz. One can make them faster by making them smaller to reduce capacitance limitations. We close the first optical switch to generate the impulse, and the sampling beam closes the second switch to examine the pulse after it goes through the device, as shown in Figure 3. The sample beam can be suitably time-delayed to account for the transit time through the device. The devices are wire-bonded, as we are unable to make them monolithic. This wire bonding introduces inductance, which is the major limitation people in this field face in going to high frequencies with this technique. Monolithic devices are possible, however,as Dwight Striet has made a new series of FETs that are supposed to work up to 350 GHz. It would be nice to be able to measure them.

An example of the utility of this technique is shown in Figure 4, which shows the current gain of an AlInAs/GaInAs HEMT device as a function of frequency, obtained by Fourier analysis of the input and output electrical pulses. This particular device was thought to work at 150 GHz; the data shows the actual cutoff at 100 GHz. This cutoff is caused by the inductance due to the wire bond. The mode at about 60 GHz is also due to the wire bond. We compared amplitude and phase data for this device as obtained with our technique and with other available techniques (e.g., a Hewlett Packard network analyzer [NWA]). We found that the NWA shows ripple, whereas the optical technique is smooth from 75 GHz to 100 GHz (data not shown). We have used this technique to characterize AlGaAs/GaAs heterojunction bipolar transistors (HBTs) at 20 K and 300 K, as well. HBTs can be extremely fast, but we cannot measure them beyond 100 GHz due to the inductance in the wire bond. Character-ization by a professional laboratory (like NIST) would help to address this problem.

This technique has application in characterizations that reveal information about fundamental physics phenomena. One example is the case of superconducting delay lines. Sample data for delay time as a function of input current are shown in Figure 5; the temperature dependence of the device is shown in Figure 6. The phenomena being measured here are amenable to analysis from fundamental physical principles. As shown in Figure 7, the measured response shows a better fit to a $(T/T_c)^2$ relationship rather than $(T/T_c)^4$, as predicted by S-wave pairing of the BCS model. This indicates that either D-wave pairing or other factors are at work in high-T_c superconductors, and that a "straight" BCS model is inadequate to describe the phenomena observed here.

In order to address the limitations of the wire-bonding technique, as described above, one recently developed technique includes the use of contactless optoelectronic coupling, as shown in Figure 8, so that the device is not wire-bonded. Electro-optic material is placed in proximity to the output line of the device being examined, and the resultant electric field is measured. We are just beginning to do these measurements. There is a fundamental calibration problem in these measurements, and there is no reproducibility from laboratory to laboratory. Refinements to this technique obviate the need for an external optoelectronic material: It is now possible to irradiate with a laser using coplanar guides or microstrip lines and measure changes in optoelectronic coefficients. This works well on the output side, but the input still requires wire-bonding. Another variation of this technique allows for sampling at THz frequencies, as shown in Figure 9, and as Dan Grischkowsky described earlier in this meeting. Additional refinements allow for direct irradiation of a device without intermediate switches (thereby bypassing any input parasitics), and subsequent monitoring of the output. Such techniques demonstrate that some HBTs have fast response times, on the order of 10 ps. HEMT devices may be similarly characterized, but their underlying physics makes the task more difficult to interpret. These devices are very fast. They can be made to generate high frequencies, as diagramed in Figure 10. This produces a stable, low power output at 60 GHz, as shown in Figure 11. However, this arrangement occupies an entire table top. This approach is further refined (and miniaturized) by using a mode-locked laser shown in Figure 12. In using these mode-locked lasers you are not mixing lasers, but rather use the devices as opto-electronic oscillators, in this case at 830 nm. It is also a transit time device, with the optical wave oscillating 65 GHz. As shown in Figure 13, this laser light is input to the HBT; the resulting radiated output is at 65.12 GHz with a 3 dB line width of < 500 kHz, DC optical gain of about 10, and a power conversion efficiency of 0.01%. Mode-locked lasers are not, however, tunable. The HBT can be operated as a three terminal device; putting current on the base one can generate side bands, as shown in Figure 14. In other words, one could put information on it, and move the side bands accordingly. As noted previously, these laser sources are now available up to 350 GHz or more.

One way to integrate the capabilities afforded by these high-speed devices, lasers, and assorted optoelectronic components is through the use of optical wave propagation in polyimide channels (waveguides), fabricated as shown in Figure 15. The capability to make polyimide waveguides allows us to produce directly on a chip substrate complex structures like delay lines, power splitters and repetition multipliers etc., as shown in Figure 16. What it is still lacking in this scheme is a modulator. However, recently we have been able to find electro-optical polymers that have dyes that will have responses out to 200 GHz. Figure 17 shows a schematic of this device. We could examine its response up to 40 GHz using a heterodyne setup shown in Figure 18. Mixing the output from two stable diode-pumped YAG lasers allows for heterodyne detection of the modulated signal up to some 100 GHz.

These approaches allow us to design electro-optical communication devices containing multiple channels on small

wafers, as diagramed in Figure 19. The output from two lasers is mixed in various MMIC-like devices that provide amplification and that radiate. Phase information is applied by such materials as the polymer modulators described above; amplitude information may be similarly applied by Mach Zender interferometers. Optical interconnection to other systems would be possible as shown in the Figure. A futuristic vision of the possibility for optical communication using THz technology is shown in Figure 20.

Based on our work, we can draw some conclusions, as shown in Figure 21. Optical testing requires standards. Picosecond techniques using high-power optoelectronic sources is the method of choice. But methods to measure this power are needed, and reproducibility is a major problem. We need standards to intercompare. Understanding how to interconnect systems and make measurements to get some reproducibility is something that NIST could address. Furthermore, characterization of the mixing process and related techniques are areas that could be addressed by NIST.

We should pursue these new application areas in communications to make our field commercially viable. The breakthrough is that light and THz frequencies can be combined to form systems for communications. In the next decade, sophisticated systems, like local area networks, etc., will emply the results of research and development in these application areas.

Round Table Discussion

As a lead-in to the round-table discussion, Neil Erickson of Millitech Corporation, as an industry representative, was asked to provide some information about the current market trend for millimeter and submillimeter components and full systems. Figures 1 and 2 show the summary in bulletized form. Based on his perspective from the commercial sector, Erickson summarized what NIST could offer to industry, as shown in Figure 3.

Using these suggestions as a jumping-off point, the Discussions chairman, Dr. Richard Harris, Chief, Cryoelectronic Metrology Division, NIST (Boulder), opened the floor for discussion by requesting that members of the three major participating groups—industry, academia, and government—tabulate what they each felt were suitable areas for NIST to address. Much discussion ensued, with key points recorded for later analysis. Topics raised included:

- support for biotechnology analysis and synthesis;
- THz modulation of optical communication;
- FTIR systems;
- industrial applications, including imaging for aircraft landing, volcanic SO_2, collision avoidance, and contraband detection;

- frequency measurements and phase noise;
- tools for high frequency measurements, (e.g., sampling, vector network analyzers);
- calibration round-robins;
- spatial measurements of antenna characteristics;
- provision of standard reference materials;
- source comparisons;
- standard attenuators;
- environmental monitoring;
- phased arrays for mapping;
- generation of standards for absolute power;
- calibrated sources;
- optical properties of materials; and
- instruments to support process monitoring in several industries.

After discussion of the relative merits of each of these suggestions, and some extended debate over NIST's proper role with specific reference to its charter, a vote was taken to determine which of the above areas should most properly be addressed by NIST. The attendees at the workshop (excluding NIST staff) were asked to vote. The most votes (in descending order) were for NIST to:

- ***take an active role in the measurement, evaluation, and dissemination of optical properties of materials* (16);**
- ***provide absolute power standards* (9 for single mode, 6 for multimode);**
- ***provide tools for frequency measurements* (5);**
- ***provide standard reference materials* (4); and**
- ***provide calibrated sources* (4).**

Several other topics received less than four votes. NIST's participation in collaborative efforts was discussed, as was its potential role in forming the nucleus of such efforts.

The attendees expressed great pleasure in the format and outcome of the workshop, and look forward to further meetings of this sort as industry, academia, and government organizations move further into the THz realm.

Appendix I
Organizing Committee

NIST WORKSHOP
"Metrology Issues in Terahertz Physics and Technology"

December 13, 1994
National Institute of Standards and Technology (NIST)
Gaithersburg, MD 20899

Dr. Charles Clark, Chief	Electron and Optical Physics Division, NIST (Gaithersburg)
Dr. Richard Suenram, Acting Chief	Molecular Physics Division, NIST (Gaithersburg)
Dr. Kenneth Evenson	Time and Frequency Division, NIST (Boulder)
Dr. Fred Walls	Time and Frequency Division, NIST (Boulder)
Dr. Leo Hollberg	Time and Frequency Division, NIST (Boulder)
Prof. Dennis Drew	Department of Physics, University of Maryland at College Park
Prof. Venky Venkatesan	Center for Superconductivity, University of Maryland at College Park
Dr. David Rudman	Cryoelectronic Metrology Group, NIST (Boulder)
Dr. Erich Grossman	Cryoelectronic Metrology Group, NIST (Boulder)
Dr. Raju Datla, Group Leader	Infrared Radiometry Group, NIST (Gaithersburg)

Appendix II
Program

NIST WORKSHOP - December 13, 1994
Metrology Issues in Terahertz Physics and Technology

Agenda with tentative titles

8:00 - 8:30	Welcome Workshop Introduction, Prior NIST Work and Future Possibilities	Raju Datla, NIST Erich Grossman, NIST
A. Applications Overviews (Chairman: Charles Clark, NIST)		
8:30 - 9:10	THz Atmospheric Science and Astronomy	Peter Siegel, JPL
9:10 - 9:50	Commercial Applications of THz Technology	Richard Huegenin, Millitech
9:50 - 10:30	Applications of Synchrotron and FEL as THz sources	Larry Carr, Grumman Jim Allen, UC Santa Barbara
10:30 - 10:50	BREAK	
10:50 - 11:30	THz MIMIC Applications	Dwight Streit, TRW
11:30 - 12:00	THz Applications in Atmospheric Sensing	Kelly Chance, Harvard Smithsonian
12:00 - 12:30	Femtosecond THz Beam Generation and Applications	Daniel Grischkowsky, Oklahoma State Univ.
12:30 - 1:30	LUNCH	
B. Specific Measurement Areas (Chairman: Kenneth Evenson, NIST)		
1:30 - 1:50	Absolute Power Measurement - A	Neil Erickson, Millitech
1:50 - 2:10	Absolute Power Measurement - B	John Mather, GSFC
2:10 - 2:30	Molecular Spectroscopy via optical photomixing	Geoff Blake, Caltech
2:30 - 2:50	Materials Properties Measurement	Bob Giles, U of Mass. at Lowell
2:50 - 3:10	Antenna Efficiency, Spatial Beam Measurement	Gabriel Rebeiz, U. of Michigan
3:10 - 3:30	Optoelectronic Measurement Techniques	Harold Fetterman, UCLA
3:30 - 3:45	BREAK	

C. Round-table Discussion (Chairman: Richard Harris, NIST)

Who Needs to Measure What?
What should be NIST's role - New Facilities/ Standards/ Collaborations ?

3:45 - 6:00 Total Power
- Materials Properties
- Spatial Distributions (Amplitude, Phase)
- Frequency, Frequency Tunability and Stability, Spectral Purity
- Other

6:00 End of Meeting

7:00 - 10:00 Reception/Dinner

Appendix III
Attendees

S. James Allen
University of California
Center for Free-Electron Laser Studies
Santa Barbara, CA 93106-5100
Phone: (805) 893-7134
Fax: (805) 893-4170
email:allen@sbfell.physics.ucsb.edu

Steven M. Anlage
University of Maryland
College Park, Maryland, U.S.A. 20742-4111
Phone: (301) 405-7321
Fax: (301) 314-9541
email:anlage@squid.umd.edu

Dr. Geoffrey Blake
California Institute of Technology
Div. of Geological & Planetary
Sciences 170-25
Pasadena, California 91125
Phone: (818) 395-8372
Fax: (818) 568-0935

Peter John Burke
Yale University
15 Prospect St.
New Haven, CT 06520
Phone: (203) 432-4275
Fax: (203) 432-4283
email: burkep@minerva.cis.yale.edu

G. Lawrence Carr
Grumman Corporate Research Center
Bethpage, New York 11714-3580
Phone: (516) 346-9073
Fax: (516) 346-3670

Dr. Kelly V. Chance
Smithsonian Astrophysical Observatory
60 Garden St.
Cambridge, MA 02138
Phone(617) 495-7389
FTS: 830-7389
Telex: 921428 Satellite Cam
email:kelly@cfa.harvard.edu

Thomas W. Crowe
University of Virginia
Charlottesville, YA 22903-2442
Phone: (804) 924-7693
Fax: (804) 924-8818
email: twc8u@virginia.edu

Dr. Raju V. Datla
NIST
Building 221, Room B208
Gaithersburg, MD 20899
Phone: (301) 975-2131
Fax: (301) 869-5700
email: rdatla@micf.nist.gov

H. Dennis Drew
University of Maryland
Physics
College Park, MD 20904
Phone: (301) 405-6146

Daniel J. Dummer
Radiometric Physics Division
Bldg. 221, Rm. A207
Gaithersburg, MD 20899
Phone: (301) 975-2381
Fax: (301) 869-5700
email: dummer@garnet.nist.gov

Franklin J. Dunmore
Department of Physics
University of Maryland
College Park, MD 20742-4111
Phone: (301) 405-7278, Lab (301) 405-6160
Fax: (301) 314-9465
email: fdl3@umail.umd.edu

Neal Erickson
Millitech & University of Massachusetts
P.O. Box 109
S. Deerfield, Massachusetts 01373
Phone:(413)665-8551 or (413)545-1873 Fax:
(413) 545-4223
email: neal@ferao1.phast.umass.edu

Harold R. Fetterman
UCLA
405 Hilgard Avenue
Los Angeles, California 90024- 1594
Phone: (310) 825-3431
Lab (310) 825-2734
Fax: (310) 206-9497
email: fetter@ee.ucla.edu

Dr. Dennis S. Friday
NIST
325 Broadway
Boulder, CO 80303-3328
Phone: (303) 497-5395
Fax:(303)497-3956
Internet: friday@bldrdoc.gov

Dr. Robert H. Giles
University of Massachusetts Lowell
450 Aiken St.
Lowell, MA 01854
Phone: (508) 458-3807
Fax: (508) 452-3333

Daniel R. Grischkowsky
Oklahoma State University
202 Engineering South
Stillwater, Oklahoma 74078
Phone: (405) 744-6622
Fax:(405)744-7554
email: grischd@master.ceat.okstate.edu

Erich N. Grossman
NIST -ANXC 814.03
325 Broadway
Boulder, CO 80303-3328

Richard E. Harris
NIST
325 Broadway
Div. 814.00
Boulder, CO 80303-3328
Phone: (303) 497-3776
Fax: (303) 497-3042
email: harris@cmg.ceee.nist.gov

Mitchell K. Hobish
5606 Rockspring Road
Baltimore, MD 21209
Phone: (410) 466-0994
Fax: (410) 466-8530

Dr. John C. Mather
NASA, Goddard Space Flight Center
Greenbelt,Maryland 20771
Phone: (301) 286-8720
Fax: (301) 286-1617
email: mather@stars.gsfc.nasa.gov

Robert J. Mattauch
University of Virginia, Thorton Hall
Charlottesville, VA 22903-2442
Phone: (804) 924-6112
Fax: (804) 924-8818

Jian Mao
University of Maryland
Dept. of Physics
College Park, Maryland 20742
Phone: (301) 405-7670
email: jml71@umail.umd.edu

John Franklin Mayo-Wells
NIST
MET, Rm.B358
Gaithersburg, MD 20899
Phone: (301) 975-2220
Fax: (301) 975-4091
email: mayowell@eeel.nist.gov

David Osterman
Hypres, Inc.
175 Clearbrook Road
Elmsford, NY 10523
Phone: (914) 592-1190 ext. 7818
Fax: (914) 347-2239

Albert C. Parr
NIST, Radiometric Physics Division
Bldg. 220, Rm. A319
Gaithersburg, Maryland 20899
Phone: (301) 975-2316
Fax: (301) 840-8551
email: parr@enh.nist.gov

Nicholas G. Paulter
NIST - Bldg. 220, Rm. B162
Gaithersburg, MD 20899
Phone: (301) 975-2405
Fax: (301) 926-3972

Michael S. Pambianchi
University of Maryland
College Park, Maryland 20742
Phone: (301) 405-7932
Fax: (301) 314-9541
email: mike@squid.umd.edu

Shing-Kuo Pan
National Radio Astronomy Observatory
2015 Ivy Road, Ste. 219
Charlottesville, VA 22903-1733
Phone: (804) 296-0262
Fax: (804) 296-0324
email: span2@nrao.edu

Ronald M. Powell
NIST Bldg. 220, Rm. B358
Gaithersburg, Maryland 20899
Phone: (301) 975-2223
Fax: (301) 975-4091
email: powellrm@eeel.nist.gov

Gabriel M. Rebeiz
University of Michigan
3238 EECS Bldg.
1301 Beal Avenue
Ann Arbor, MI 48109-2122
Phone: (313) 747-1793
Fax: (313) 747-2106

David H. Reitze
University of Florida
215 Williamson Hall
P.O. Box 118440
Gainsville,FL 32611-8440
Phone: (904) 392-3582
Fax: (904) 392-0524
email: reitze@phys.ufl.edu

Curt A. Richter
NIST
Bldg. 225, Rm. A305
Gaithersburg, MD 20899
Phone: (301) 975-2082
Fax: (301) 948-4081
email: richter@sed.eeel.nist.gov

Raphael P. Robertazzi
Hypres, Inc.
175 Clearbrook Road
Elmsford, NY 10523
Phone: (914) 592-1190 ext. 7813
Fax: (914) 347-2339

Eric Shirley
NIST
Bldg. 221, Rm. B208
Gaithersburg, Maryland 20899
Phone: (301) 975-2349
Fax: (301) 869-5700
email: shirley@molphys.nist.gov

Peter Siegel
JPL
M/S 168-314 4800 Oak Gr. Dr.
Pasadena, CA 91109
Phone: (818) 354-9089
Fax: (818) 393-4683
email: phs@merlin.jpl.nasa.gov

E. Stern
MIT LL
Box 73
Lexington, MA 01742
Phone: (617) 981-7808
email: stern@ll.mit.edu

Cha-Mei Tang
NIST
Bldg. 221, Rm. A141
Gaithersburg, Maryland 20899
Phone: (301) 975-4272
Fax: (301) 975-3038

Dr. Michael E. Thomas
John Hopkins University
Applied Physics Lab
Laurel, MD 20723
Phone: (301) 953-6000 X4414

Wen F. Tseng
NIST
Bldg. 225, Rm. A305
Gaithersburg, Maryland 20899
Phone: (301) 975-5291
Fax: (301) 948-4081
email: tseng@sed.eeel.nist.gov

Elza Vasconcellos
NIST-Boulder & Unichmp.Brazil
1250 18th St. Apt. 4
Boulder, CO 80302
Phone: (303) 497-3337
email: elza@central.bldrdoc.gov

T. (Venky) Venkatesan
Univeristy of Maryland
College Park, Maryland 20742-4111
Phone: (301) 405-7320
Fax: (301) 314-9541
Bitnet: venky@squid.umd.edu

J. M. Vrtilek
Harvard University
29 Oxford Street
Cambridge, MA 02138
Phone: (617) 495-0589
Fax: (617) 495-9837
Internet: jvrtilek@cfa.harvard.edu

John E. Walsh
Dartmouth College
6045 Wentworth Hall
Hanover,NH 03755-3526
Phone: (603) 646-1302
Fax: (603) 646-3488
email: john.walsh@dartmouth.edu

Dwight Wooland
Army Research Lab
ARL-EPSD
Fort Monmouth, NJ 07703
Phone: (908) 532-0593
Fax: (908) 544-4323
email: dwooland@arl.mil

Dong Ho Wu
Department of Physics
University of Maryland
College Park, Maryland 20742
Phone: (301) 405-7268
Fax: (301) 314-9541
email: dhwv@squid.umd.edu

Zhuomin Zhang
NIST
Bldg. 221, Rm. B208
Gaithersburg, Maryland 20899
Phone: (301) 975-2336
Fax: (301) 869-5700
email: zhuomin@garnet.nist.gov

Appendix IV
Preceeding Figures

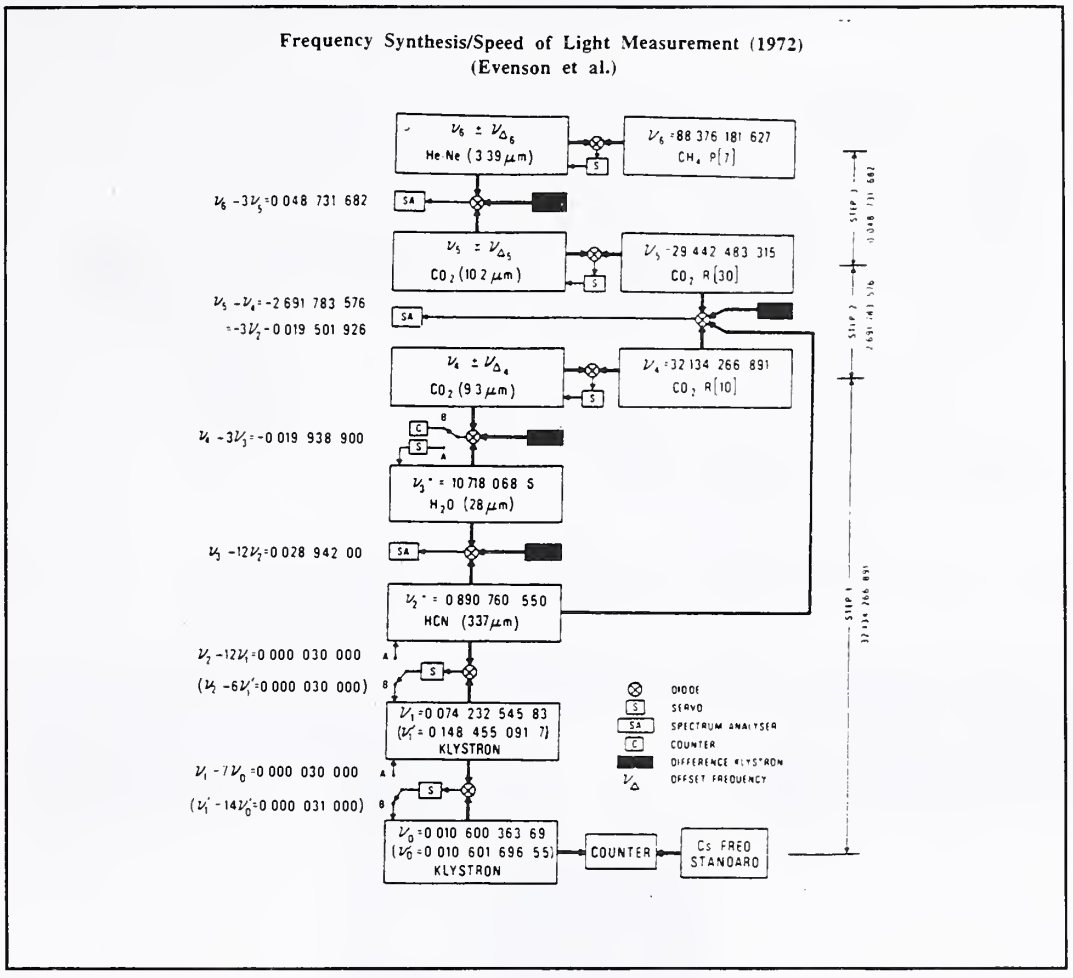

Figure 1. Stabilized laser frequency synthesis chain. All frequencies are given in THz; those marked with an asterisk were measured with a transfer laser oscillator tuned to approximate line center.

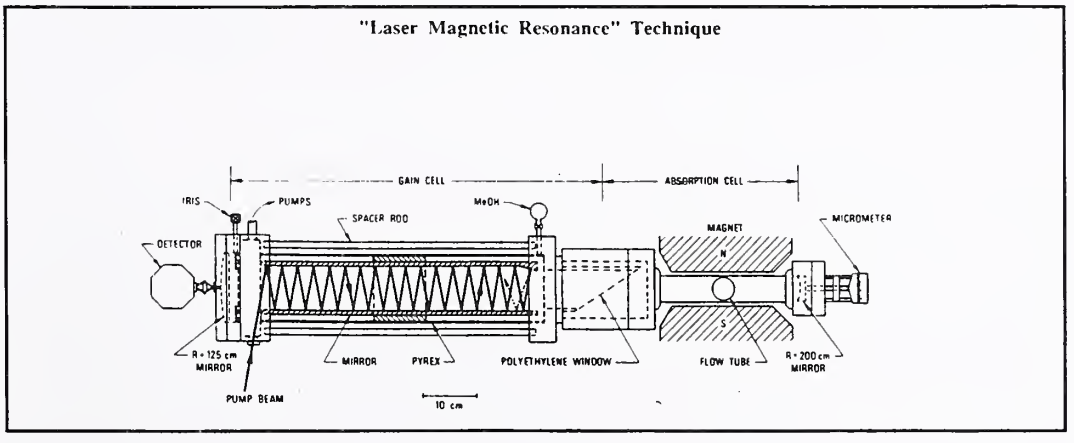

Figure 2. FIR optically pumped laser magnetic resonance spectrometer.

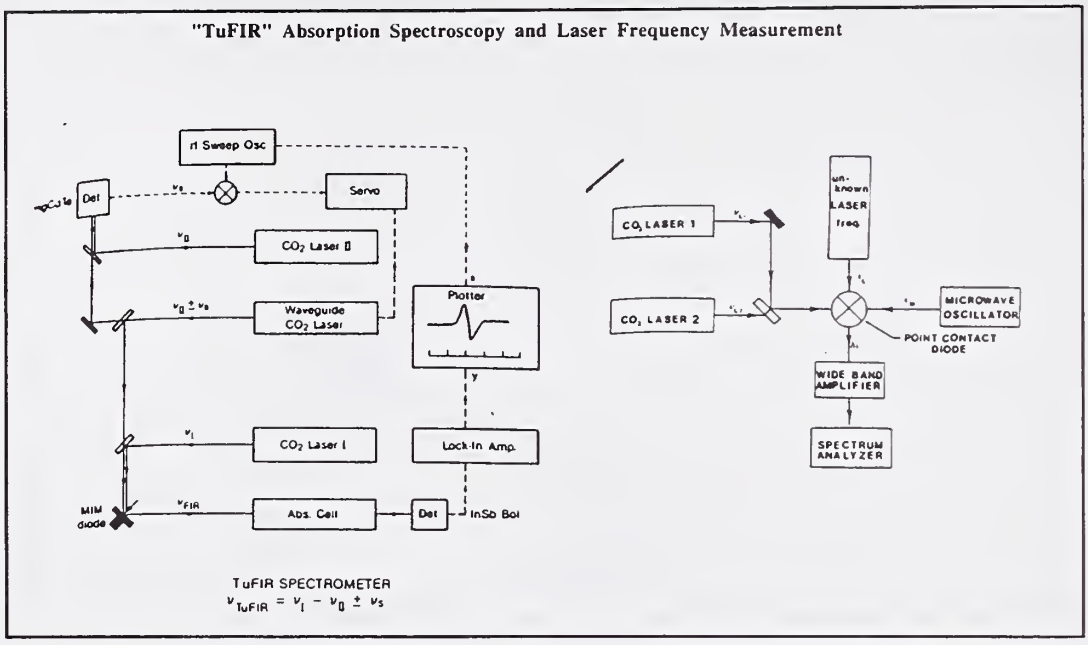

Figure 3. (left) Block diagram of TuFIR spectrometer. (right) Schematic diagram of the two CO_2 laser frequency synthesis experiment at the National Bureau of Standards, Boulder, CO. The frequencies of the two CO_2 laser ν_{L1} and ν_{L2}, the frequency ν_M of the microwave oscillator, and the unknown laser frequency ν_L are fed into a point contact MIM diode used as a harmonic generator mixer, and the beat frequency $\delta\nu$ is measured by means of a spectrum analyzer.

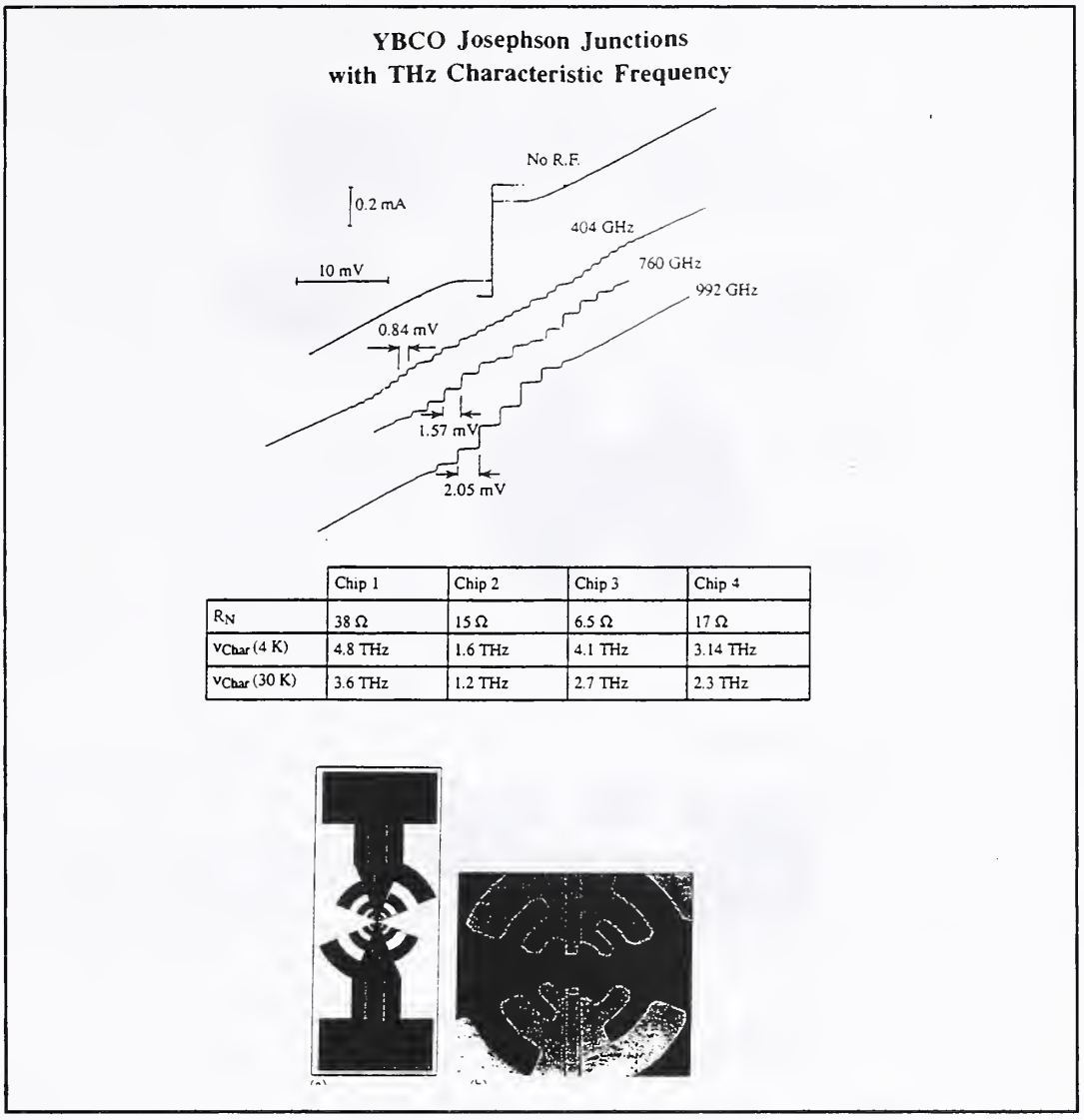

	Chip 1	Chip 2	Chip 3	Chip 4
R_N	38 Ω	15 Ω	6.5 Ω	17 Ω
ν_{Char} (4 K)	4.8 THz	1.6 THz	4.1 THz	3.14 THz
ν_{Char} (30 K)	3.6 THz	1.2 THz	2.7 THz	2.3 THz

Figure 4. YBCO Josephson Junctions with THz Characteristic Frequency

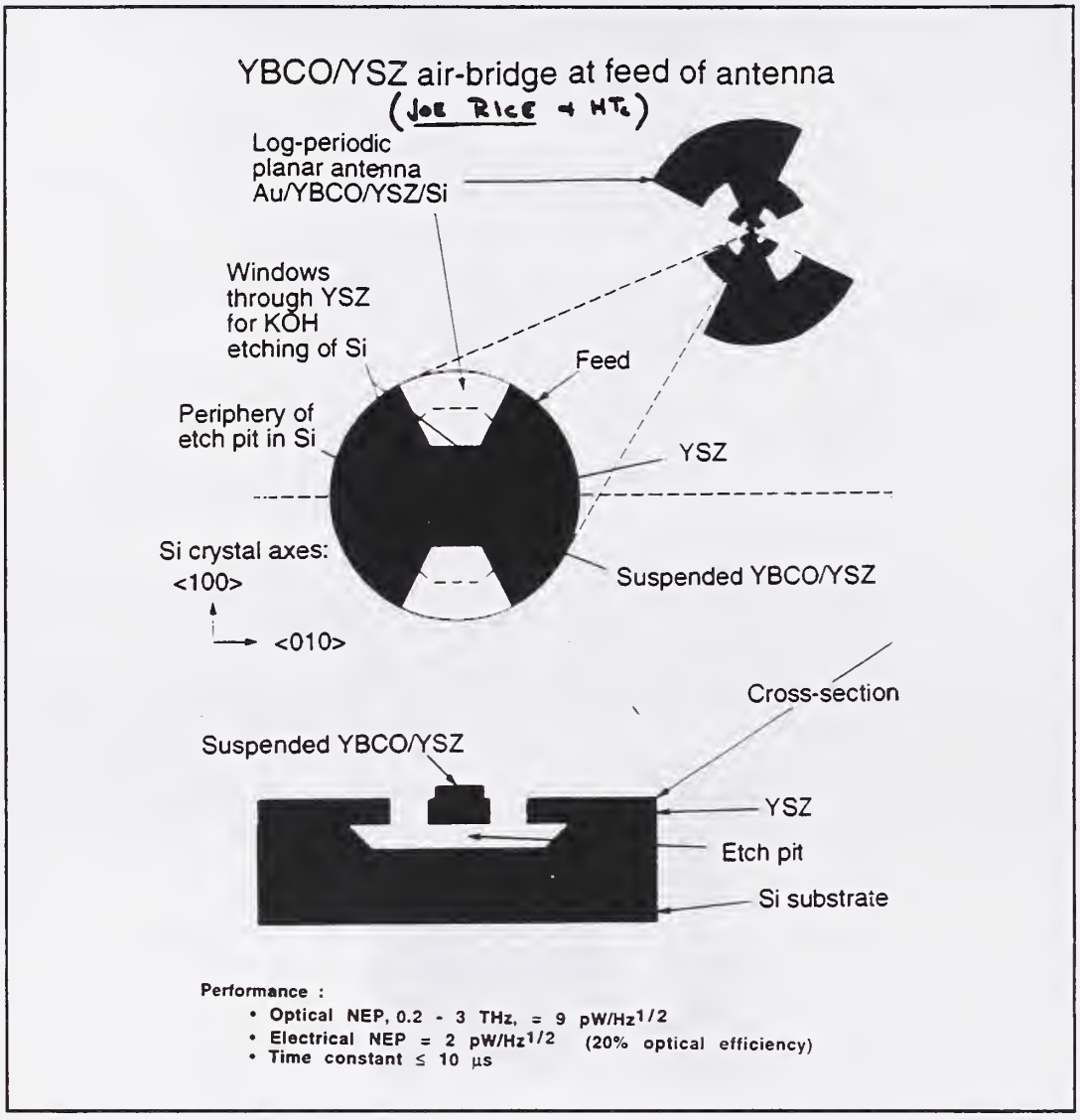

Figure 5. YBCO/YSZ air-bridge at feed of antenna

Some THz Metrology Issues

I. Absolute Power Measurement
- calibration of Scientech calorimeters (de-facto standard?)
- DC substitution and absorptance errors

II. Spatial Measurement
- beam "quality" and M^2
- antennas, (phase/intensity patterns, efficiencies)

III. Frequency-related Measurement
- reference frequencies, frequency synthesis
- spectral purity

IV. Materials Measurement
- optical constants (n,k) of bulk materials
- emittance/reflectance (diffuse and specular) of surfaces

V. Device Measurement

Figure 6. Some THz Metrology Issues

Definition of M^2, the ISO-9000 standard for beam quality

$$M^2 = \frac{\pi D_{0L}^2}{4\lambda(L_3 - L_1)}\left[\left(\frac{D_1}{D_{0L}}\right)^2 - 1\right]^{1/2}$$

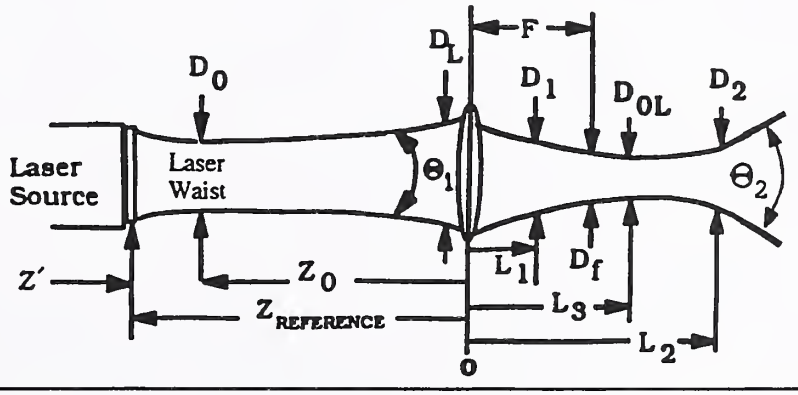

Figure 7. ISO definition of symbols used for laser beam spatial parameters [2].

Heterodyne Radiometry for Millimeter and Submillimeter-Wave Earth Remote Sensing

Peter Siegel & Joe Waters
Jet Propulsion Laboratory

Science Priorities Addressed by Millimeter- and Submillimeter-Wave Earth Remote Sensing

1. Stratospheric Ozone Chemistry
   Monitor ozone and key molecular species in all chemical cycles thought to be significant (radicals, reservoirs+, source gasesΨ)*
   O_3, (ClO, OH, BrO, HO_2), (HNO_3, HCl, HOCl)+, (H_2O, N_2O)Ψ*

2. Upper Tropospheric and Stratospheric Greenhouse Gases
   Measurement of chemical species thought to play a role in the transformation of greenhouse gases and in radiative forcing of climate change (H_2O, N_2O, O_3)

3. Measurement of Volcanic Pollutants in the Lower Stratosphere
   SO_2, HCl

4. Measurements through Ice Clouds and Aerosols
   Investigation of heterogeneous chemistry in the stratosphere

Figure 1

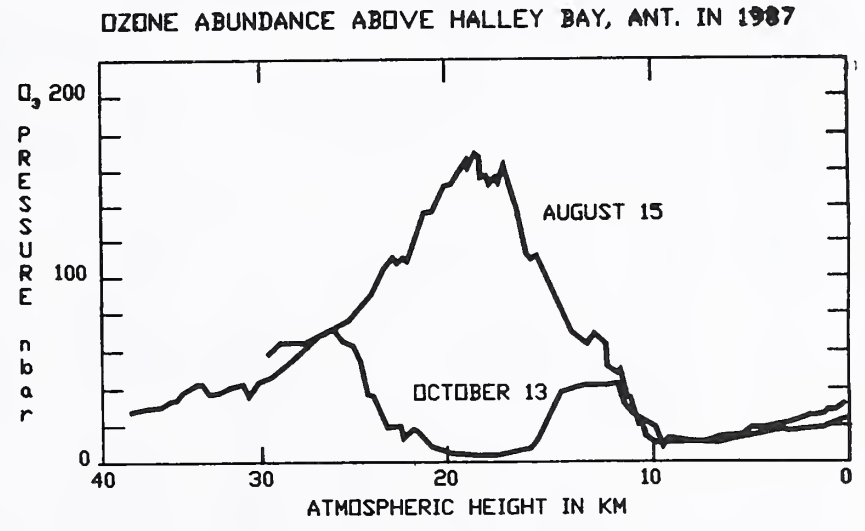

Figure 2

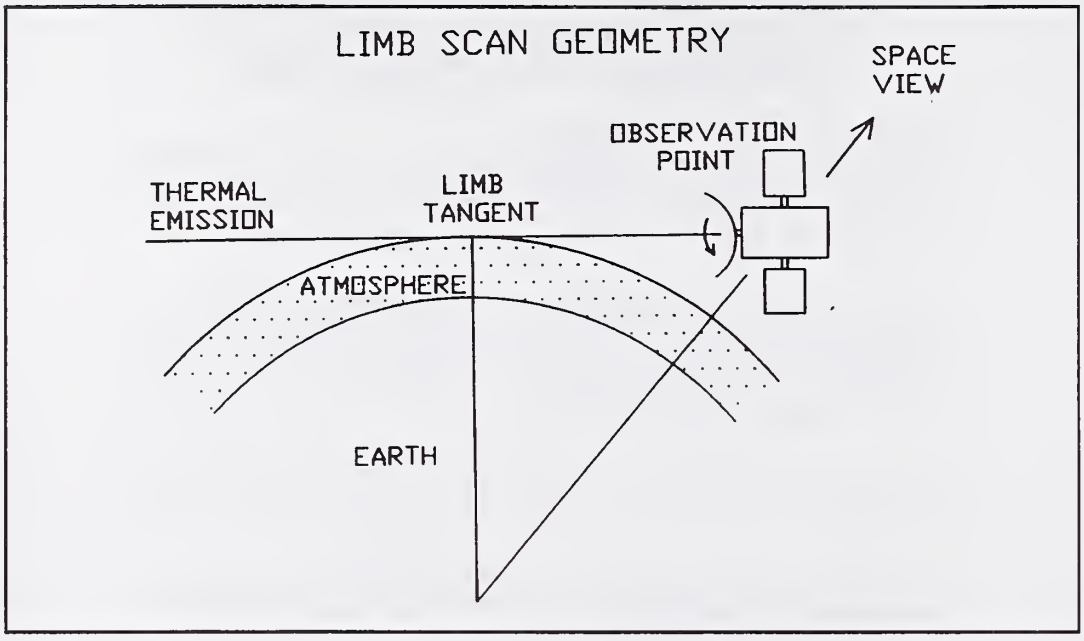

Figure 3

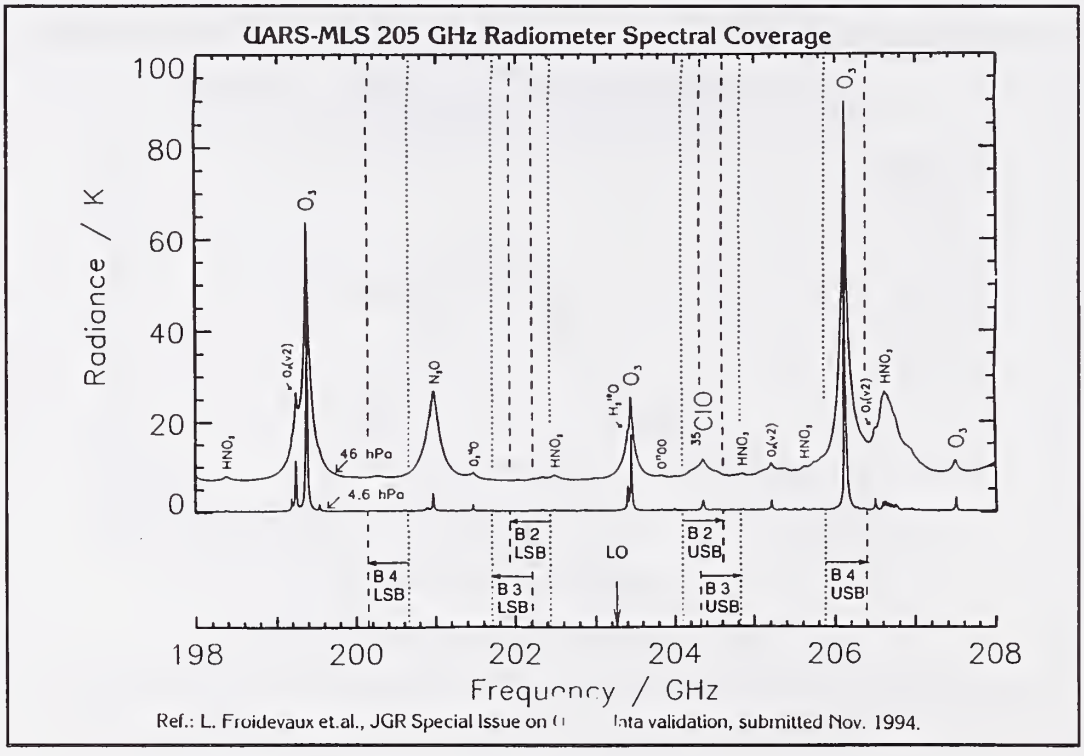

Figure 4

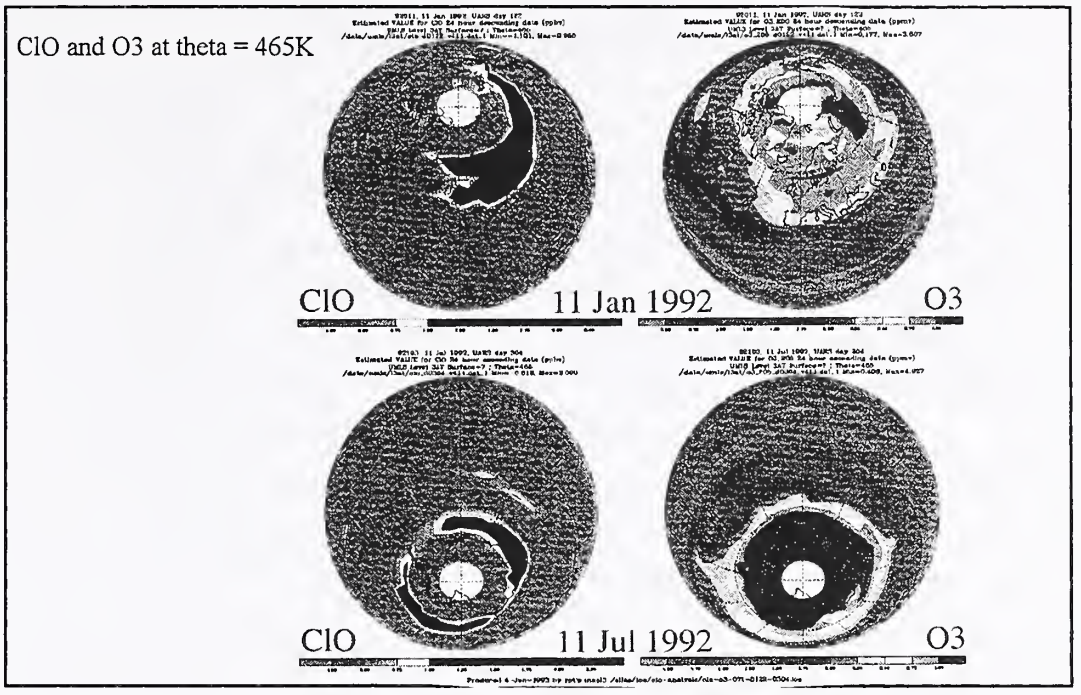

Figure 5

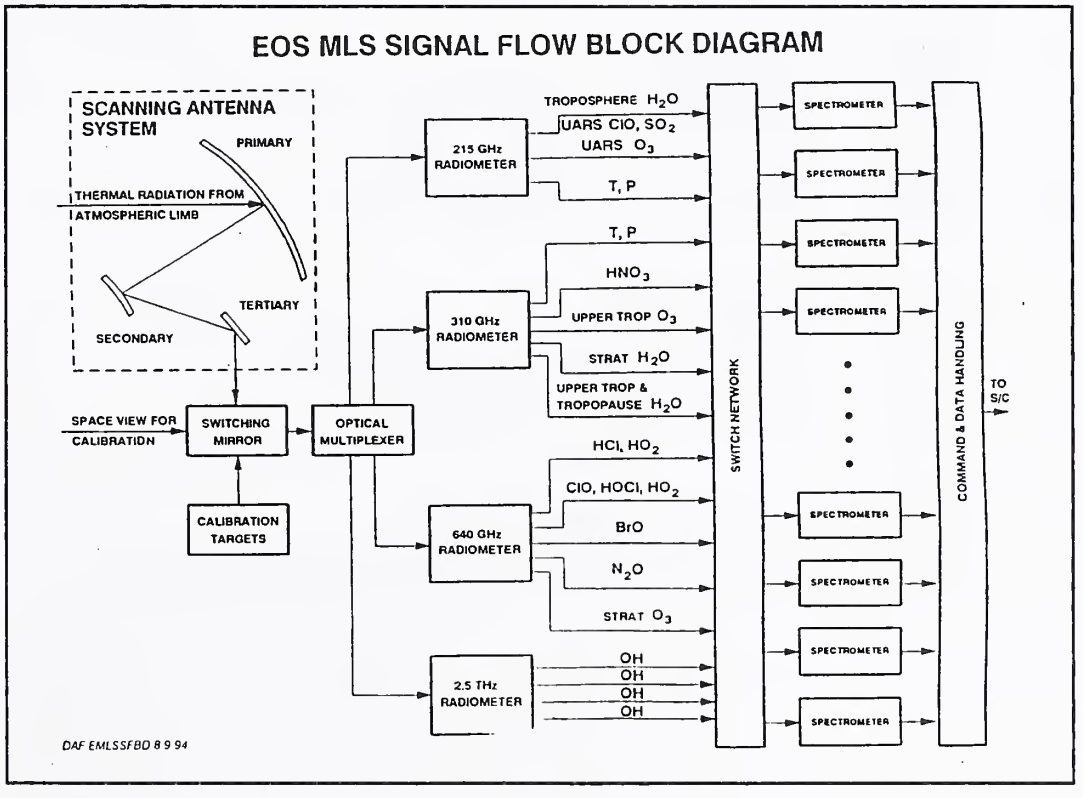

Figure 6

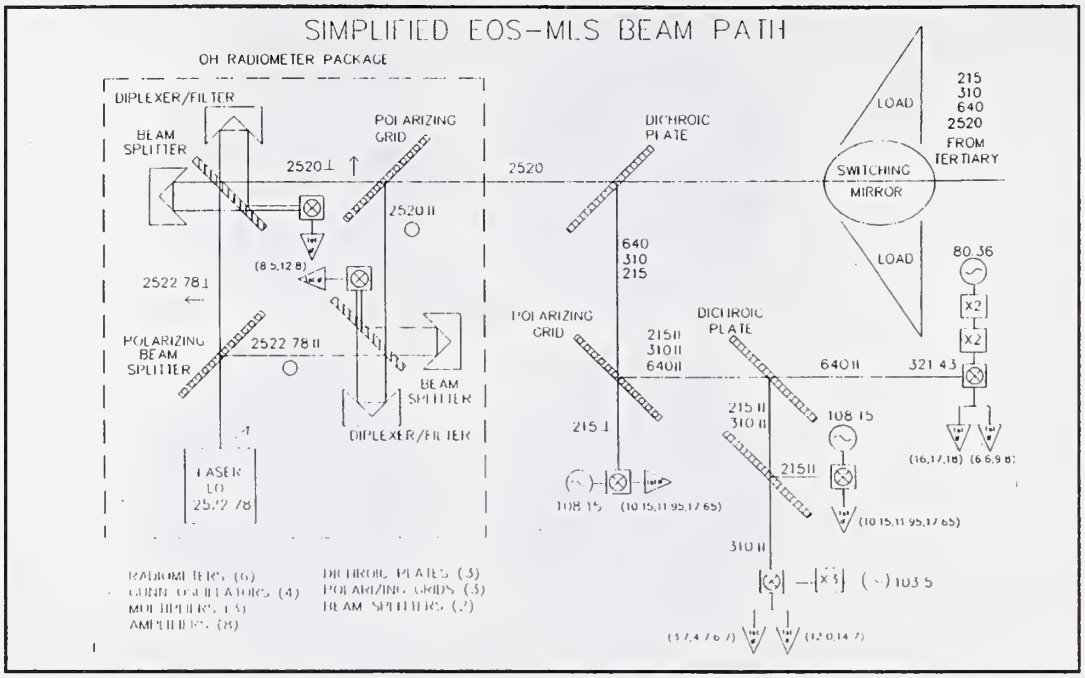

Figure 7

UARS-MLS 1980's technology:

Mixers:	Whisker-contacted Schottky diodes at 183 & 205 GHz
Loc. Osc.:	GaAs GUNN driving whisker-contacted varactor tripler
1st IF:	Discrete narrow band FET amplifiers
Diplexer:	Optical injection via Folded Fabry-Perot
Back-end:	Discrete component filter banks, variable channel width

EOS-MLS 1990's technology:

Mixers:	Planar-diode antiparallel-pair subharmonically pumped
Loc. Osc.:	InP GUNN driving planar-diode doublers
1st IF:	Broadband MMIC HEMT amplifiers in mixer blocks
Diplexer:	Waveguide injection internal to mixers
Back-end:	1 GHz wide, 1000 channel acousto-optic spectrometers?

Additional EOS-MLS 2000 technology for OH:

Mixers:	Open structure with integrated submicron diode for 2.5 THz
Loc.Osc.:	RF excited CO_2 laser pumping far IR methanol gas laser

Figure 8

Standards Used in EOS-MLS Measurements

For Radiance Calculations:

Spectral line shape vs. pressure/temperature
Emissivity of materials from 100 to 2520 GHz for Cal. Loads
Antenna Beam Patterns across all RF bands up to 2.5 THz
Spillover/Emissivity differences in Signal/Space View Paths
Absolute Frequency reference for removal of Doppler shift
Absolute Radiometric Sideband Calibration

For Instrument Design/Specifications

Absolute Power at Submillimeter Wavelengths
Absolute Frequency at Submillimeter Wavelengths
Black Body Emissivity/Equivalent Load Temperatures
Calibrated Spot Noise Temperature
Relative Sideband Response

Figure 9

THz Applications in Atmospheric Sensing

Kelly Chance
Harvard Smithsonian Institution

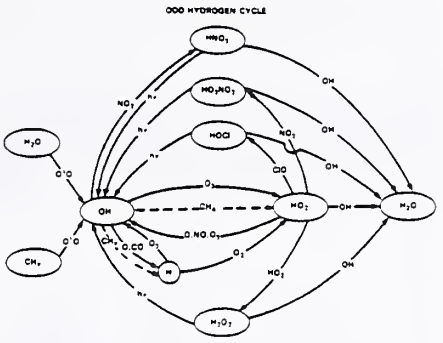

Schematic of the Odd-Hydrogen Cycle.

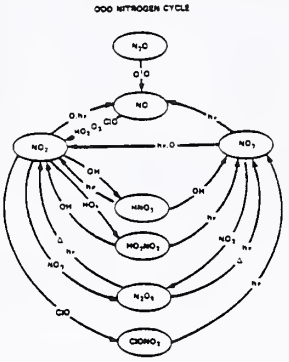

Schematic of the Odd-Nitrogen Cycle.

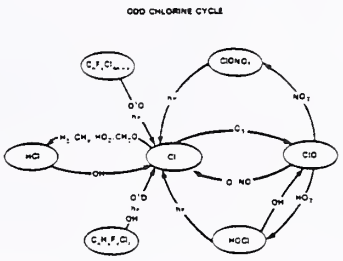

Schematic of the Odd-Chlorine Cycle

From *Present State of Knowledge of the Upper Atmosphere: An Assessment Report*, NASA Reference Publication 1162, 1986.

Figure 1

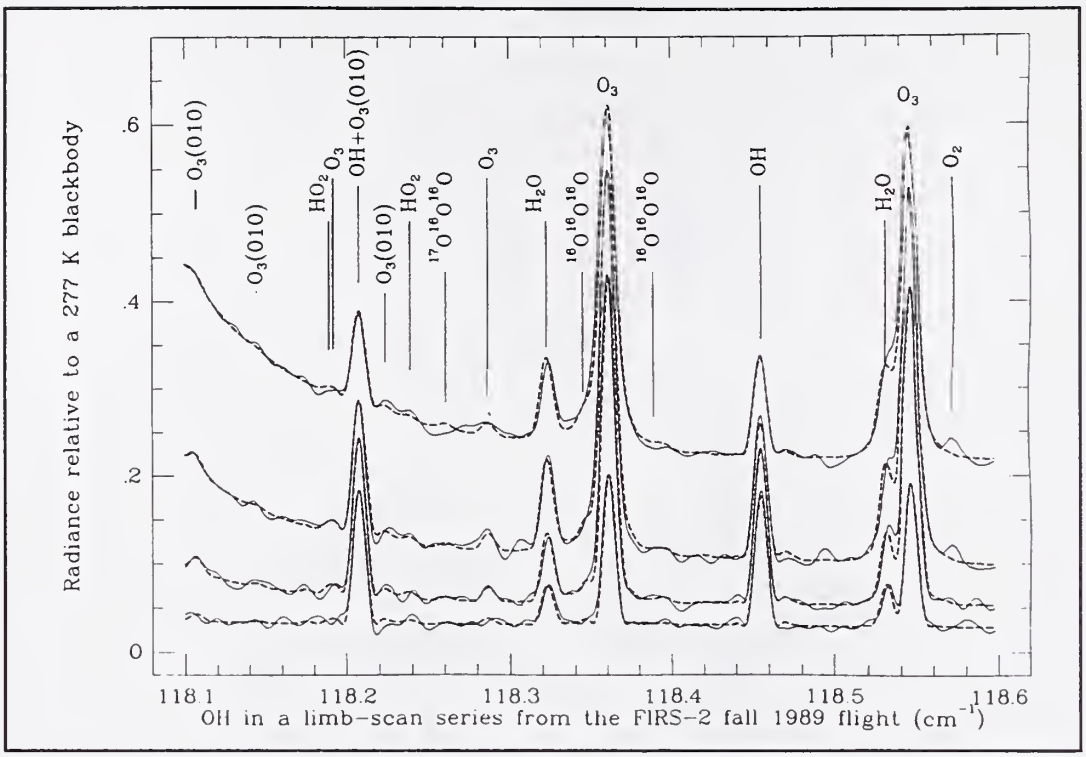

Figure 2

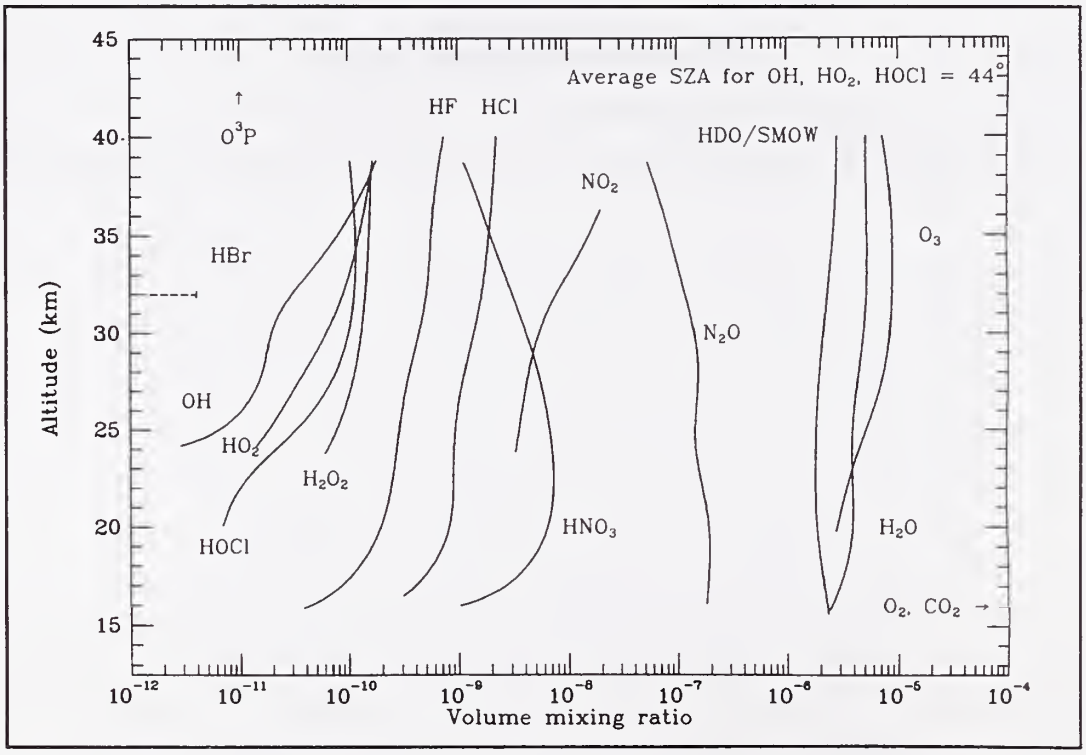

Figure 3

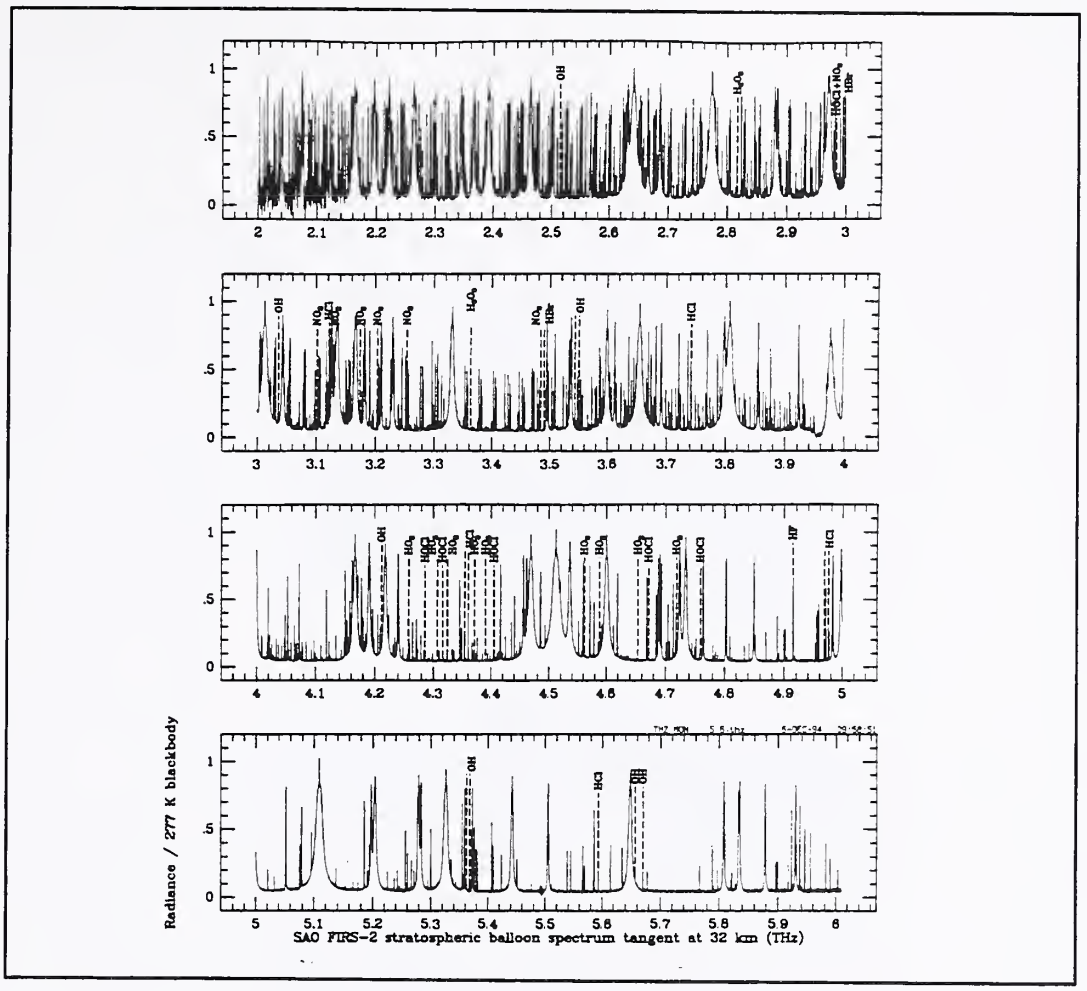
Radiance / 277 K blackbody
SAO FIRS-2 stratospheric balloon spectrum tangent at 32 km (THz)

Figure 4

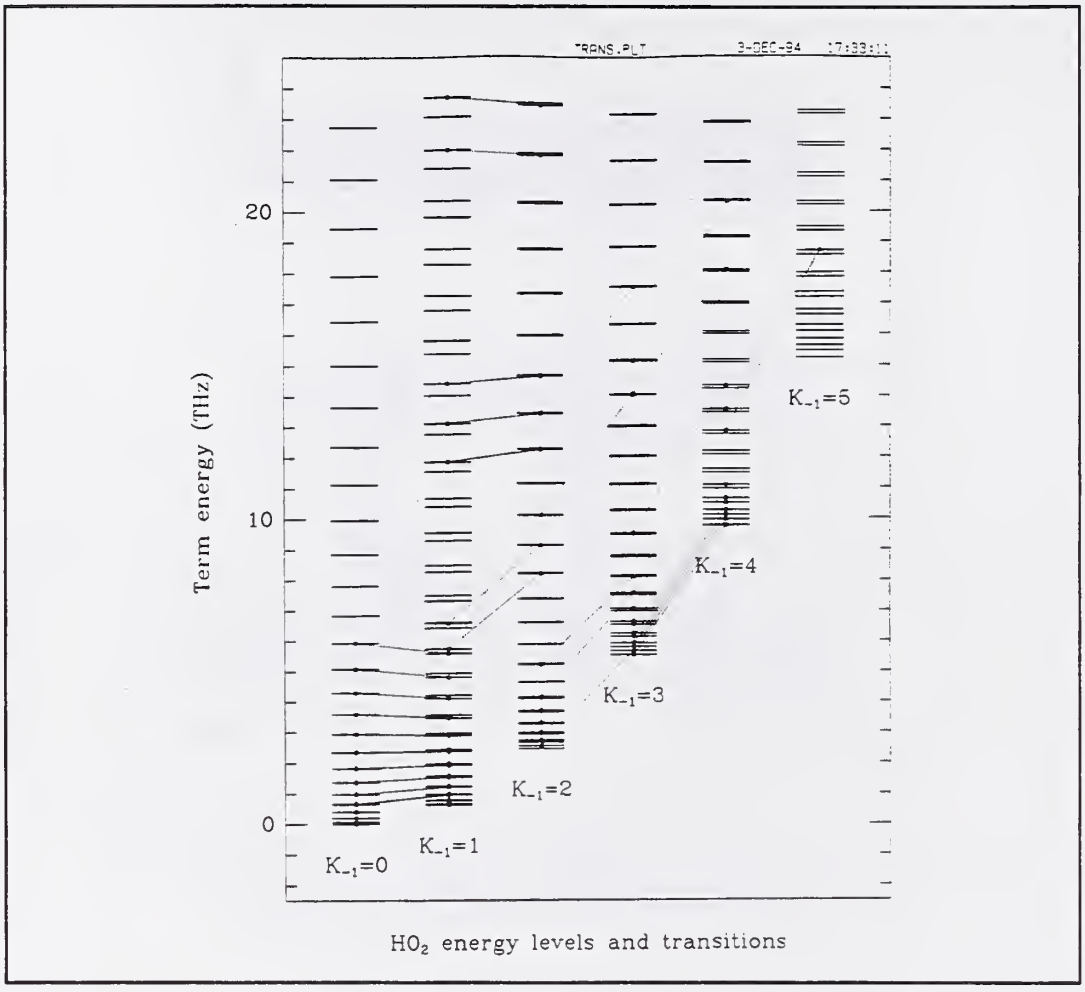
TRANS.PLT
3-DEC-94
Term energy (THz)
20
10
0
K-1=0
K-1=1
K-1=2
K-1=3
K-1=4
K-1=5
HO2 energy levels and transitions

Figure 5

Pergamon

J. Quant. Spectrosc. Radiat. Transfer Vol. 52, No. 3/4, pp. 447–457, 1994
Elsevier Science Ltd. Printed in Great Britain

0022-4073(94)00054-9

THE SMITHSONIAN ASTROPHYSICAL OBSERVATORY DATABASE SAO92

K. CHANCE, K. W. JUCKS, D. G. JOHNSON, and W. A. TRAUB
Harvard-Smithsonian Center for Astrophysics, 60 Garden Street, Cambridge, MA 02138, U.S.A.

Abstract—The Smithsonian Astrophysical Observatory (SAO) maintains a molecular line database (the SAO line database) for analysis of atmospheric spectra in the far i.r. and longer-wave mid i.r., from 10–800 cm^{-1}. This database combines the best currently available line parameters, including the HITRAN[1,2] molecular database, the JPL submillimeter, millimeter, and microwave spectral line catalog[3] (JPLSMM), and other available measurements and calculations. The current version of the database contains 154,895 lines from H_2O, CO_2, O_3, N_2O, CO, CH_4, O_2 (including the $^1\Delta$ state), NO, SO_2, NO_2, NH_3, HNO_3, OH, HF, HCl, HBr, HI, ClO, OCS, H_2CO, HOCl, HCN, H_2O_2, $O(^3P)$, and HO_2. The database is available in both HITRAN-type 80 character (SAO92) and 100 character (SAO92A) formats.

1. L. S. Rothman, R. R. Gamache, A. Goldman, L. R. Brown, R. A. Toth, H. M. Pickett, R. L. Poynter, J.-M. Flaud, C. Camy-Peyret, A. Barbe, N. Husson, C. P. Rinsland, and M. A. H. Smith, *Appl. Opt.* 26, 4058 (1987).
2. L. S. Rothman, R. R. Gamache, R. H. Tipping, C. P. Rinsland, M. A. H. Smith, D. Chris Benner, V. Malathy Devi, J.-M. Flaud, C. Camy-Peyret, A. Perrin, A. Goldman, S. T. Massie, L. R. Brown, and R. A. Toth, *JQSRT*. 48, 469 (1992).
3. R. L. Poynter and H. M. Pickett, Submillimeter millimeter and microwave spectral line catalog, Publ. 80–23, revision 2, Jet Propulsion Laboratory, Pasadena, CA (1984).

INTRODUCTION

Far i.r. techniques have now been successfully used in thermal emission from balloon-borne stratospherie spectrometers to measure atmospheric OH, HO_2, H_2O_2, H_2O (including a number of hot bands and minor isotopic species), $O(^3P)$ atoms (in the mesosphere and thermosphere), O_2, O_3 (including a number of hot bands and minor isotopic species), HCl, HOCl, HF, NO_2, HCN, HNO_3, and a significant upper limit for HBr. The SAO FIRS-2 balloon-borne spectrometer, which is configured to take spectra in the far i.r. from 80–210 cm^{-1}, has made measurements of most of these species. FIRS-2 also has a measurement channel in the longer-wave mid i.r. from 350–700 cm^{-1}, where CO_2, HNO_3, N_2O, and H_2O have been measured. The analysis of flight spectra obtained with this instrument is the prime motivation for maintaining the SAO database. Our concern has been to perform the best possible quantitative analyses of the flight spectra to obtain atmospheric measurements, including a rigorous consideration of the effects of line parameters and their uncertainties on the analysis. This consideration has led in some cases to laboratory measurements and calculations specifically aimed at the improvement of line parameters in order to support the analysis of flight spectra.[4–10]

Figure 1 shows a summary of the result of fitting of FIRS-2 flight spectra (in this case from a balloon flight from Fort Sumner, NM in the Fall of 1989) used to obtain atmospheric concentration profiles. This figure provides a visual summary of most of the current thermal i.r. stratospheric measurement capability; it is these molecules whose measurement must be supported by an appropriate database. A typical portion of a summed limb-scan of FIRS-2 spectra from the Fall 1989 flight, which illustrates the level of detail available in this type of measurement is shown in Fig. 2. This portion of the summed (50 min integration per spectrum) limb-scan, from 99–100 cm^{-1}, includes emission lines from the entire dynamic range of far i.r. measurement capability, from the very strong H_2O lines near 99.1 cm^{-1} to the very weak lines visible at below the 1% level of the spectra (the signal to noise ratio in these spectra is > 500). Figure 3 shows the result of an analysis of FIRS-2 spectra to determine the largest measurable far i.r. features of those species we measure in our spectra (this includes one upper limit, HBr). This analysis represents the average midday

Figure 6

The OHIO Concept: Refinements on a Design for Satellite-Based Measurements of Stratospheric OH

Kelly Chance
Smithsonian Astrophysical Observatory, Cambridge, MA, USA

The hydroxyl radical, OH, is of primary importance in the regulation of the ozone concentration in the earth's stratosphere (the ozone layer). OH has not been monitored on a world-wide basis from space because of the lack of an instrumental technique for doing so. We have developed a concept for an instrument that could make the necessary measurements using currently-available technology, and are in the process of developing a laboratory prototype.

The OH Interferometer Observations (OHIO) concept is an option for the generalized far infrared Fabry-Perot instrument, optimized for satellite-based measurement of the OH radical in the earth's stratosphere with the simplest possible instrument configuration. This paper gives refined design parameters for OHIO. The design presented uses entirely existing, demonstrated technology, does not require stored cryogens, and concentrates on thermal emission measurements of OH, the one stratospheric species which can be measured uniquely and well in the far infrared from a satellite. Measurements are of the $F_1, 7/2^+ \rightarrow F_1, 5/2^-$ transition at 118.455 cm^{-1} (84.42 μm), which has been demonstrated to be the best spectral feature for atmospheric measurements of OH. The current design parameters, including realistic values for Fabry-Perot transmission, detector performance, and filtering required to suppress radiation passed in the higher orders of the grating monochromator, are demonstrated to be within a comfortable margin of providing what is required for global measurements of OH. Thus, we should soon be able to demonstrate a working model for a potential satellite instrument.

The proposed satellite-based measurements of OH have been enabled by atmospheric spectroscopy studies at the Smithsonian Astrophysical Observatory, development of far infrared Fabry-Perot technology at the National Air and Space Museum and the Naval Research Laboratory, and the commercial development of high-T_c superconductor detectors under sponsorship of the NASA Sensors and Instrument Technology program. OHIO includes collaboration with scientists in The Netherlands and Germany.

Figure 7

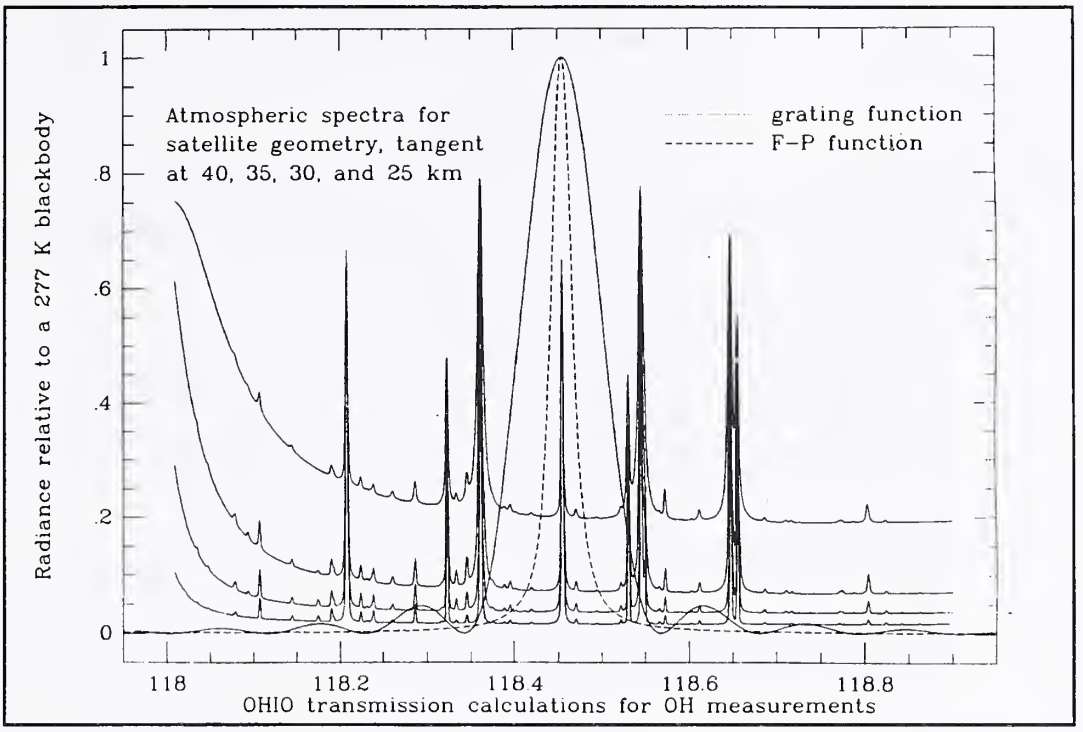
Atmospheric spectra for
satellite geometry, tangent
at 40, 35, 30, and 25 km
grating function
F-P function
Radiance relative to a 277 K blackbody
1
.8
.6
.4
.2
0
118
118.2
118.4
118.6
118.8
OHIO transmission calculations for OH measurements

Figure 8

THz Applications in Atmospheric Sensing

Kelly Chance
13 December 1994

- **THz Species:** Measurements in the 0.6-6 THz range are particularly useful for stratospheric remote sensing measurements of the altitude profiles of trace gases involved in ozone layer chemistry.
  - Unique measurements of OH, HO_2, H_2O_2, and HBr
  - Favorable measurements of HOCl, ClO, HCl, HF
  - Measurements are made in emission: diurnal behavior can be monitored
  - Tropospheric lines are too broad and too obscured (by H_2O) to be measured by THz techniques, except in special cases
  - There are potentially valuable applications in mesospheric and thermospheric physics and chemistry. Thermospheric $O(^3P)$ atoms are a particular possibility.

- **Current Techniques:**
  - Balloon-borne FTS (OH, HO_2, H_2O_2, $O(^3P)$, O_2, O_3, HF, HCl, HOCl, HBr, NO_2, HCN, CO)
  - Balloon-borne submillimeterwave limb sounder (HO_2, O_3, HCl, ClO); THz bands for EOS-MLS (HF, HCl, ClO, BrO)

- **The Future:** Satellite-based stratospheric OH measurements. Several techniques are being developed.
  1. Fabry-Perot/grating instrument (the **OHIO** program). This is a joint, U.S./European program which proposes to use currently-available technology (YBCO bolometer detectors at 80 K; NRL/NASM meshes) to make OH measurements from space.
  2. Heterodyne measurements. Efforts are underway in the U.S. and in Europe to develop the technology for heterodyne measurements of OH.

Figure 9

Applications of Synchrotron Far-IR to Studies of Electronic Materials

Larry Carr
R&D Center – Electronic Materials Laboratory
Grumman Aerospace and Electronics
Bethpage, NY

Infrared Synchrotron Radiation (IR-SR)

Features:

- continuous spectral coverage from microwaves thru x-rays.
- power per bandwidth ($dP/d\omega$) is less than from a thermal source.
  - except for $\omega < 100$ cm^{-1}.
  - $dP/d\omega$ (IR-SR) ~ $\omega^{1/3}$.

    (thermal) ~ ω^2.
- 2 to 3 orders of magnitude brighter than thermal source.
- pulsed (due to electron bunching) , 10s of ps to 100s of ps.
- spatially coherent (due to small source size).

NSLS-VUV for $0 < \omega < 300$ cm^{-1} => 10mW peak power (1/2 ns duration).
70 μW average (cw).

Figure 1

U.S. Synchrotron radiation sources - pulse characteristics

(2nd generation and beyond)

Source	pulse width (ps)	min. sep (ns)	max. sep (ns)
SRC-Aladdin	500	20	297
NSLS-VUV	500	18.9	170
NSLS-Xray	500	18.9	568
CAMD	50	2	184
ALS	50	2	656
APS	75	2.8	3683

Figure 2

AT&T Quantum Well Infrared Photodetector (QWIP)
$GaAs/Al_xGa_{1-x}As$ (B.F. Levine et al)

200 micron diam. mesas

70A/500A x50 periods

x=0.10

19 μm cutoff (long wavelength)

IR-SR Source

≤ 500ps incident pulse

≈ 600MHz system bandwidth

$\tau_{response}$ < 500 ps (upper bound)

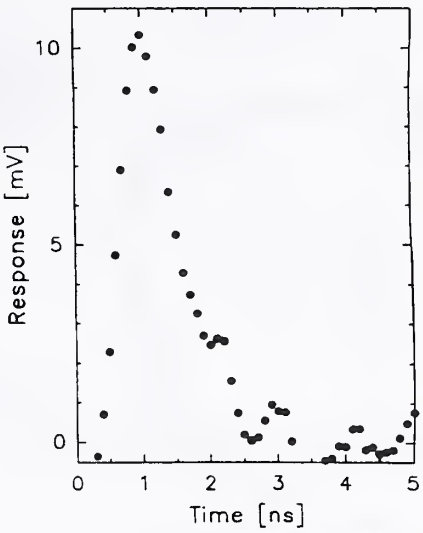

GRUMMAN Corporate Research Center

Figure 3

Time-resolved (pump-probe) spectroscopy technique

1. Laser pulse creates photo-excitations in a sample. Infrared pulse follows.

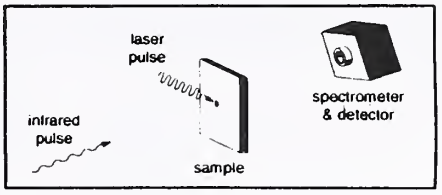

2. Photoexcitations evolve during time interval Δt, after which infrared pulse is incident and probes the excitations.

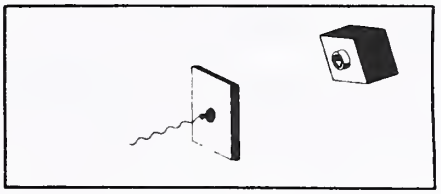

3. Infrared pulse is detected and spectroscopically analyzed. Process is repeated for various Δt to extract time-dependence of spectral features.

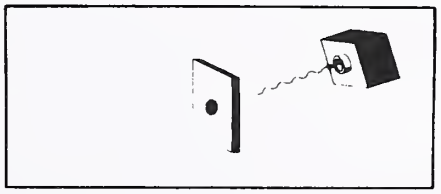

Figure 4

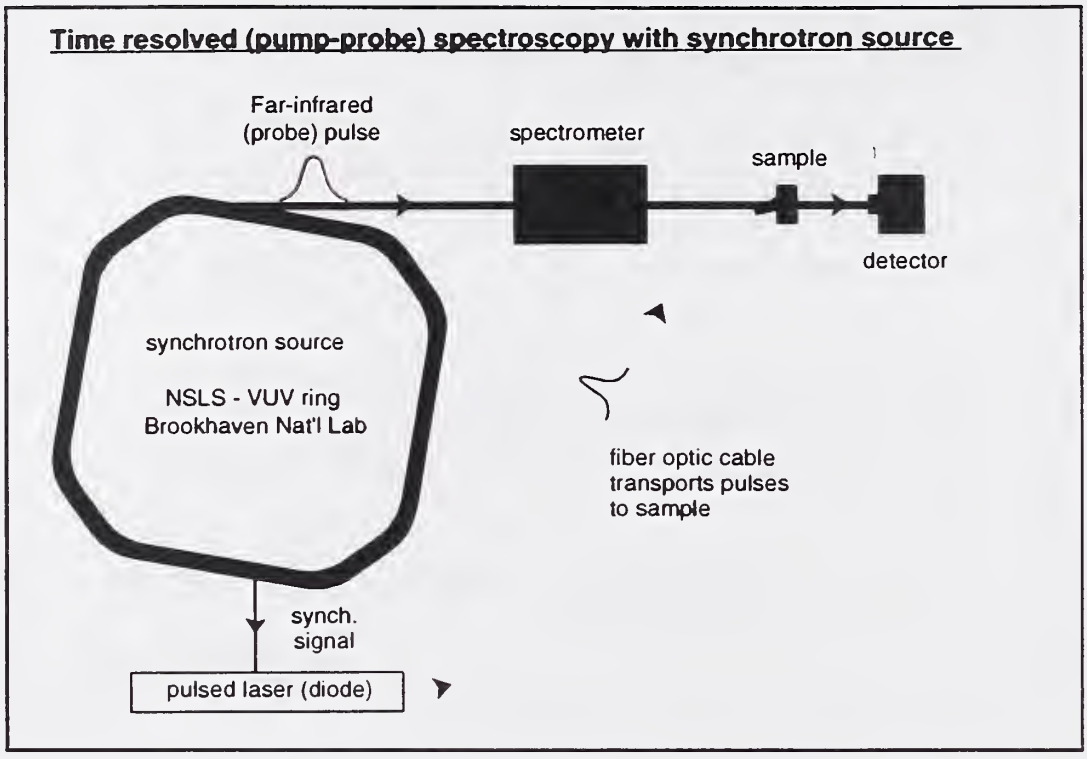

Figure 5

Photo-induced spectroscopy

$$-\Delta T/T \equiv -(T_{light\ on} - T_{light\ off}) / T_{light\ off}$$

- Magnitude of typical signals ~ 10^{-3}.
- Often, absorption coefficient for photoexcitation is high, e.g. $\alpha \sim 10^4$ cm^{-1}

  => penetration depth d ~ 1 μm.

For a nominally transparent material (undoped semiconductor),

$$\frac{-\Delta T}{T} \equiv \frac{2}{n+1} (377\ \Omega)\ d\ \Delta\sigma$$

- For GaAs, n=3.5; d = 1 μm => $\Delta\sigma \equiv 60\ (-\Delta T/T)$ [Ω-cm]$^{-1}$.

Figure 6

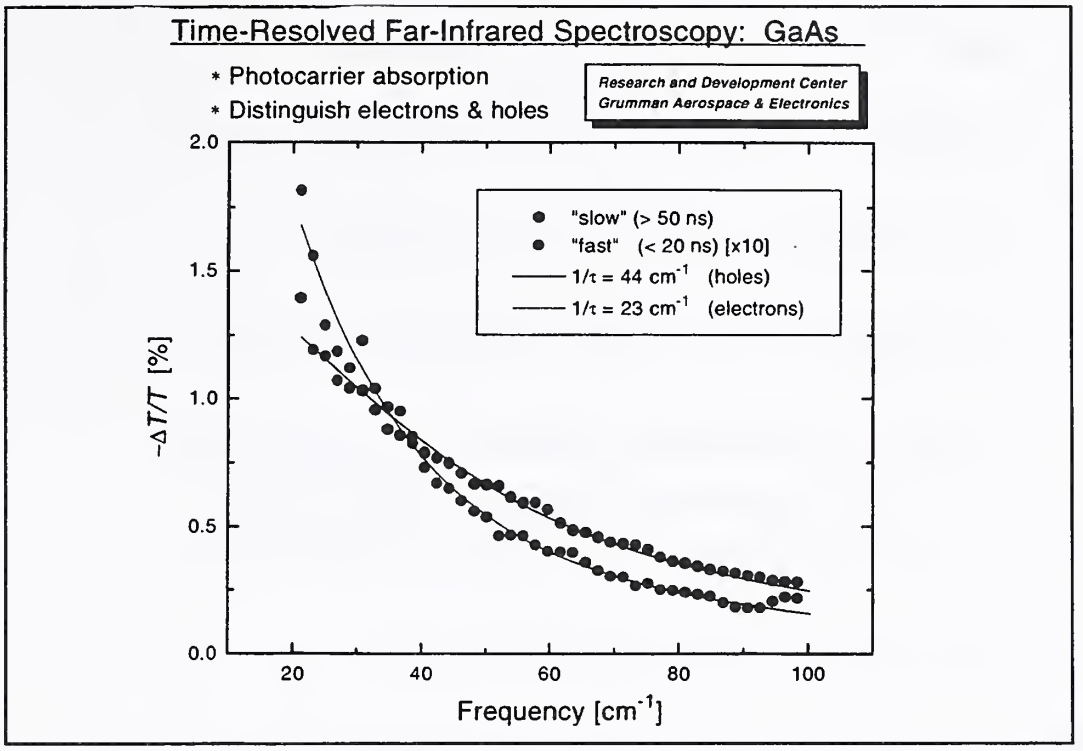

Figure 7

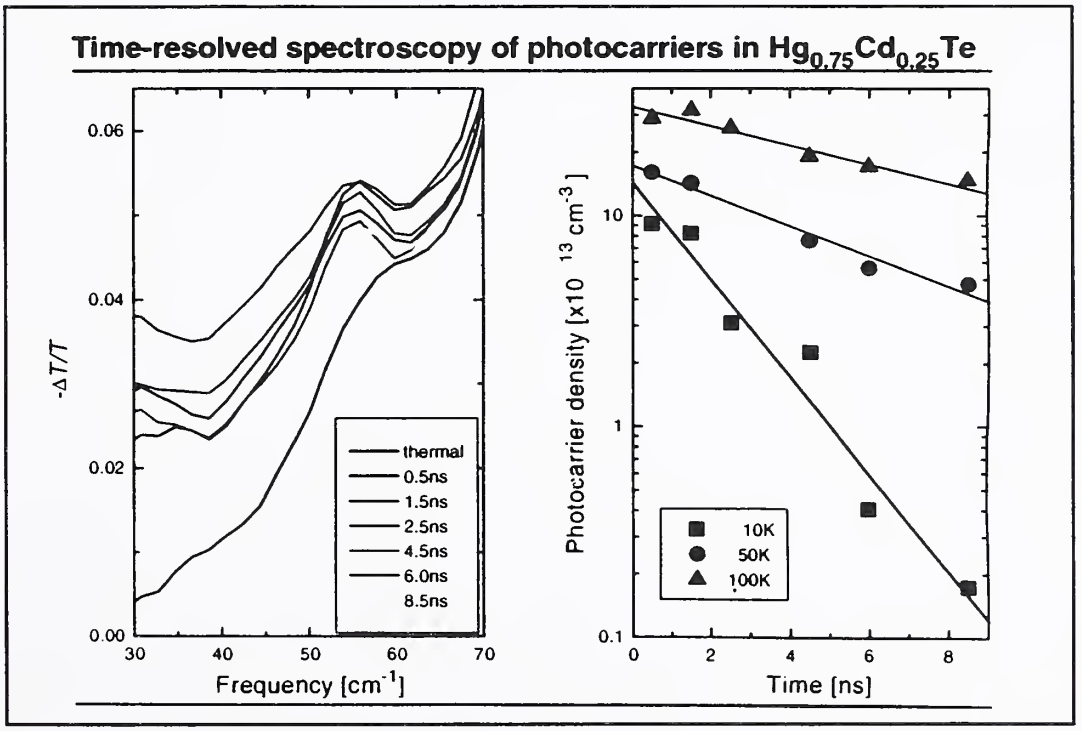

Figure 8

Summary / Conclusions

- IR-SR is useful source for both cw and time-dependent spectral studies of materials.
- Power is NOT high (10 mW peak, 70 μW avg. across FIR).
- Source must be very stable (many SR sources are not) to reach S/N requirements.
- Nanosecond time-resolved far-IR spectroscopy has been demonstrated
  1) High PRF necessitates careful choice of experimental system design.
  2) Time resolution approaching a few 10s of ps can be anticipated in future.
- Synchrotron's RF allows for electrical synchronization.

Figure 9

Application of Free-Electron Lasers as Terahertz Sources

S. James Allen
Center for Free-Electron Laser Studies
University of California, Santa Barbara

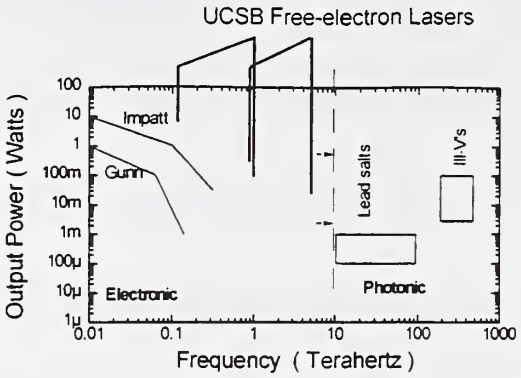

A Scientific Thrust:

Non linear quantum transport
in semiconductor nanostructures
in terahertz electnc fields.

Novel phenomena in
semiconductor nanostructures.

Potential Technology Impact:

Define the high frequency limits of
conventional electronics.

Enable new electronics
at terahertz frequencies.

Figure 1

Terahertz Dynamics in Resonant Tunneling Diodes

Office of Naval Research, Hughes Research Lab, UC-Micro

J.S. Scott, M. Wanke, J. Kaminski
UCSB

D. Chow, M. Lui, T.Y. Liu
Hughes Research Lab

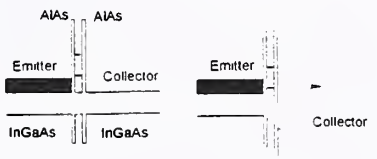

- High peak current densities 10^5 A/cm^2
- High peak to valley ratios ≈ 25:1 at 300 K
- Terahertz oscillations, (E.R. Brown et al. Lincoln Lab.)
- Picosecond switching, (D. Bloom et al. Stanford U.)

Figure 2

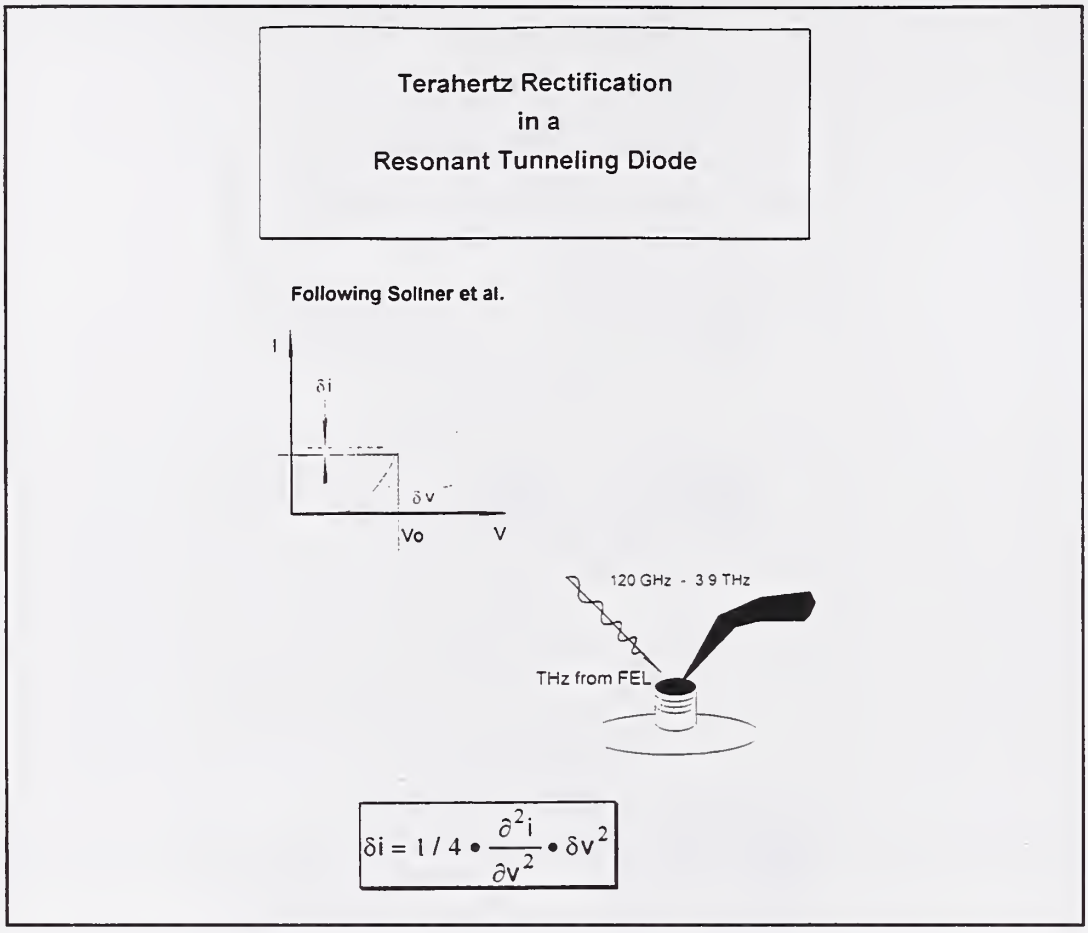
Terahertz Rectification
in a
Resonant Tunneling Diode
Following Sollner et al.
I
δi
δv
Vo
V
120 GHz - 3 9 THz
THz from FEL
$\delta i = 1/4 \bullet \frac{\partial^2 i}{\partial v^2} \bullet \delta v^2$

Figure 3

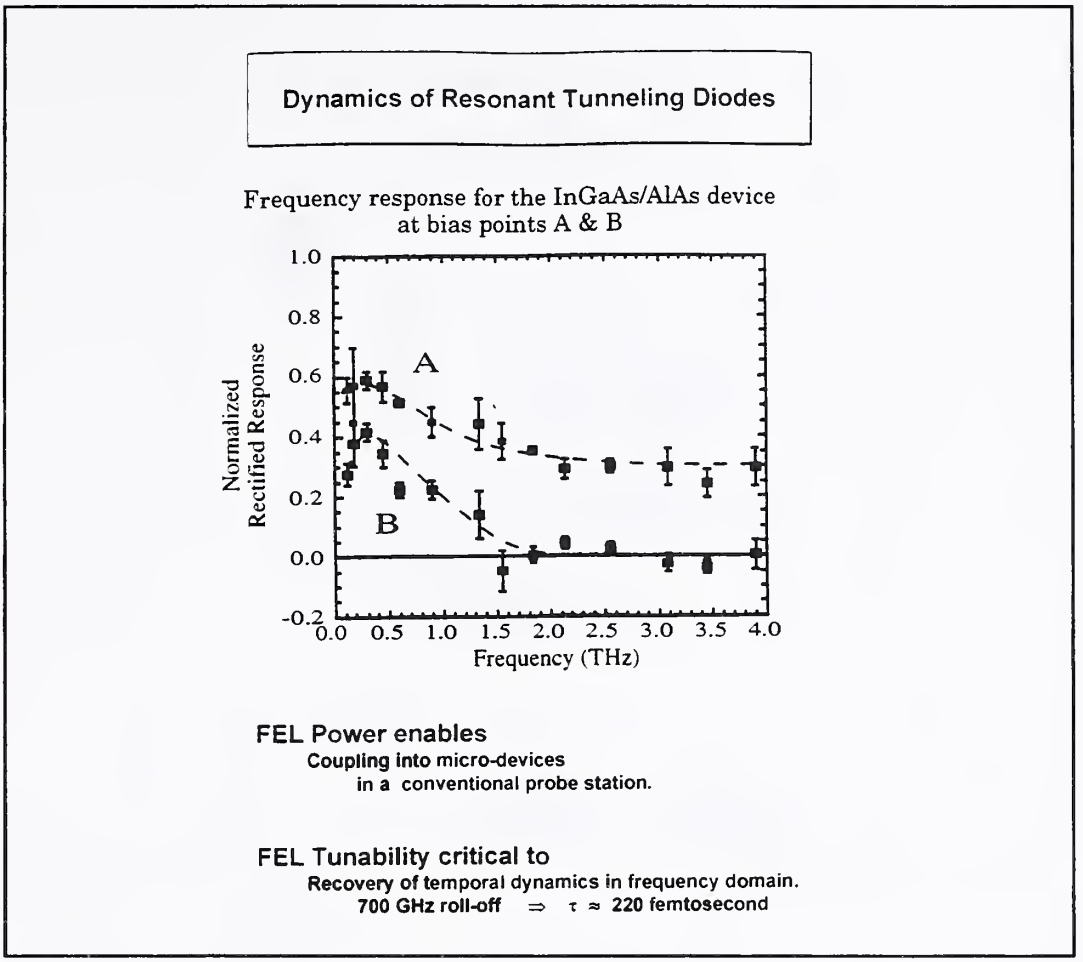
Dynamics of Resonant Tunneling Diodes
Frequency response for the InGaAs/AlAs device
at bias points A & B
Normalized
Rectified Response
1.0
0.8
0.6
0.4
0.2
0.0
-0.2
A
B
0.0 0.5 1.0 1.5 2.0 2.5 3.0 3.5 4.0
Frequency (THz)
FEL Power enables
Coupling into micro-devices
in a conventional probe station.
FEL Tunability critical to
Recovery of temporal dynamics in frequency domain.
700 GHz roll-off ⇒ τ ≈ 220 femtosecond

Figure 4

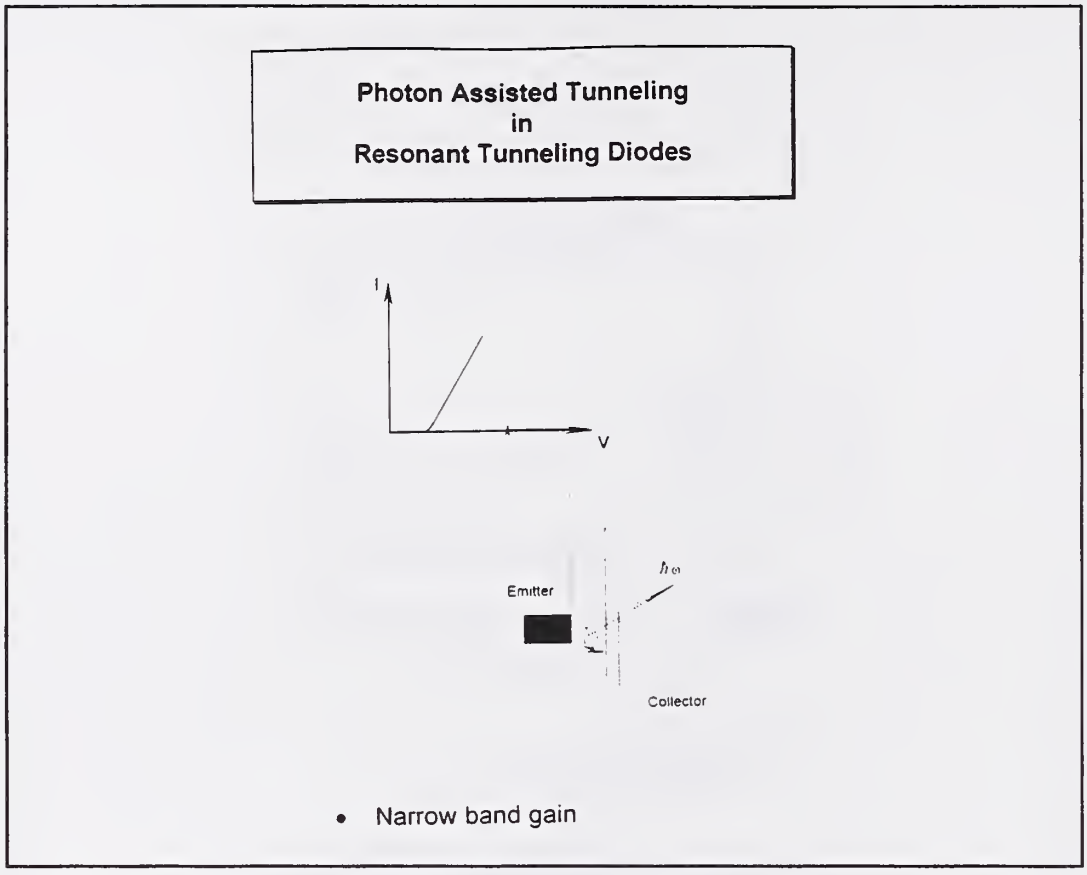
Photon Assisted Tunneling
in
Resonant Tunneling Diodes
I
V
Emitter
$\hbar\omega$
Collector
• Narrow band gain

Figure 5

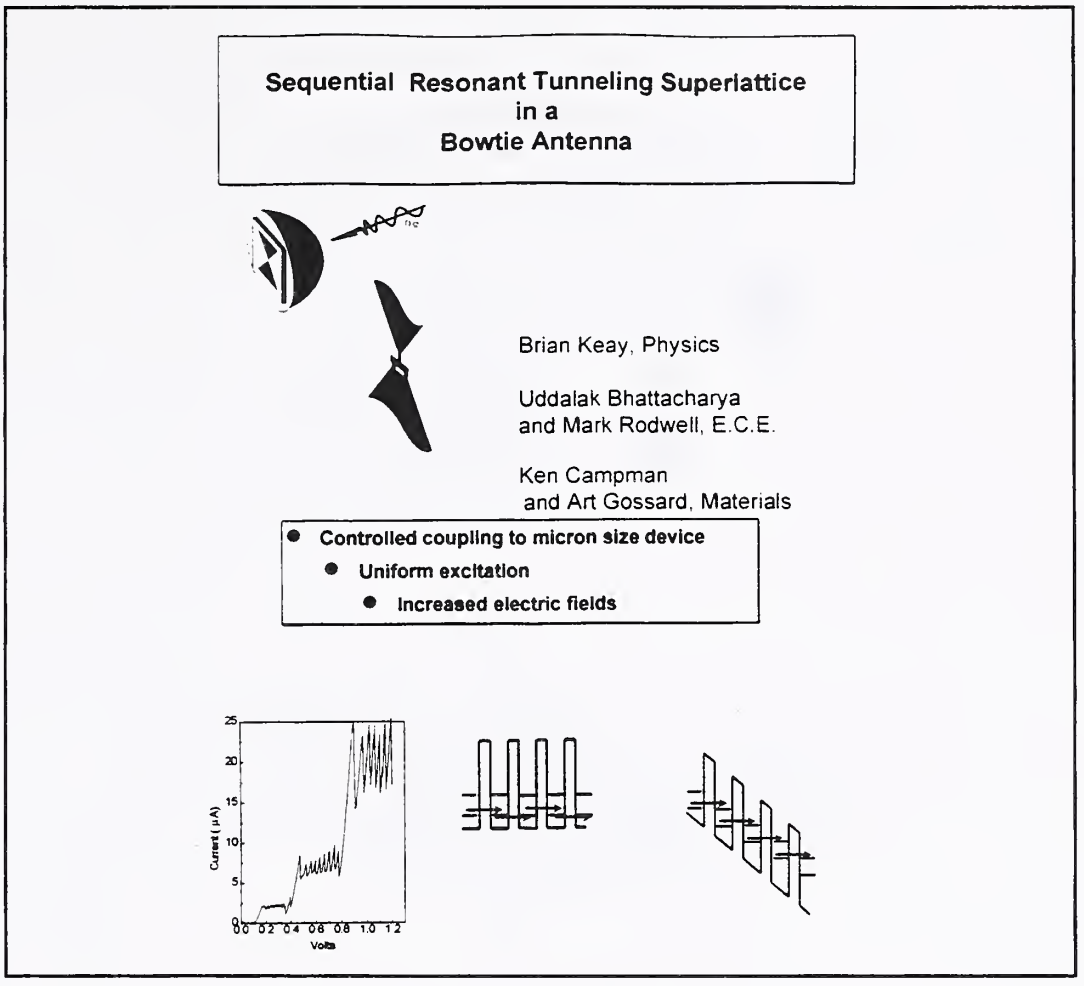
Sequential Resonant Tunneling Superlattice
in a
Bowtie Antenna
Brian Keay, Physics
Uddalak Bhattacharya
and Mark Rodwell, E.C.E.
Ken Campman
and Art Gossard, Materials
Controlled coupling to micron size device
Uniform excitation
Increased electric fields
Current (μA)
Volts

Figure 6

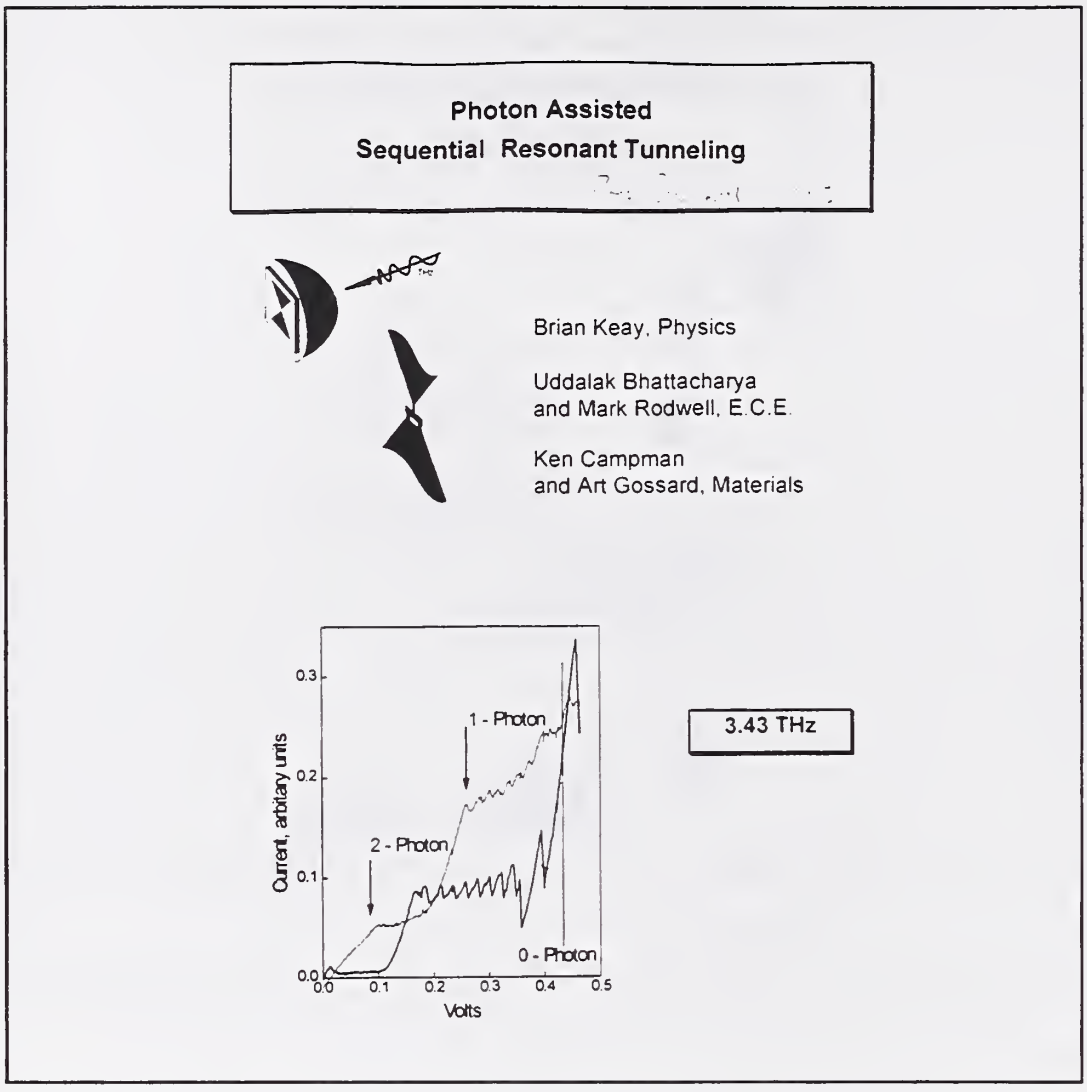
Photon Assisted
Sequential Resonant Tunneling
Brian Keay, Physics
Uddalak Bhattacharya
and Mark Rodwell, E.C.E.
Ken Campman
and Art Gossard, Materials
Current, arbitary units
Volts
1 - Photon
2 - Photon
0 - Photon
0.0
0.1
0.2
0.3
0.4
0.5
3.43 THz

Figure 7

Femtosecond THz Beam Generation and Applications

Daniel Grischkowsky
School of Electrical and Computer Engineering
Oklahoma State University

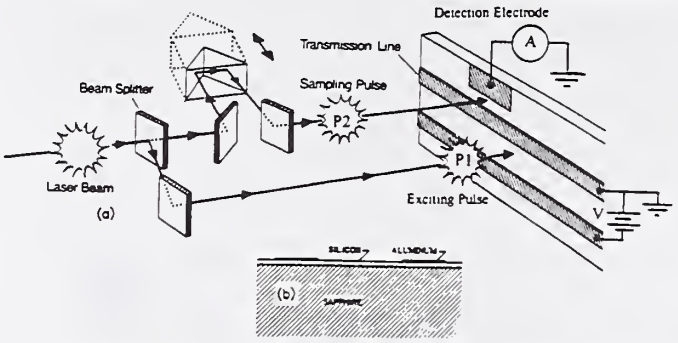

M.B. Ketchen, D. Grischkowsky, T.C. Chen, C-C. Chi, I.N. Duling III, N.J. Halas, J-M. Halbout, J.A. Kash and G.P. Li, "Generation of Sub-Picosecond Electrical Pulses on Coplanar Transmission Lines," Appl. Phys. Lett., Vol.48, 751 (1986).

D. Grischkowsky, M.B. Ketchen, C-C. Chi, I.N. Duling III, N.J. Halas, J-M. Halbout, and P.G. May, "Capacitance Free Generation and Detection of Sub-Picosecond Electrical Pulses on Coplanar Transmission Lines," IEEE J. Quantum Electronics, Vol. 24, 221 (1988).

Figure 1

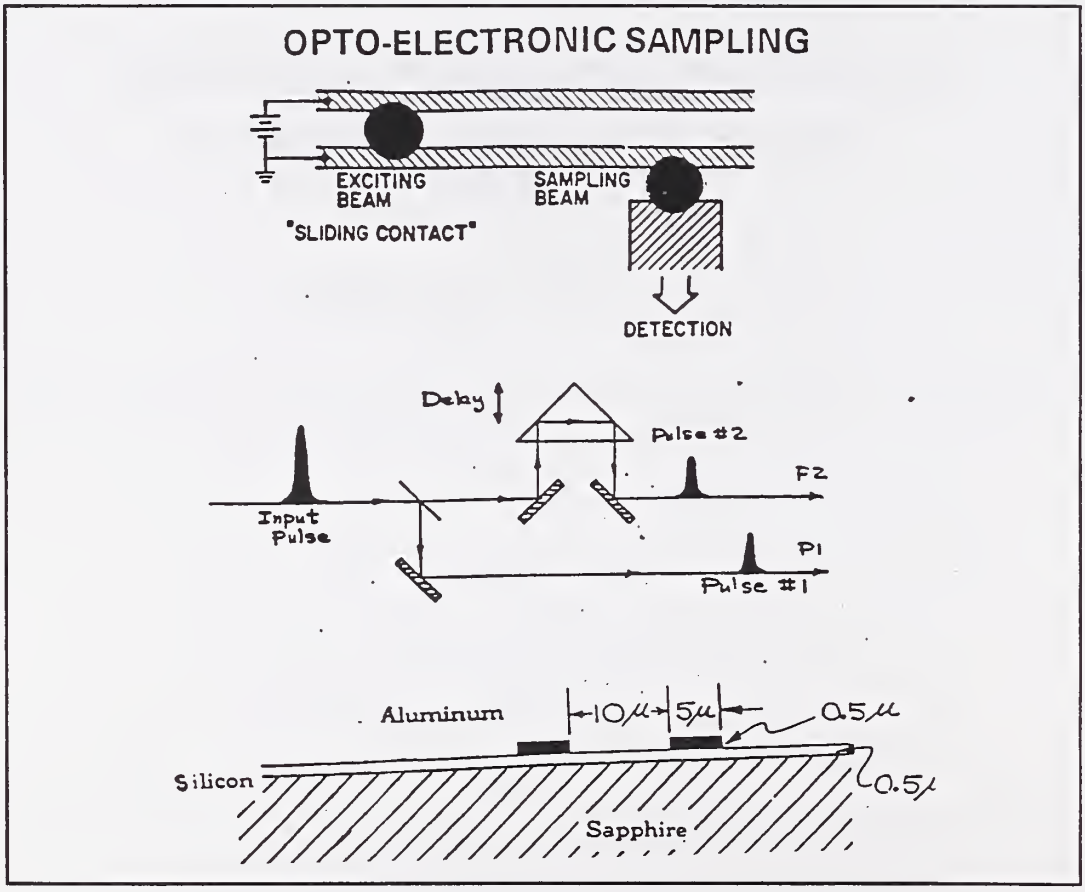

Figure 2

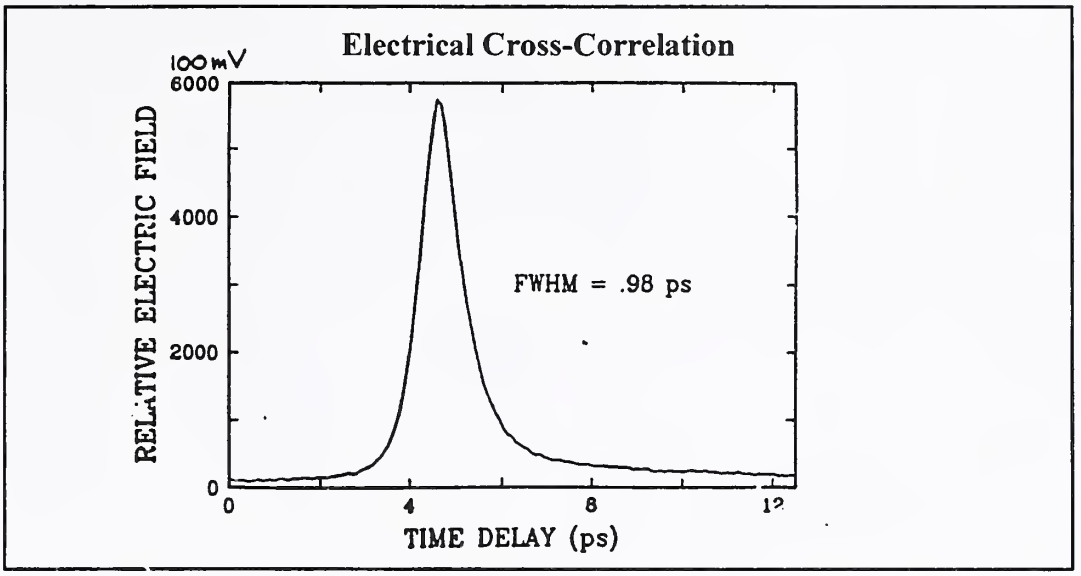

Figure 3

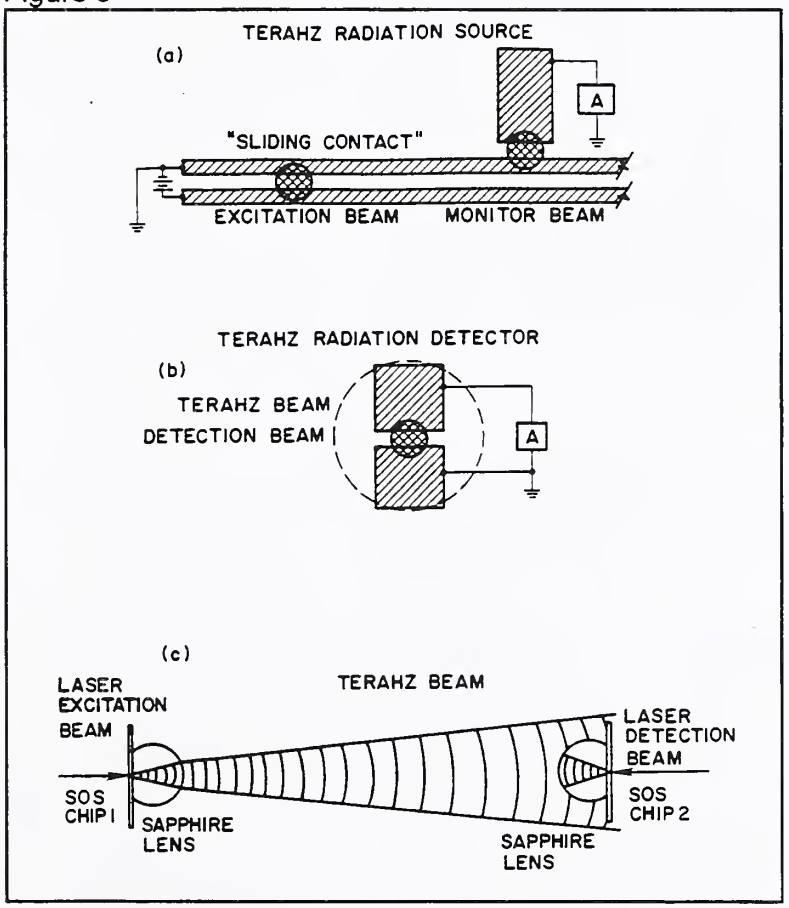

Figure 4

Figure 5

Figure 6

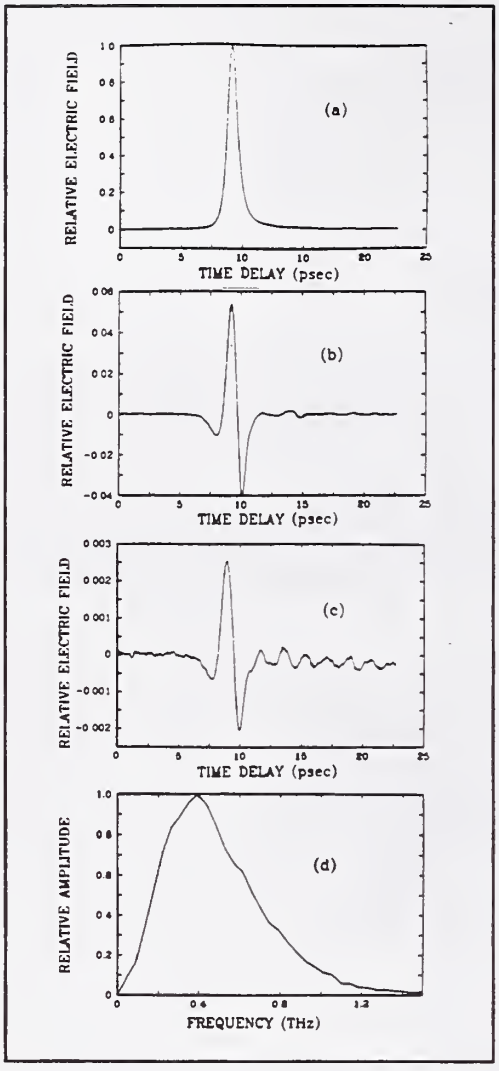

Figure 7

Figure 8

Figure 9

Figure 10

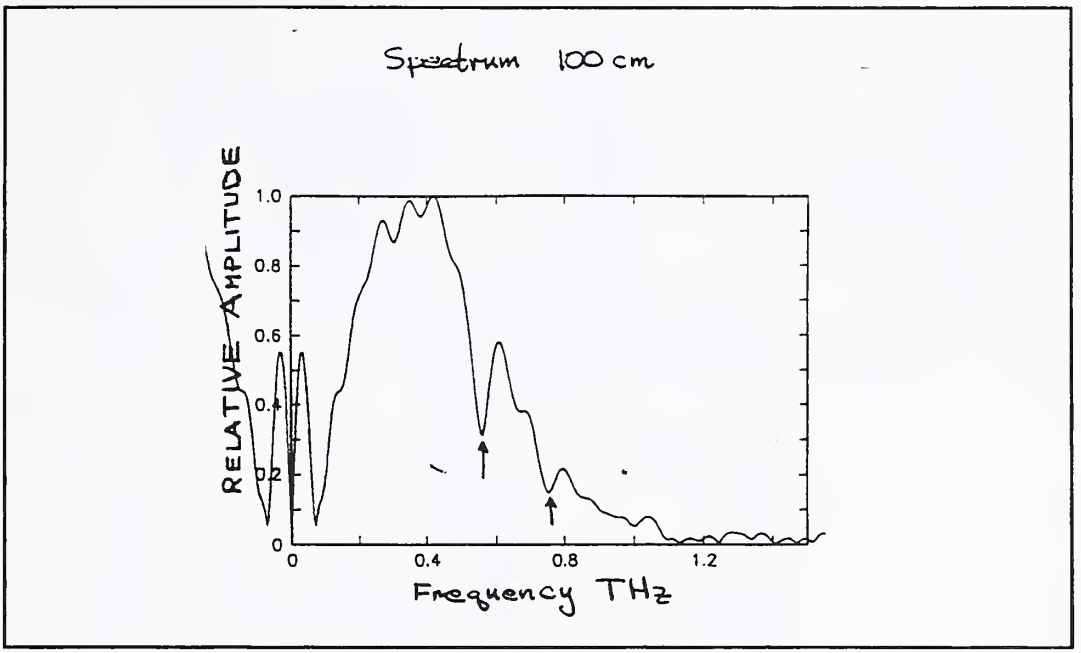

Figure 11

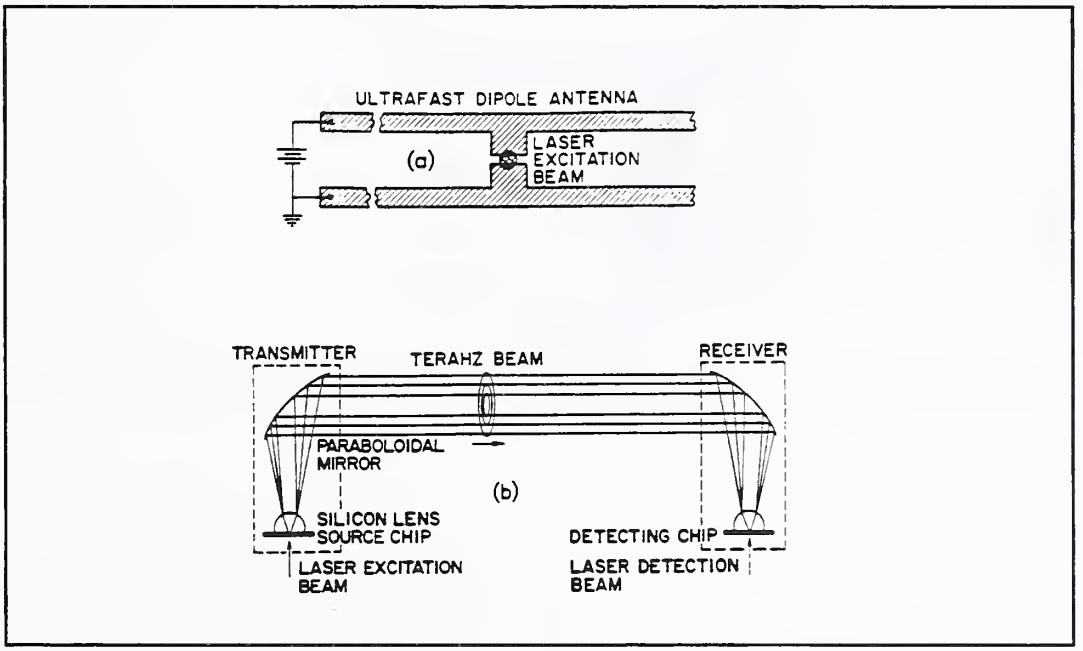

Figure 12

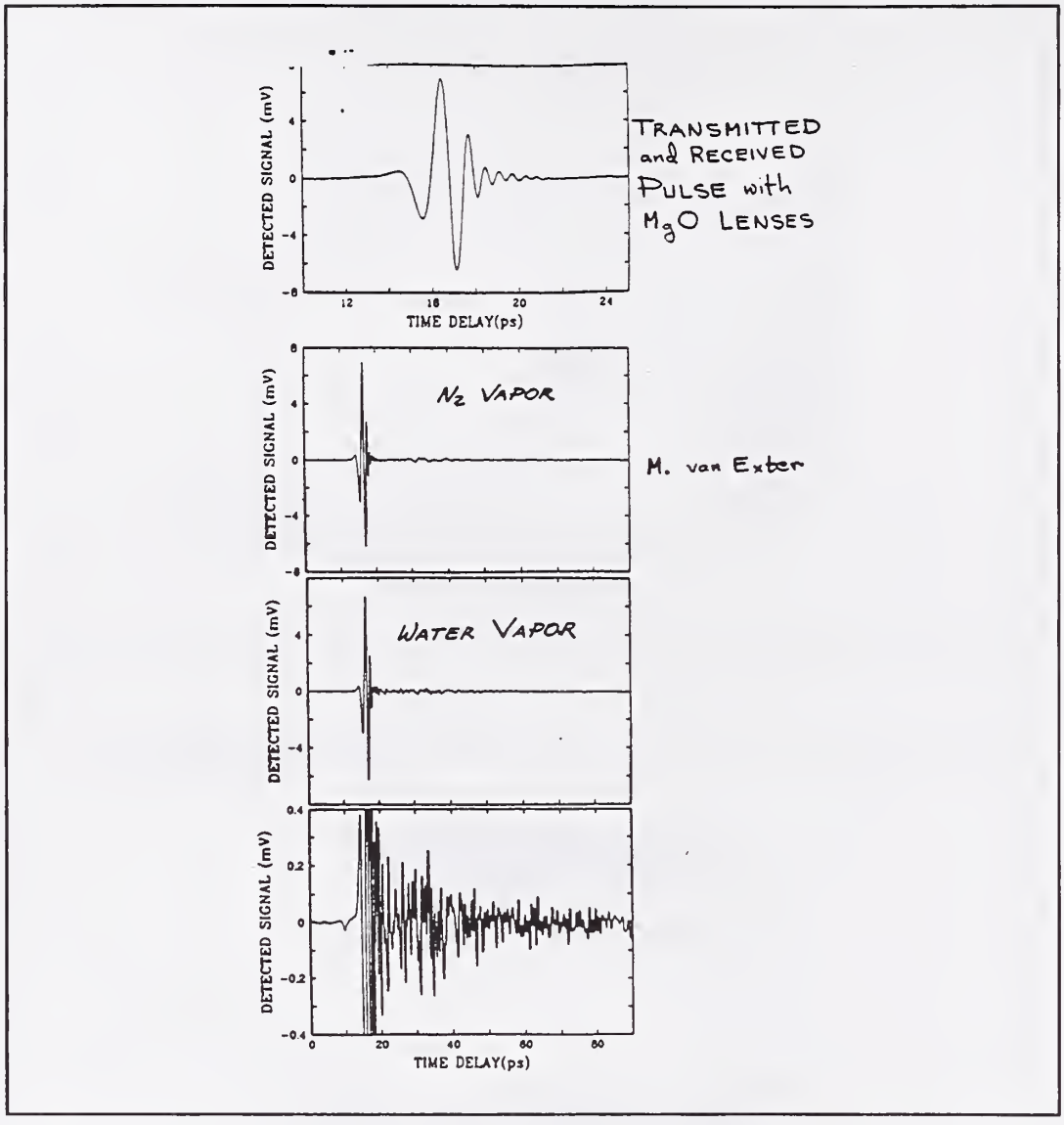
DETECTED SIGNAL (mV)
TIME DELAY(ps)
TRANSMITTED and RECEIVED PULSE with MgO LENSES
N_2 VAPOR
M. van Exter
WATER VAPOR

Figure 13

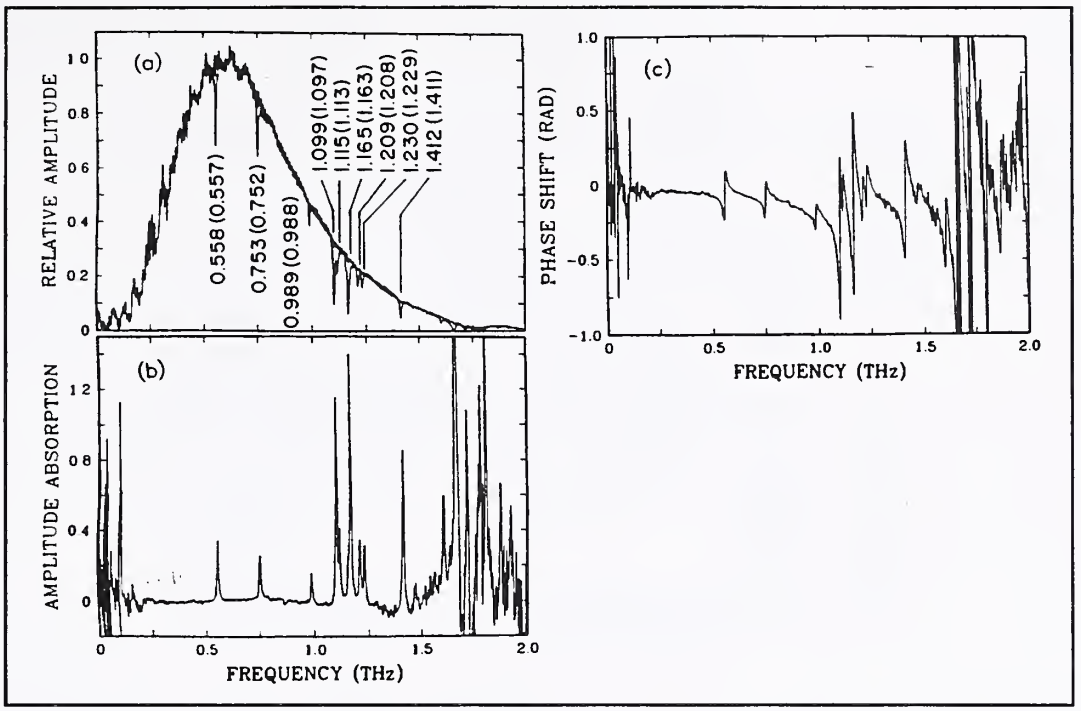
(a)
RELATIVE AMPLITUDE
0.558 (0.557)
0.753 (0.752)
0.989 (0.988)
1.099 (1.097)
1.115 (1.113)
1.165 (1.163)
1.209 (1.208)
1.230 (1.229)
1.412 (1.411)
(b)
AMPLITUDE ABSORPTION
FREQUENCY (THz)
(c)
PHASE SHIFT (RAD)
FREQUENCY (THz)

Figure 14

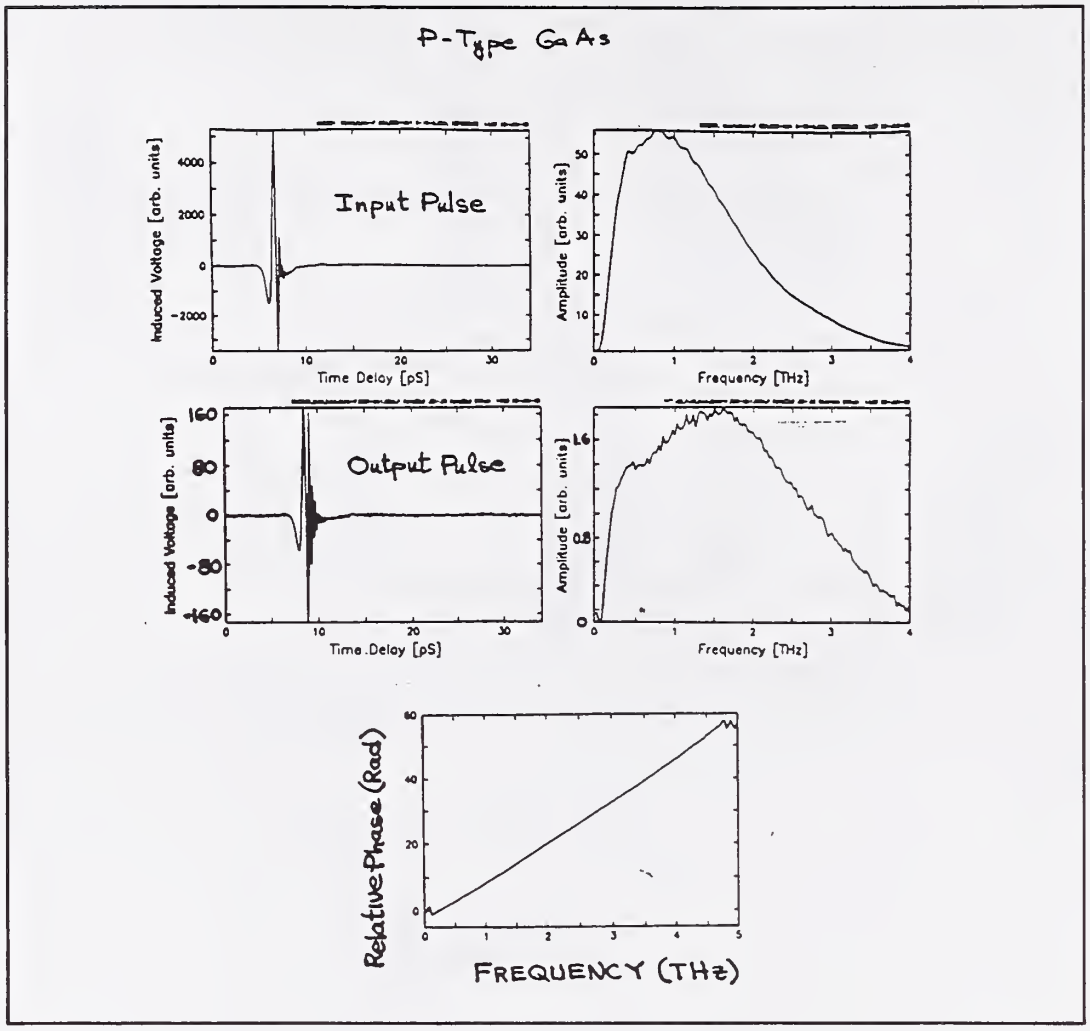
P-Type GaAs
Input Pulse
Induced Voltage [arb. units]
Time Delay [pS]
Amplitude [arb. units]
Frequency [THz]
Output Pulse
Induced Voltage [arb. units]
Time Delay [pS]
Amplitude [arb. units]
Frequency [THz]
Relative Phase (Rad)
FREQUENCY (THz)

Figure 15

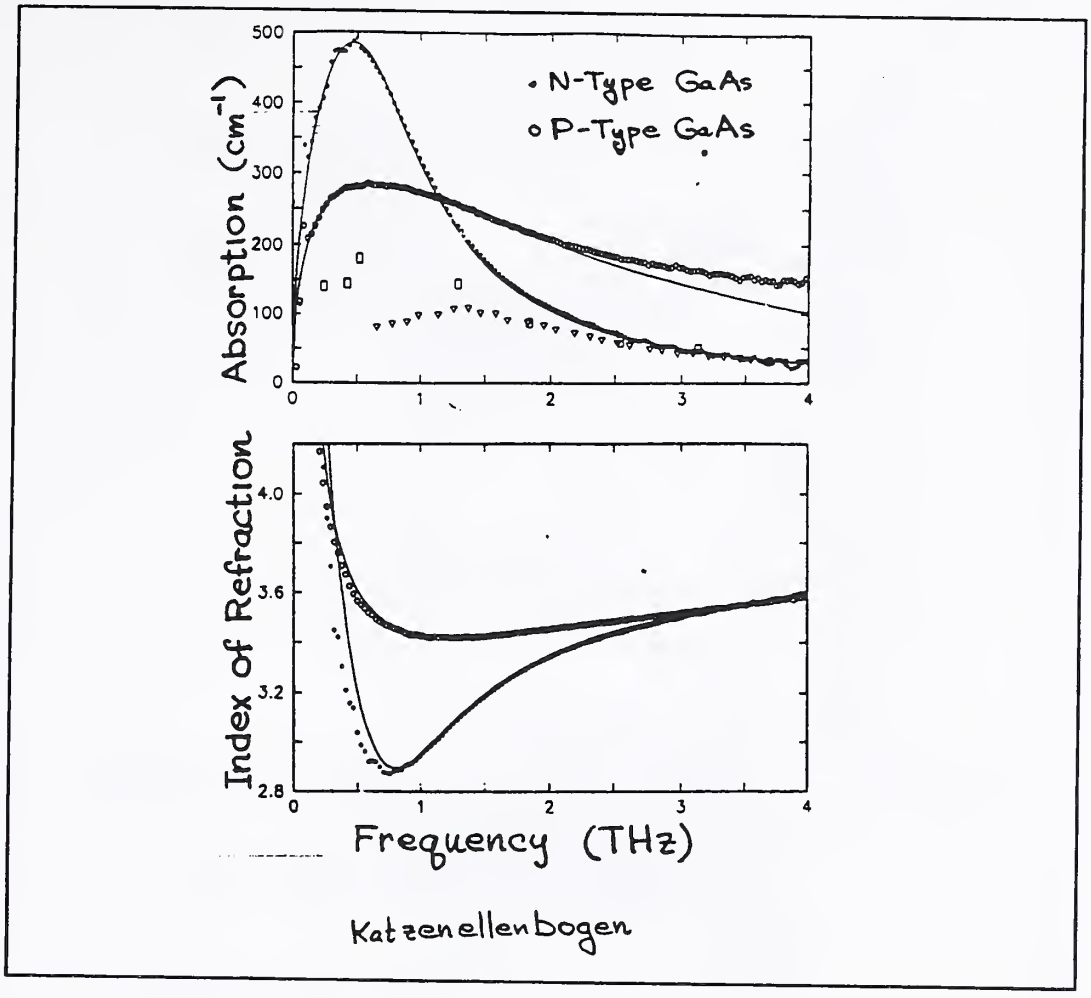
Absorption (cm⁻¹)
500
400
300
200
100
0
0
1
2
3
4
• N-Type GaAs
○ P-Type GaAs
Index of Refraction
4.0
3.6
3.2
2.8
0
1
2
3
4
Frequency (THz)
Katzenellenbogen

Figure 16

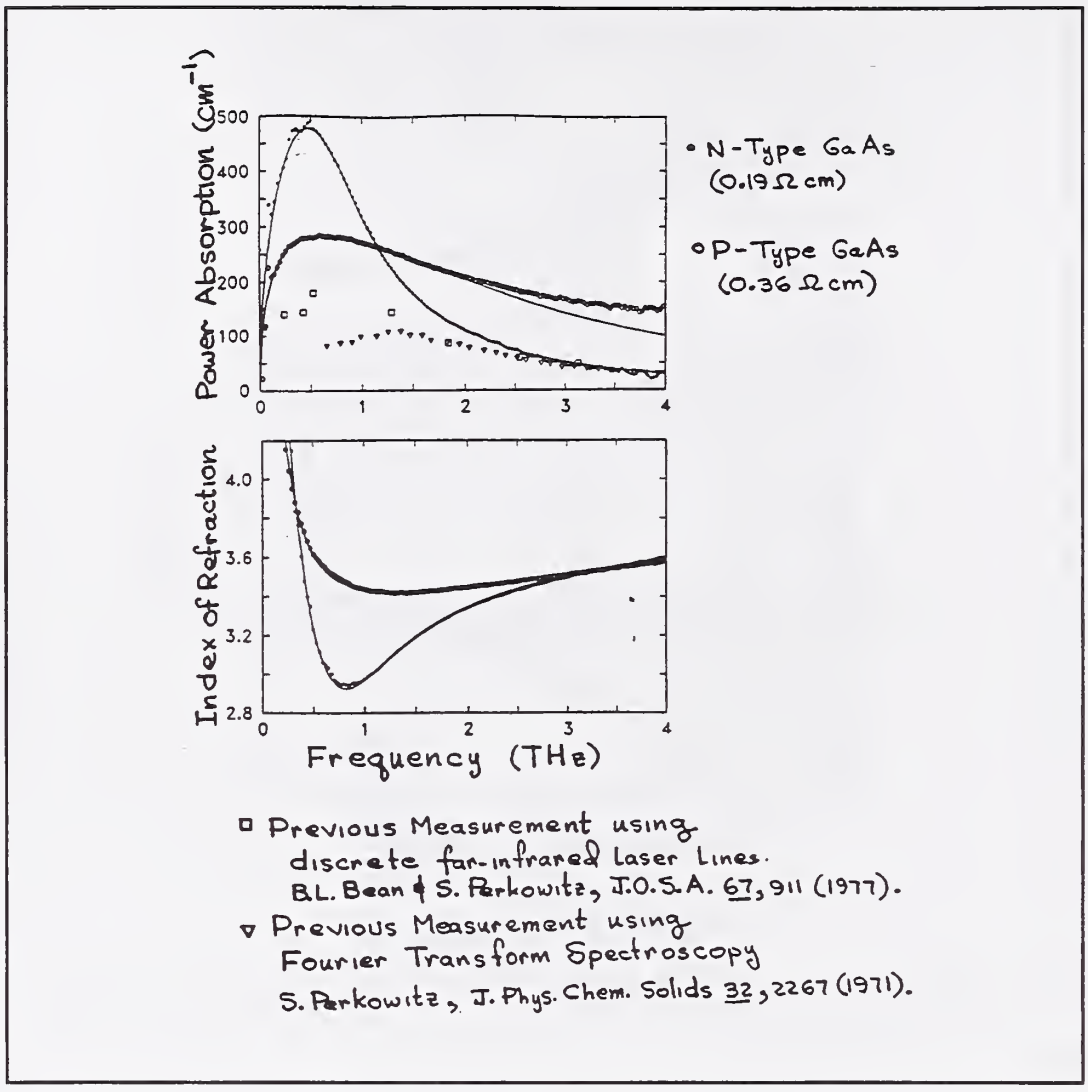
Power Absorption (cm⁻¹)
500
400
300
200
100
0
0
1
2
3
4
• N-Type GaAs
(0.19 Ω cm)
○ P-Type GaAs
(0.36 Ω cm)
Index of Refraction
4.0
3.6
3.2
2.8
0
1
2
3
4
Frequency (THz)
□ Previous Measurement using
discrete far-infrared laser lines.
B.L. Bean & S. Perkowitz, J.O.S.A. 67, 911 (1977).
▽ Previous Measurement using
Fourier Transform Spectroscopy
S. Perkowitz, J. Phys. Chem. Solids 32, 2267 (1971).

Figure 17

Power Standards for the Near Millimeter and Submm Region

Neil Erickson
Millitech Corporation

Power Measurement Problems in the Submm Region

- Available power is small from most sources.
  Accurate calorimeters are not sufficiently sensitive.
- Difficult to verify spectral purity.
  Unknown harmonic content, spurious oscillation, contaminating lines.
- Output tends to be optically coupled (feed horns or other antenna structure).
  Poor coupling efficiency to any small (particularly single mode) structure.
- Propagation loss is high, even in air.
  Unknown attenuation.
- No test equipment to make even the most basic measurements.
  No way to verify VSWR, frequency or make swept measurements.
- Mode purity is poor.
  Unknown fraction of power in higher modes with very poor coupling.
- Frequency range is very large, > 10/1.
  No single solution is likely to be workable.

Figure 1

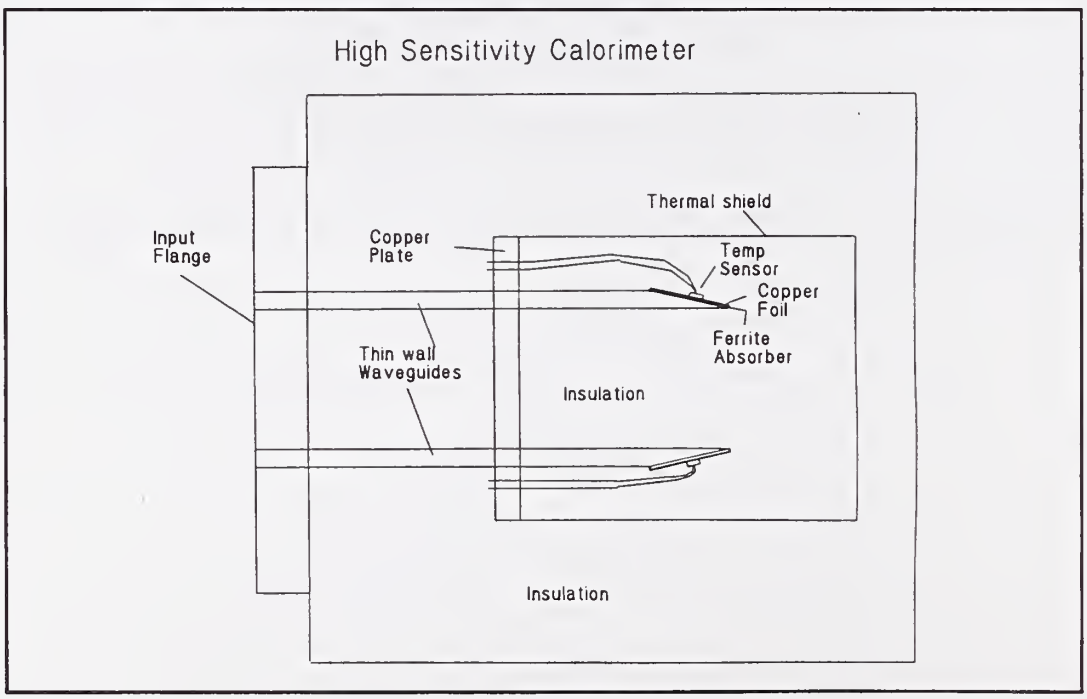

Figure 2

Far Infrared Absolute Spectrophotometer (FIRAS)

John Mather
NASA Goddard Space Flight Center

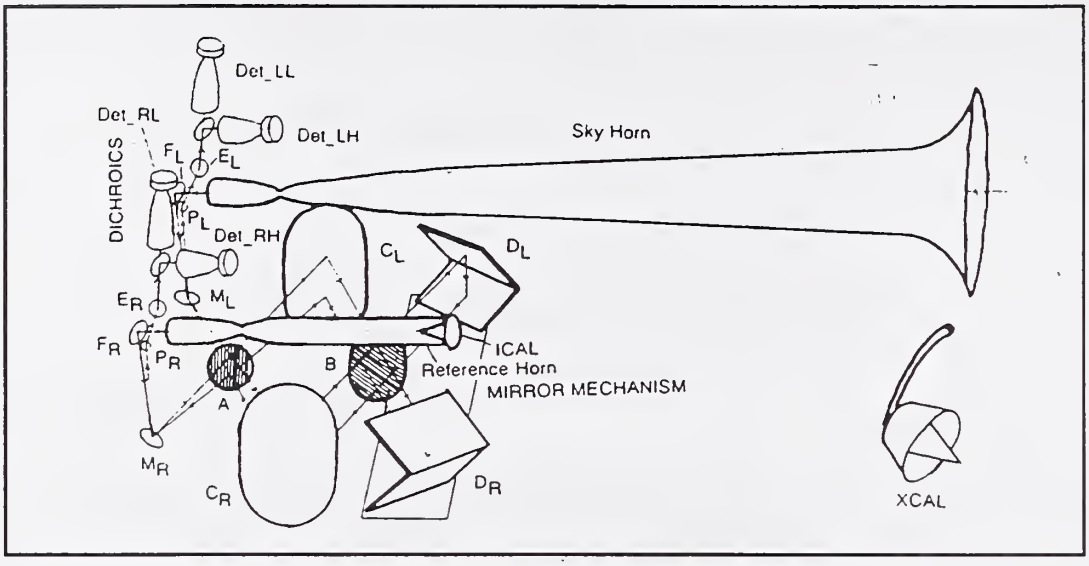

Figure 1

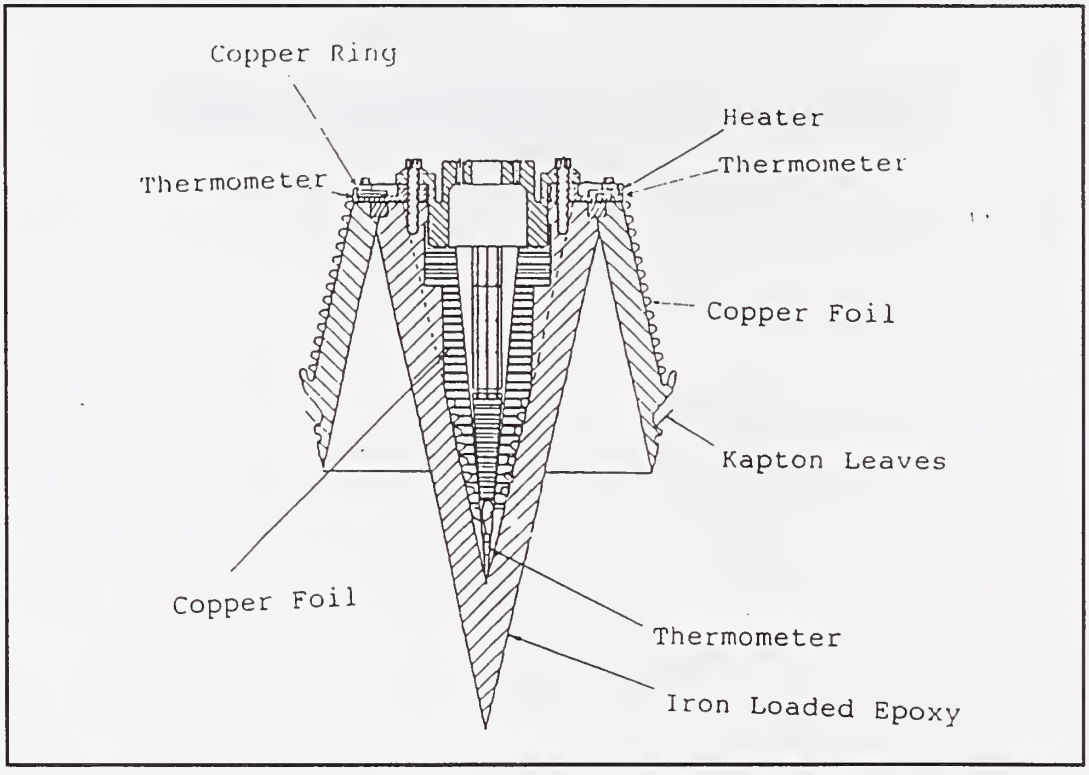

Figure 2

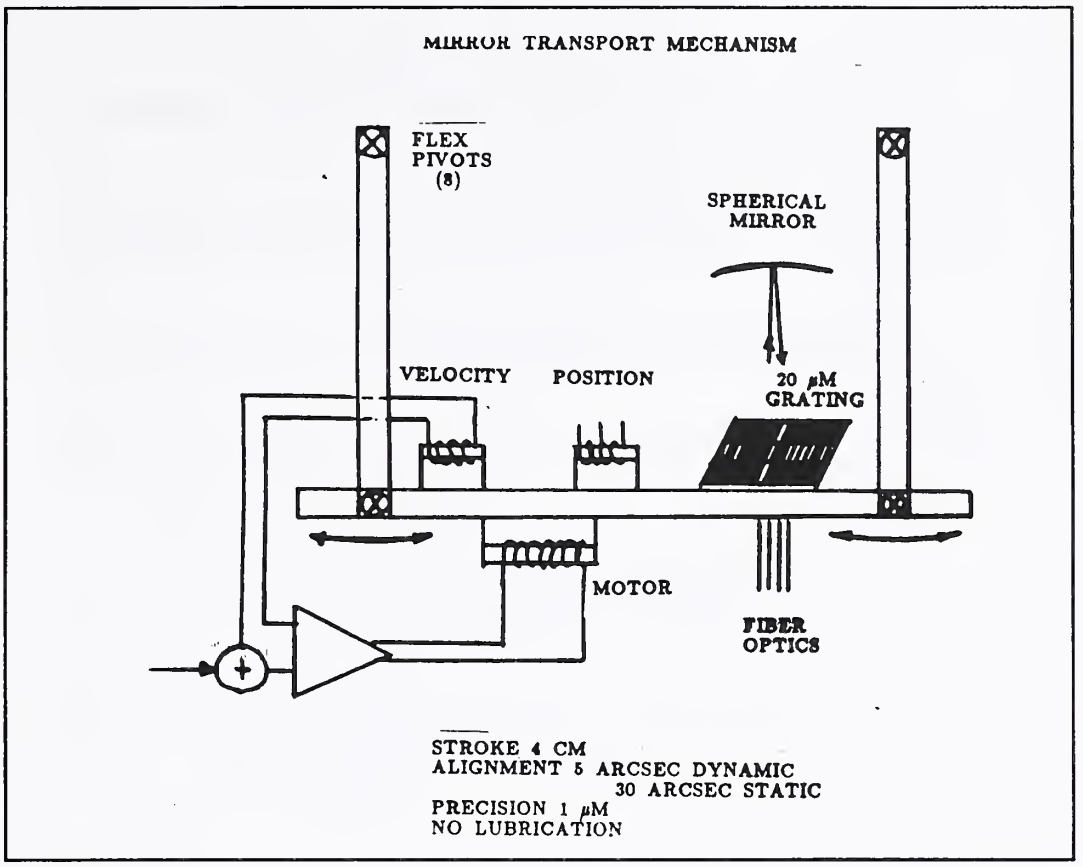
MIRROR TRANSPORT MECHANISM
FLEX
PIVOTS
(8)
SPHERICAL
MIRROR
VELOCITY
POSITION
20 μM
GRATING
MOTOR
FIBER
OPTICS
STROKE 4 CM
ALIGNMENT 5 ARCSEC DYNAMIC
30 ARCSEC STATIC
PRECISION 1 μM
NO LUBRICATION

Figure 3

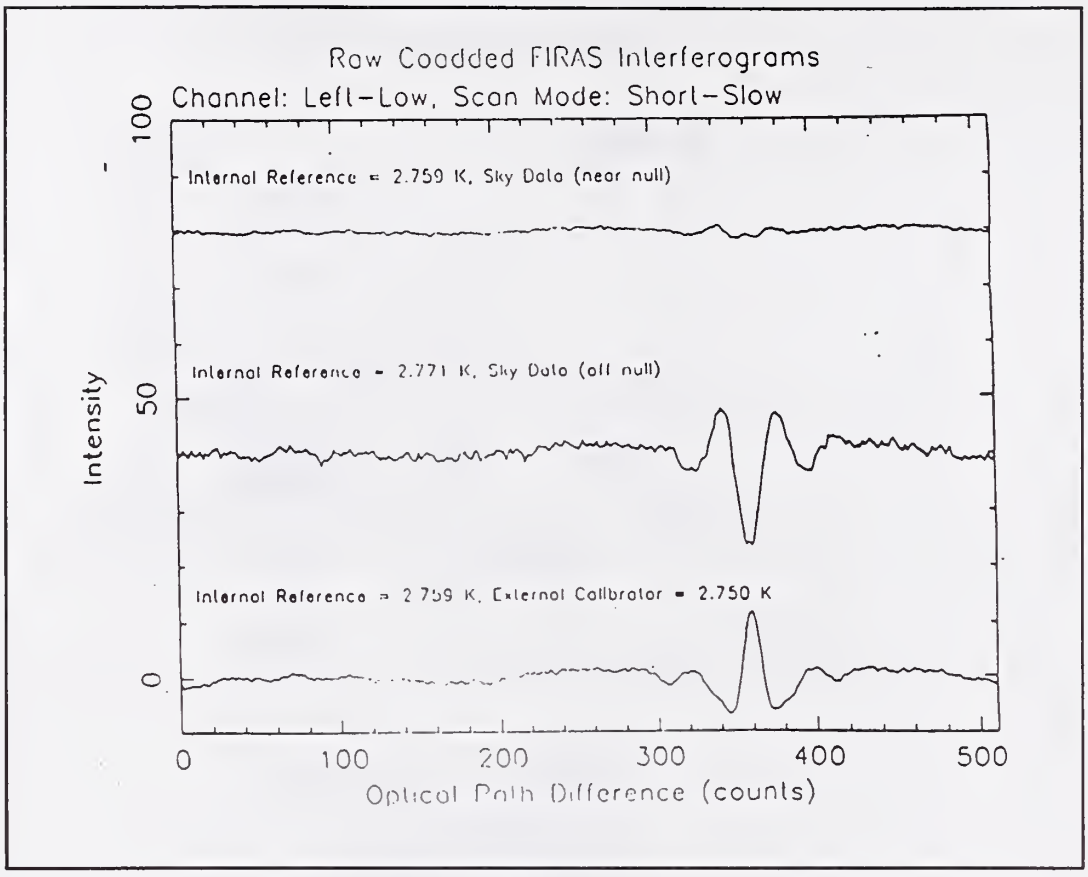
Raw Coadded FIRAS Interferograms
Channel: Left-Low, Scan Mode: Short-Slow
Internal Reference = 2.759 K, Sky Data (near null)
Internal Reference = 2.771 K, Sky Data (off null)
Internal Reference = 2.759 K, External Calibrator = 2.750 K
Intensity
100
50
0
0
100
200
300
400
500
Optical Path Difference (counts)

Figure 4

FIRAS Calibration Procedure

- External calibrator (XCAL) in sky horn
- Independently control temperatures of all internal objects with significant emissivity
- Take cal data in both null and off-null conditions to make FIRAS a direct-substitution experiment.
- Solve the linear system for all internal emissivities $\varepsilon_{i,\nu}$ and optical efficiency H_ν at frequency ν.
- Calibrate by inverting the linear equation

$$S_\nu OBS = H_\nu [S_{\nu,true} + \Sigma_i \varepsilon_{i,\nu} B_\nu (T_i)]$$

... where, during cal procedures, $S_{\nu,true}$ is the XCAL's Planck curve.

Figure 5

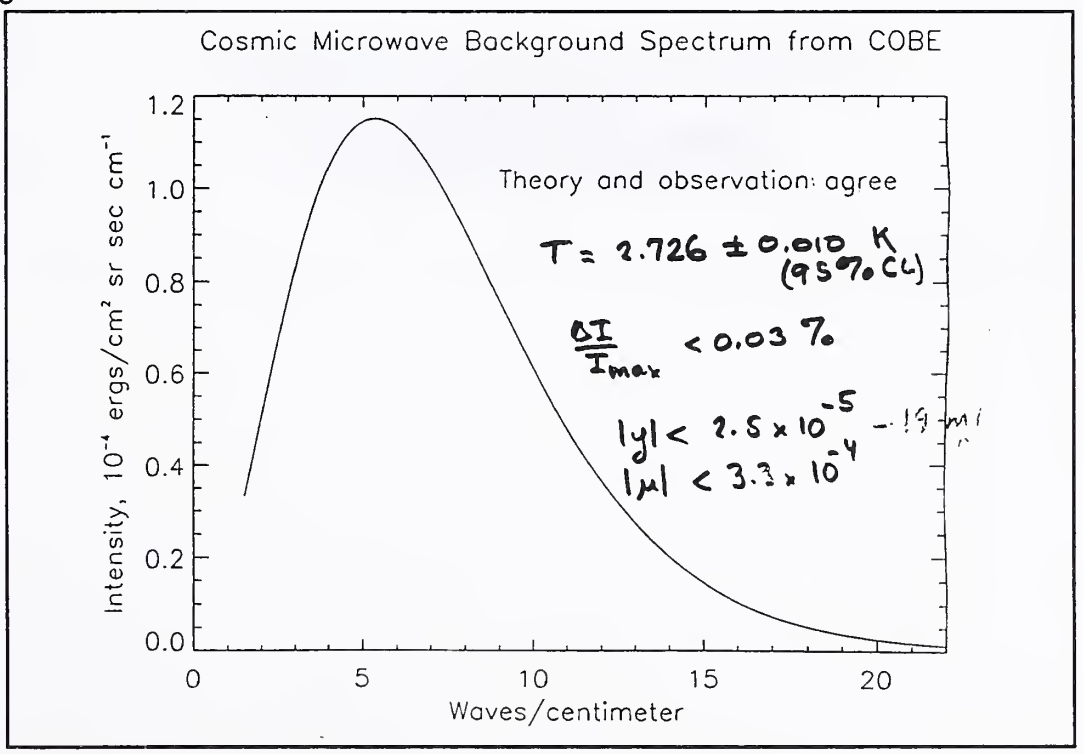

Figure 6

Laboratory Spectroscopy in the THz Region

Geoff Blake
California Institute of Technology

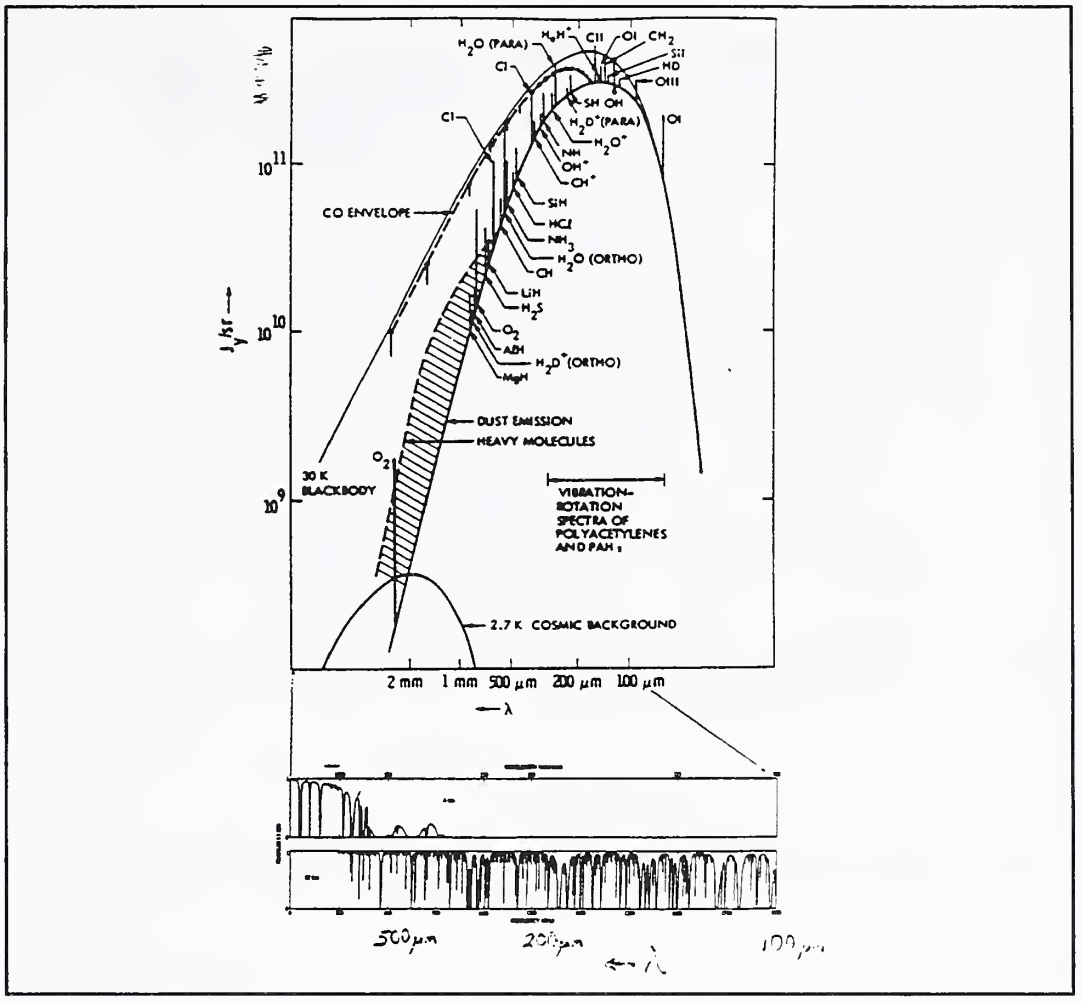
H_2O (PARA)
H_3O^+
CII
OI
CH_2
SII
HD
OIII
Cl
SH OH
H_2D^+(PARA)
H_2O^+
NH
OH^+
CH^+
SiH
HCl
NH_3
H_2O (ORTHO)
CH
LiH
H_2S
O_2
ABH
H_2D^+(ORTHO)
MgH
CO ENVELOPE
DUST EMISSION
HEAVY MOLECULES
30 K BLACKBODY
VIBRATION-ROTATION SPECTRA OF POLYACETYLENES AND PAH's
2.7 K COSMIC BACKGROUND
10^{11}
10^{10}
10^9
2 mm
1 mm
500 μm
200 μm
100 μm
λ
500μm
100μm

Figure 1

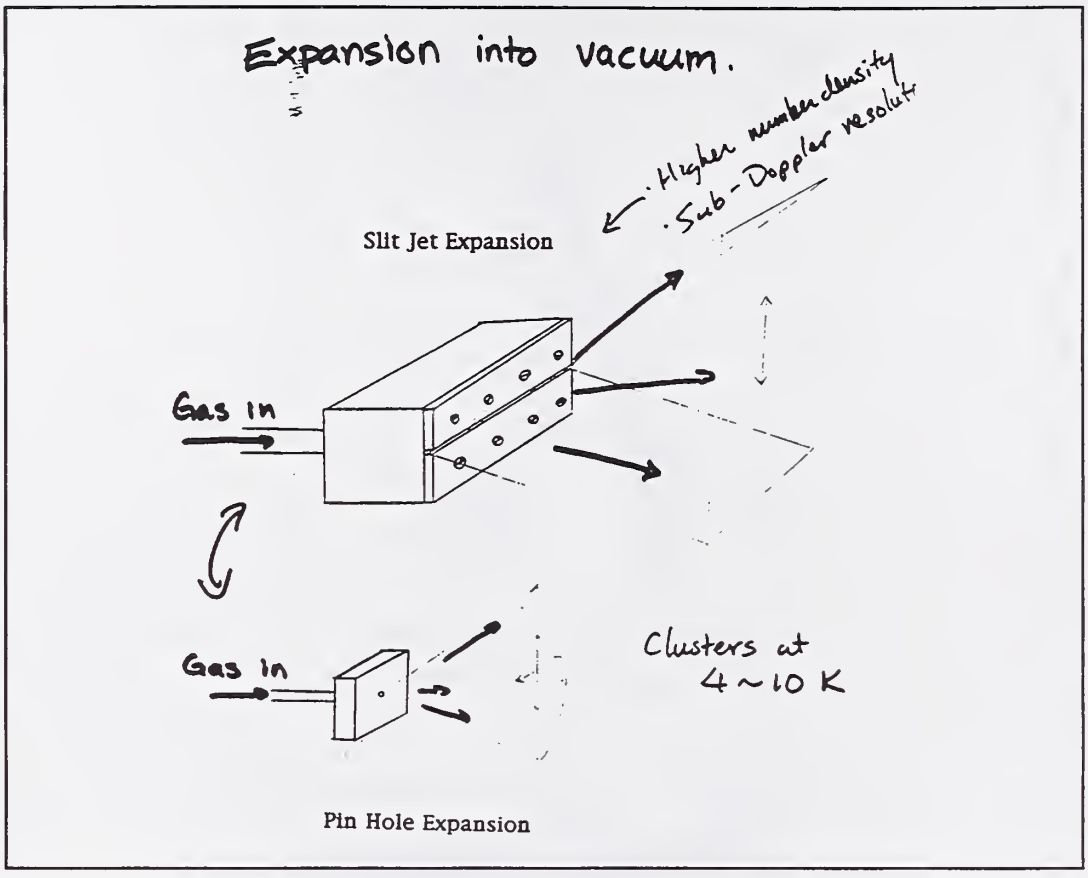
Expansion into vacuum.
· Higher number density
· Sub-Doppler resolution
Slit Jet Expansion
Gas in
Gas in
Clusters at
4 ~ 10 K
Pin Hole Expansion

Figure 2

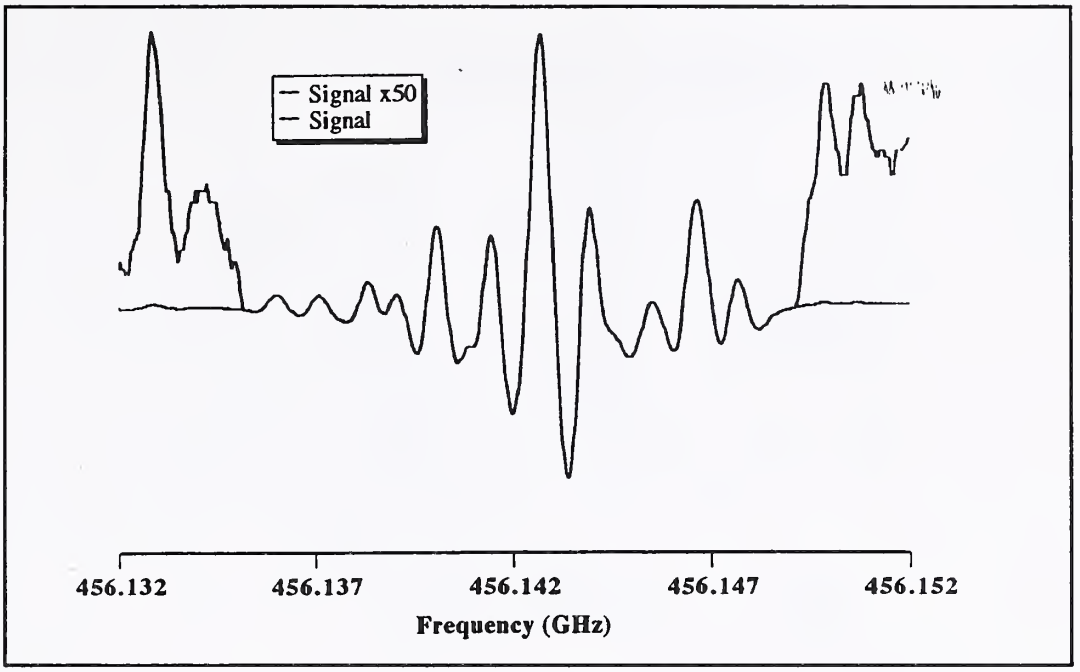
Signal x50
Signal
456.132
456.137
456.142
456.147
456.152
Frequency (GHz)

Figure 3

Summary of laser power necessary to obtain a minimum detectable fractional absorption of 1 part in 10^8 as a function of frequency in the far and near infrared.

ν		Power in 2×10^{16} Photons/s	Shot noise: P=1μW
100 GHz	3.3 cm^{-1}	2.7 μW	1.2×10^{-8}
300 GHz	10 cm^{-1}	4 μW	2×10^{-8}
1 THz	33 cm^{-1}	13 μW	3.6×10^{-8}
3 THz	100 cm^{-1}	40 μW	6.3×10^{-8}
10 THz	333 cm^{-1}	133 μW	1.1×10^{-7}
33 THz	1000 cm^{-1}	436 μW	2.1×10^{-7}
100 THz	3333 cm^{-1}	1450 μW	3.6×10^{-7}

Quant Limit

$$\frac{\Delta P}{P_0} = 2\left[\eta M^2 \left(\frac{P_0}{h\nu}\right)\tau\right]^{-1/2}$$

For $P_0 = 1\mu W$ $\eta = .25$ $M = .1$

$h\nu = 100\ cm^{-1}$

$$\frac{\Delta P}{P_0} \gtrsim 10^{-6} \quad \text{in } \tau = 1\ sec.$$

Figure 4

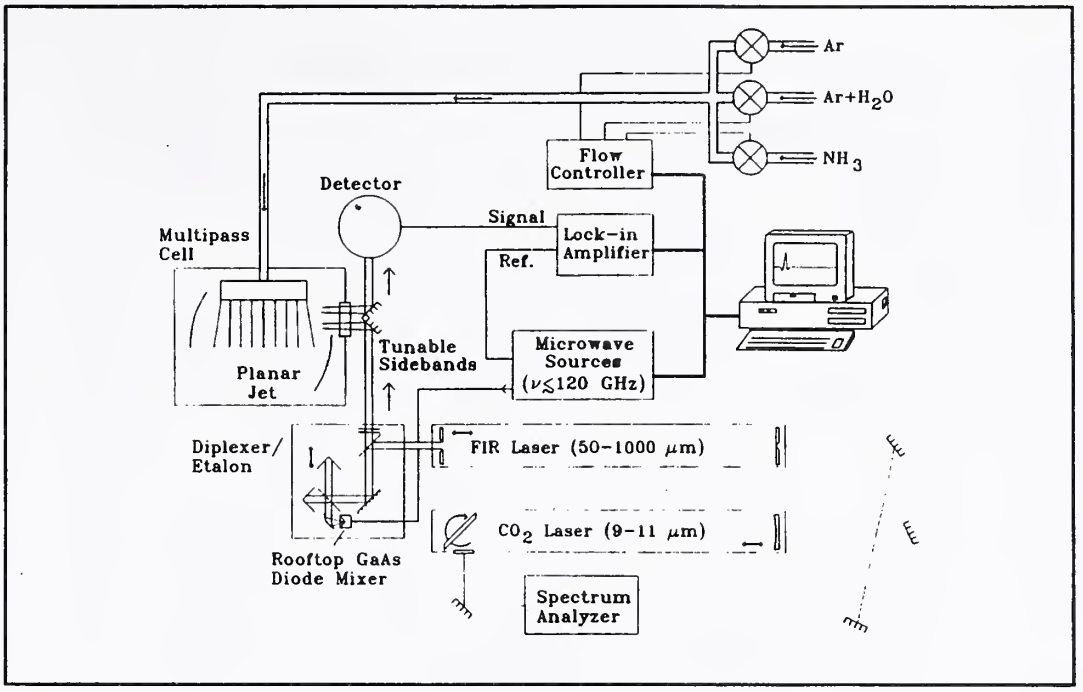

Figure 5

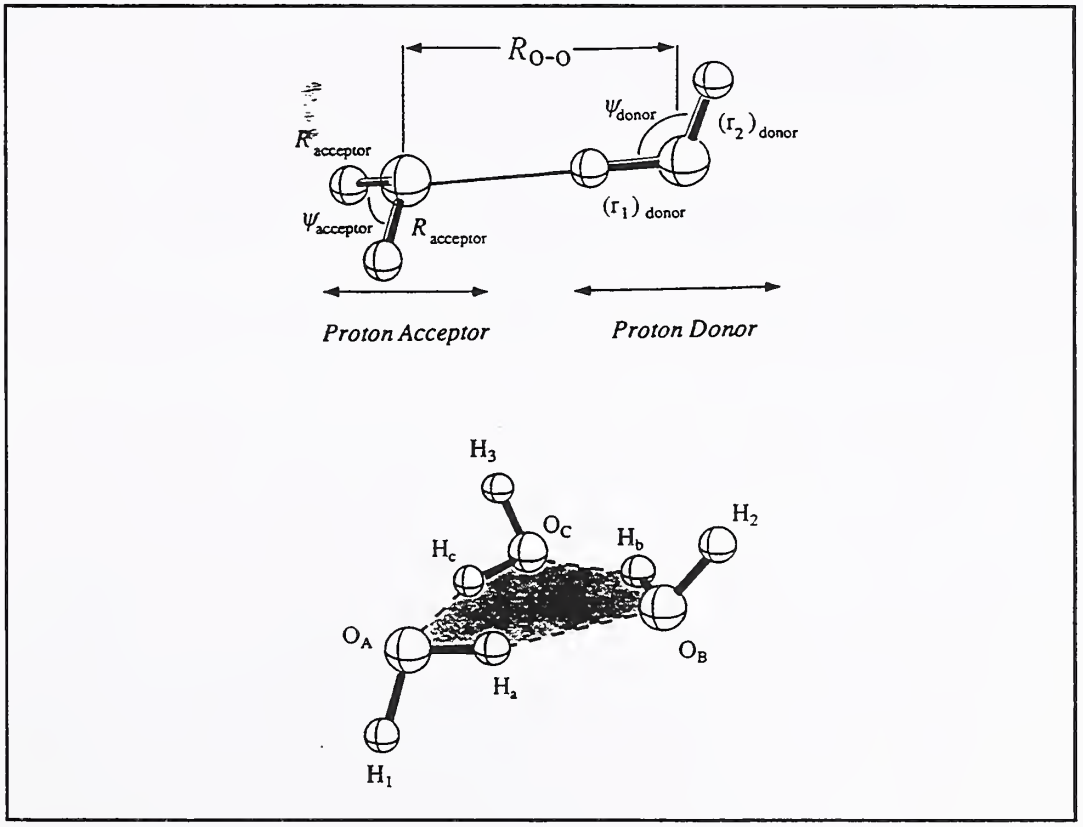

Figure 6

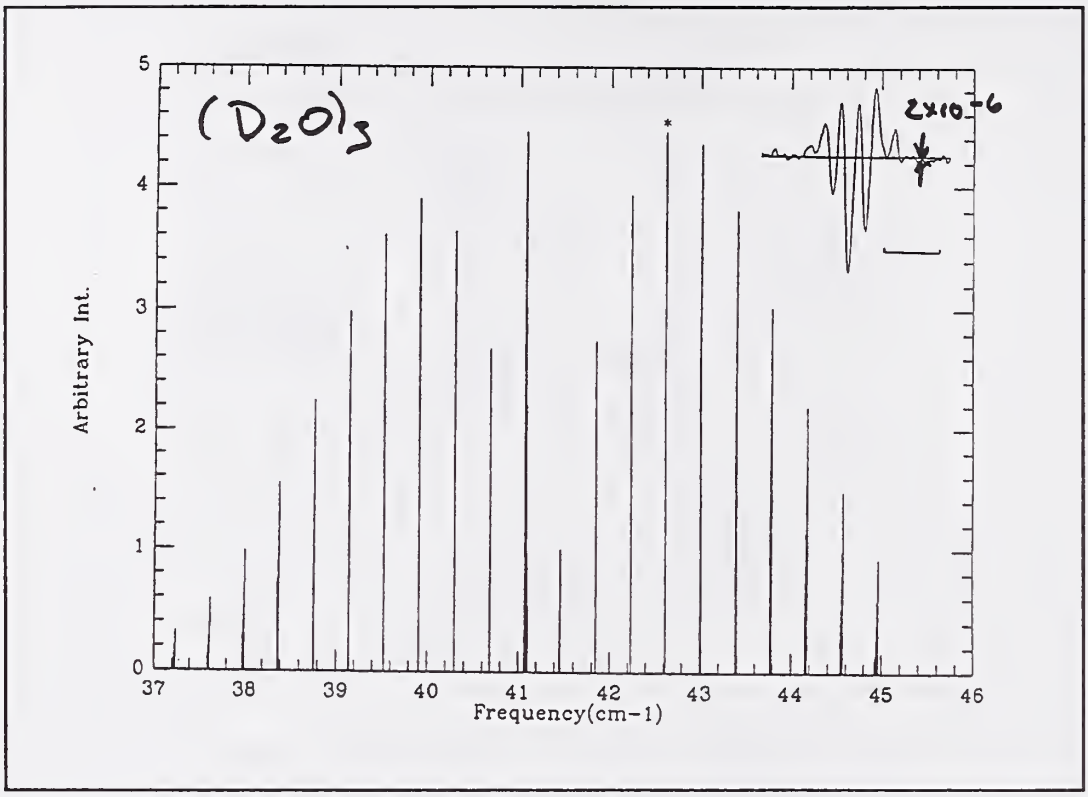
(D2O)3
2x10-6
Arbitrary Int.
0
1
2
3
4
5
37
38
39
40
41
42
43
44
45
46
Frequency(cm-1)

Figure 7

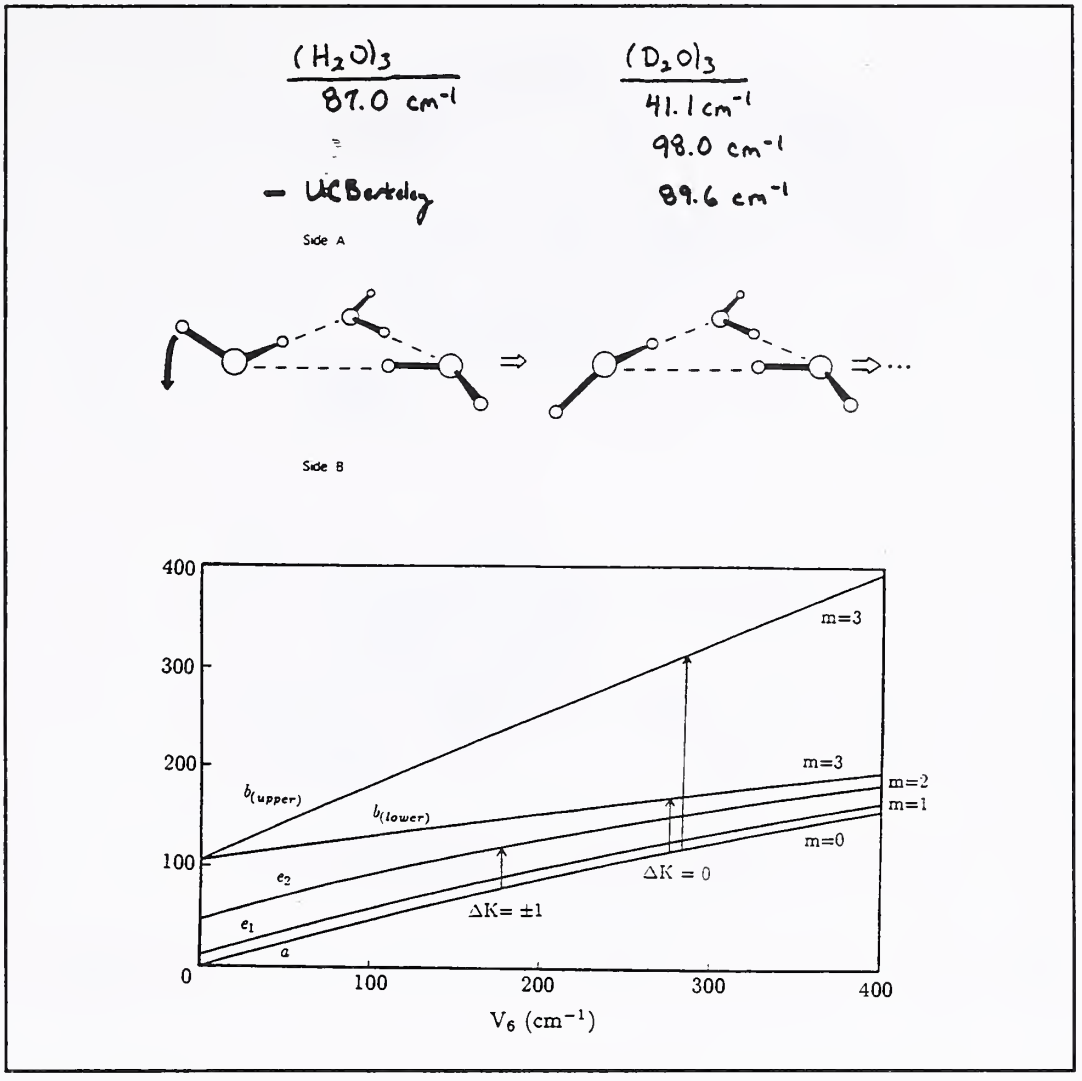
(H2O)3
87.0 cm-1
(D2O)3
41.1 cm-1
98.0 cm-1
89.6 cm-1
— UCBerkeley
Side A
Side B
400
300
200
100
0
100
200
300
400
V6 (cm-1)
m=3
m=3
m=2
m=1
m=0
b(upper)
b(lower)
e2
e1
a
ΔK= ±1
ΔK = 0

Figure 8

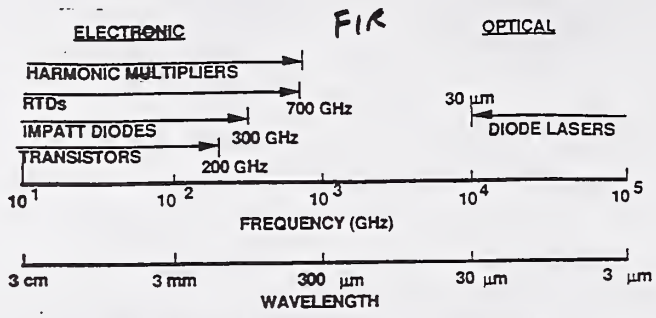

Fig. 1. Solid-state source technology in the far-infrared region.

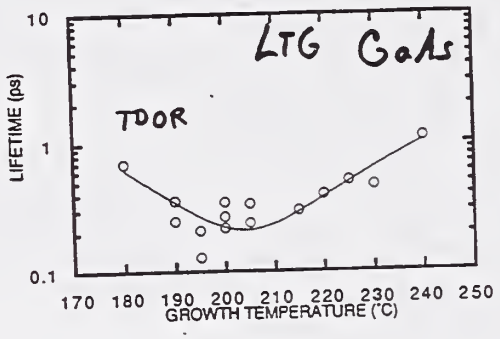

Figure 9

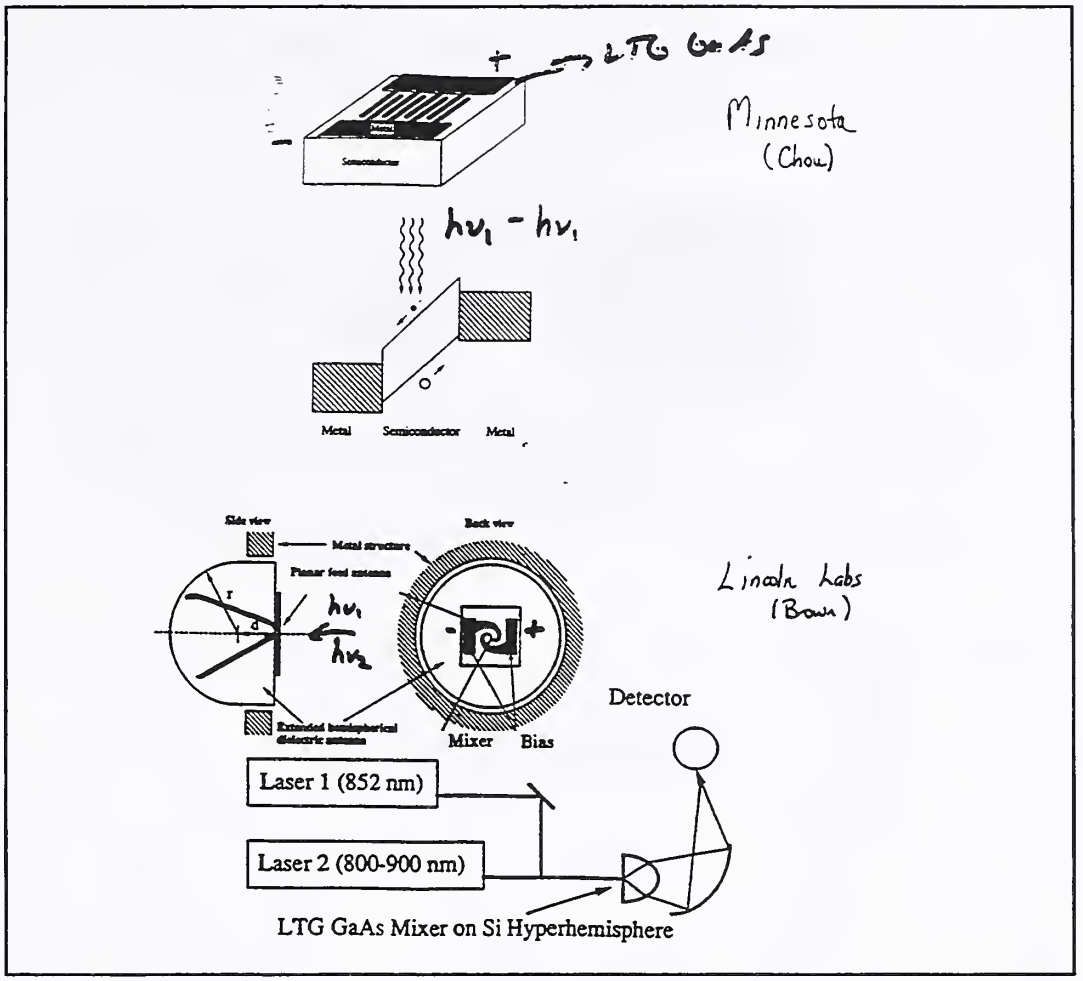
+
LTG GaAs
Minnesota
(Chou)
$h\nu_1 - h\nu_1$
Metal
Semiconductor
Metal
Side view
Back view
Metal structure
Planar feed antenna
$h\nu_1$
$h\nu_2$
Extended hemispherical dielectric antenna
Mixer
Bias
Lincoln Labs
(Brown)
Detector
Laser 1 (852 nm)
Laser 2 (800-900 nm)
LTG GaAs Mixer on Si Hyperhemisphere

Figure 10

Brown et al. 1994, SPIE vol. 2145A

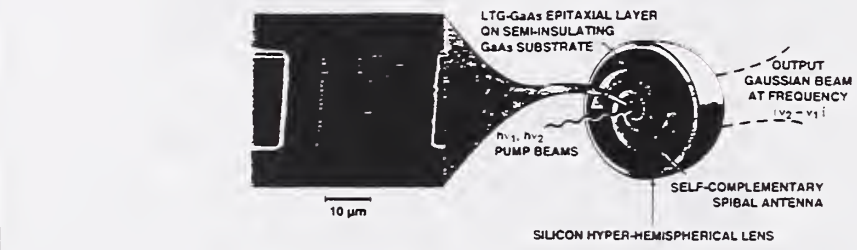

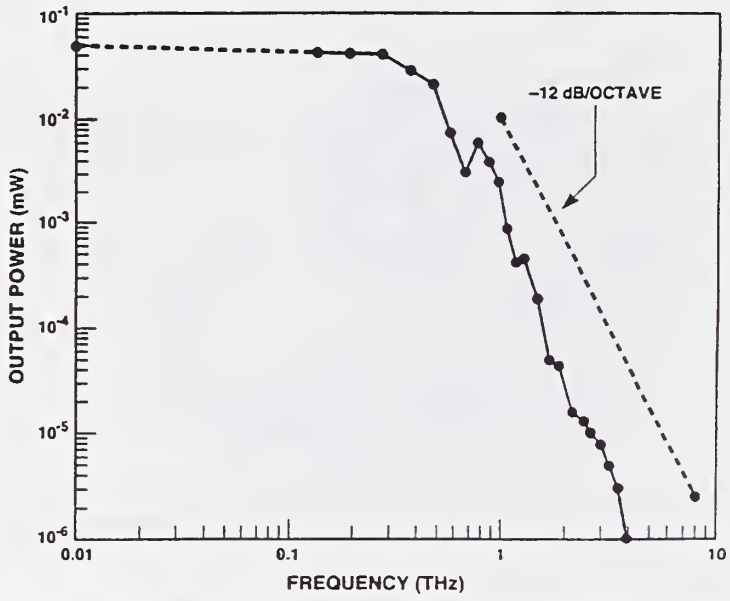

Figure 11

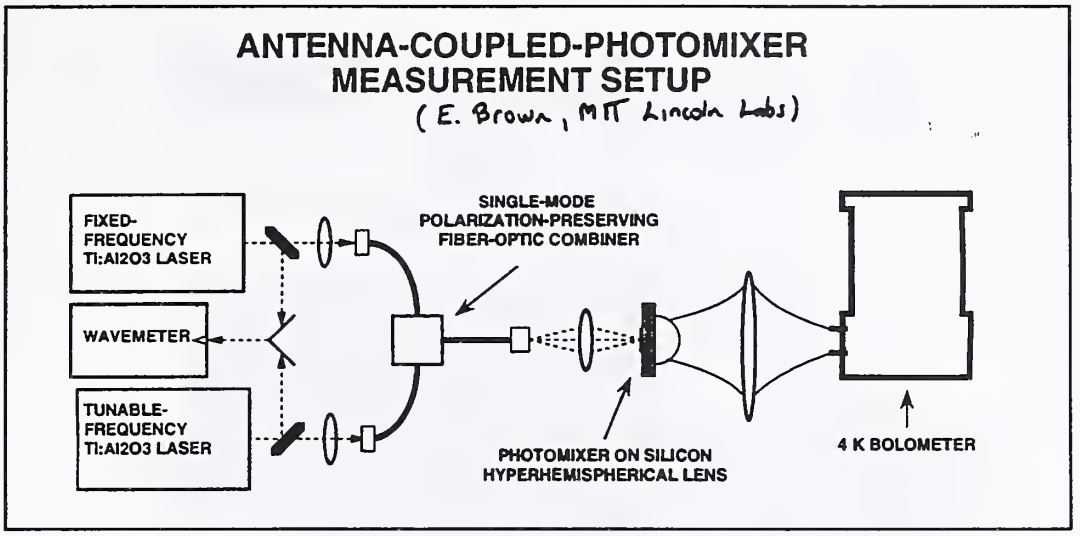

Figure 12

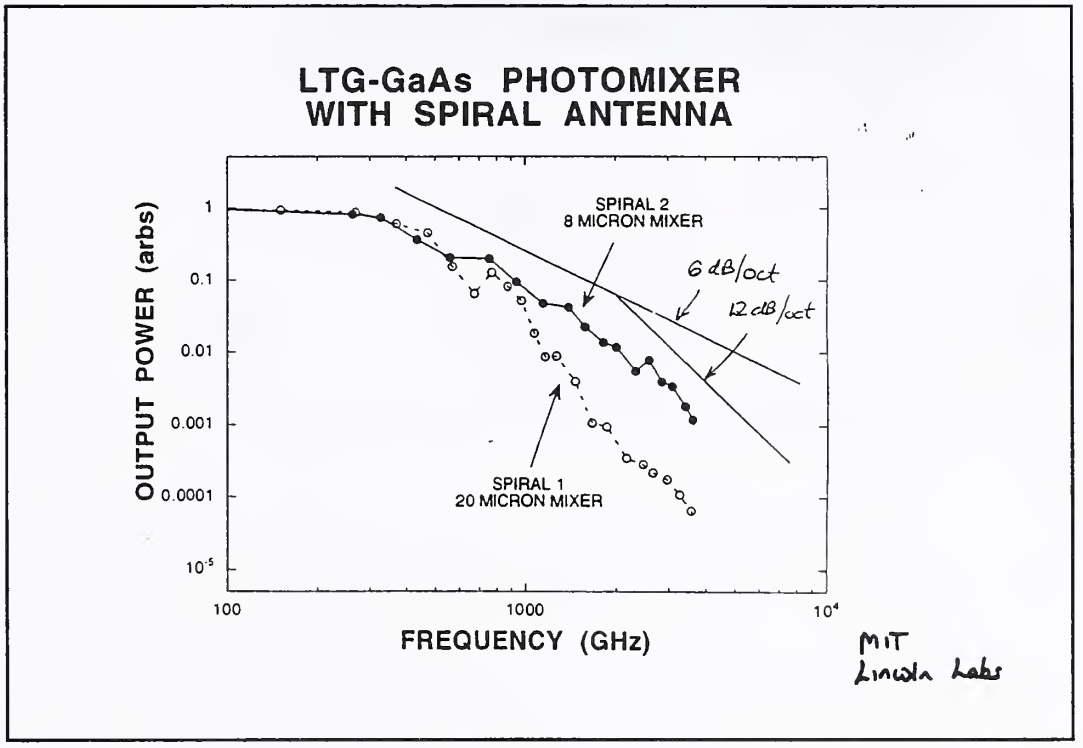

Figure 13

PRELIMINARY DATA SHEET

100 mW cw Distributed Bragg Reflector Laser Diodes

SDL™-5700 SERIES
SDL™-6700 SERIES

Features

- **852 nm or 1083 nm**
- **Up to 100 mW cw Power at 852 nm**
- **Up to 50 mW cw Power at 1083 nm**
- **25 dB Sidemode Suppression**
- **3 MHz Spectral Width**
- **Cs or He Pump Source**

High power distributed Bragg reflector (DBR) laser diodes provide frequency stable optical power for excitation of cesium vapor in atomic clocks or helium in magnetometers. The DBR structure nearly eliminates spectral shifts due to external optical feedback and provides a stable wavelength precisely tuned to the electronic transition.

Fabry-Perot cavity laser diodes are readily available at the absorption wavelengths of Cs or He. However, optical feedback from external surfaces or minor environmental changes cause mode hops or spectral shifts and a reduction of pump efficiency. The SDL-5700 Series DBR laser diode provides both the power of Fabry-Perot laser diodes and the spectral stability required for optical pumping of atomic transitions.

A GaAlAs strained layer active region allows low threshold and operating current for the 852 nm devices, while strained InGaAs provides the active layer for 1083 nm lasers. A grating reflector determines the stable wavelength. The wavelength is repeatable at turn-on.

The SDL-5700 Series DBR laser diodes are available in TO-3 packages with internal thermoelectric cooler. Output power of 10 mW cw or 100 mW cw are available options. The SDL-6700 Series laser diodes are available with an output power of 50 mW cw.

SDL

Figure 14

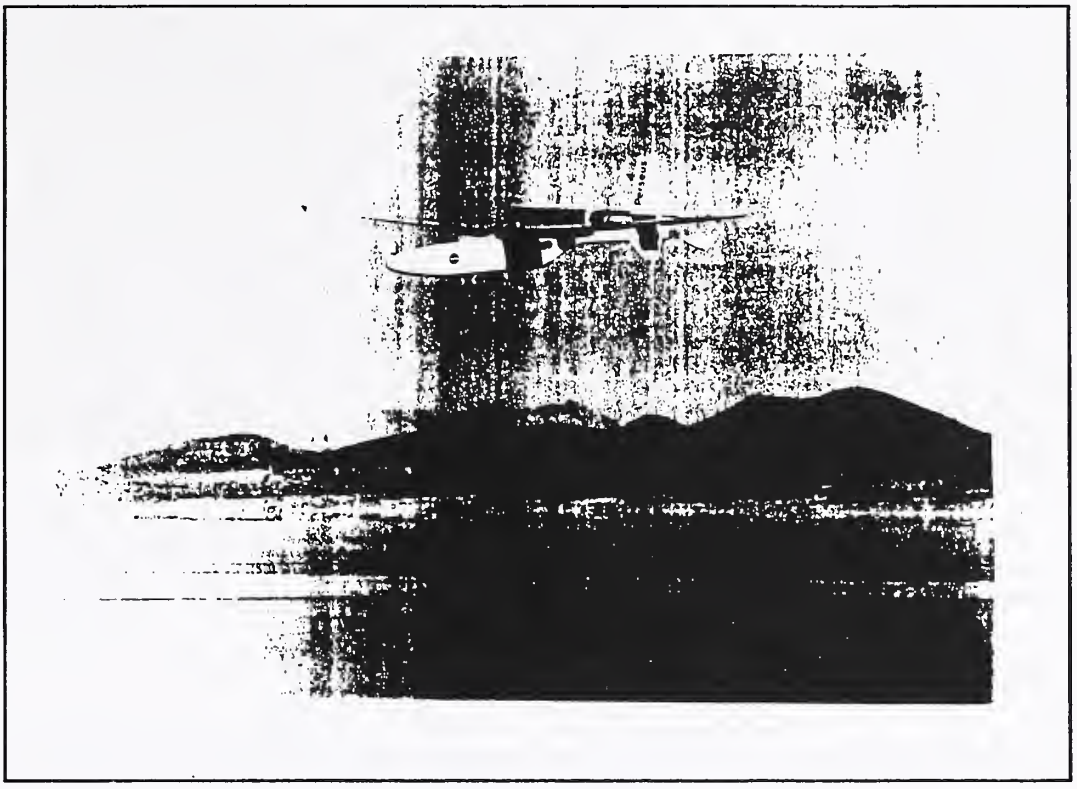

Figure 15

Characterization of Material Properties at Terahertz Frequencies

Robert H. Giles
Submillimeter Technology Laboratory
University of Massachusetts, Lowell

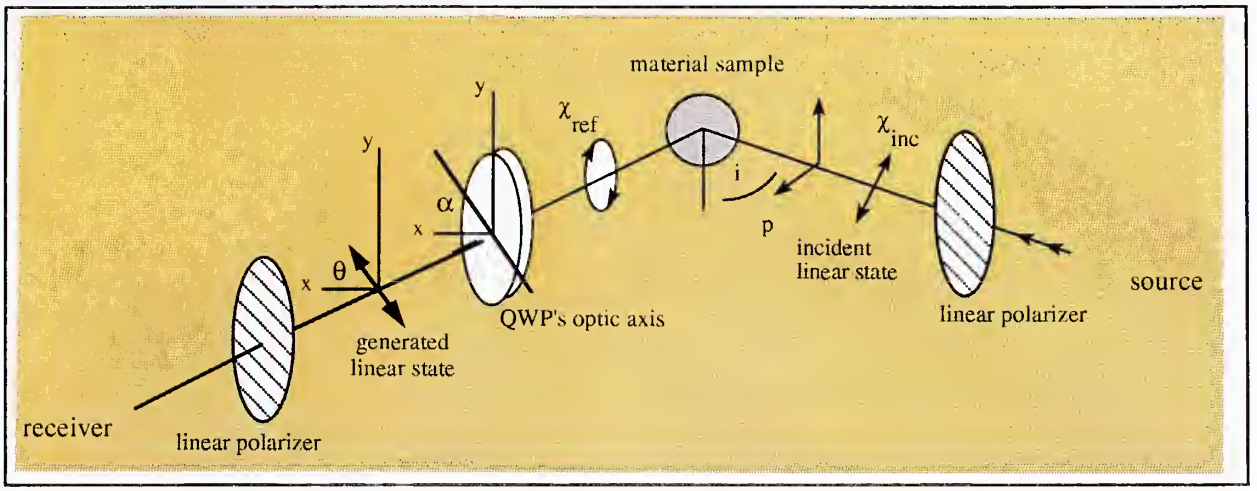

Figure 1. The ellipsometric measurement technique using a quarter-wave plate.

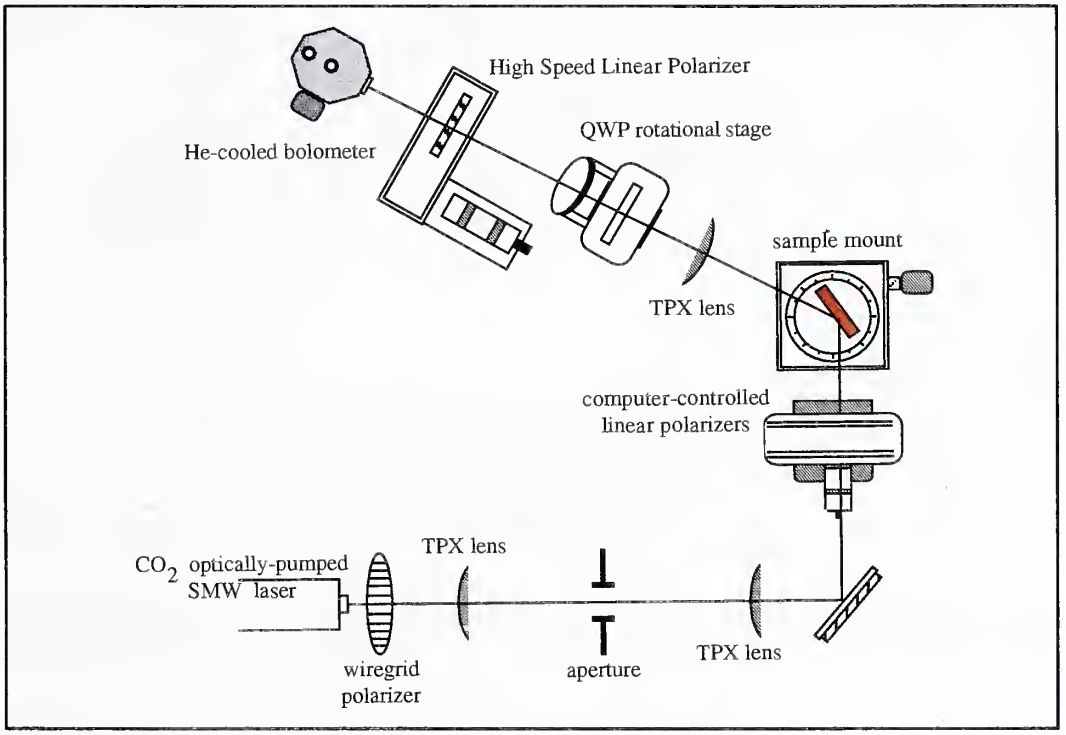

Figure 2. STL's automated submillimeter-wave ellipsometric measurement system.

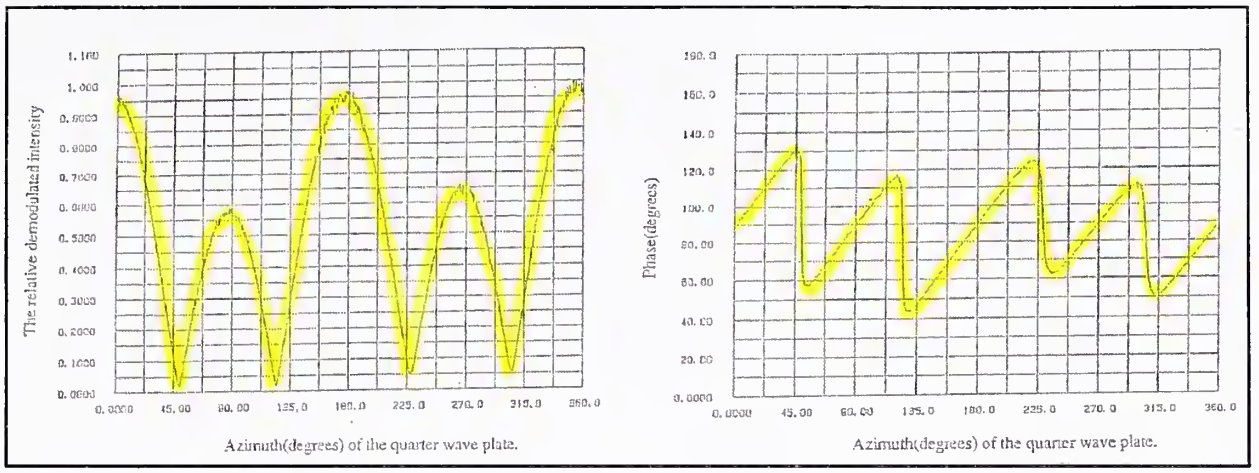

Figure 3. The demodulated intensity as a function of the QWP's azimuth.

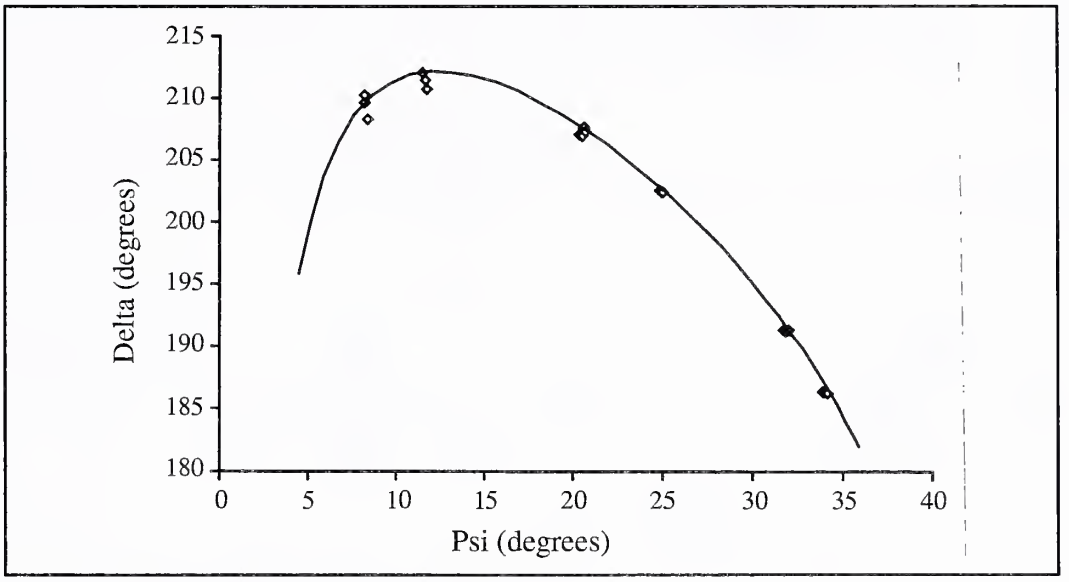

Figure 4. Ellipsometric measurement of high purity silicon at a wavelength of 513.0157μm.

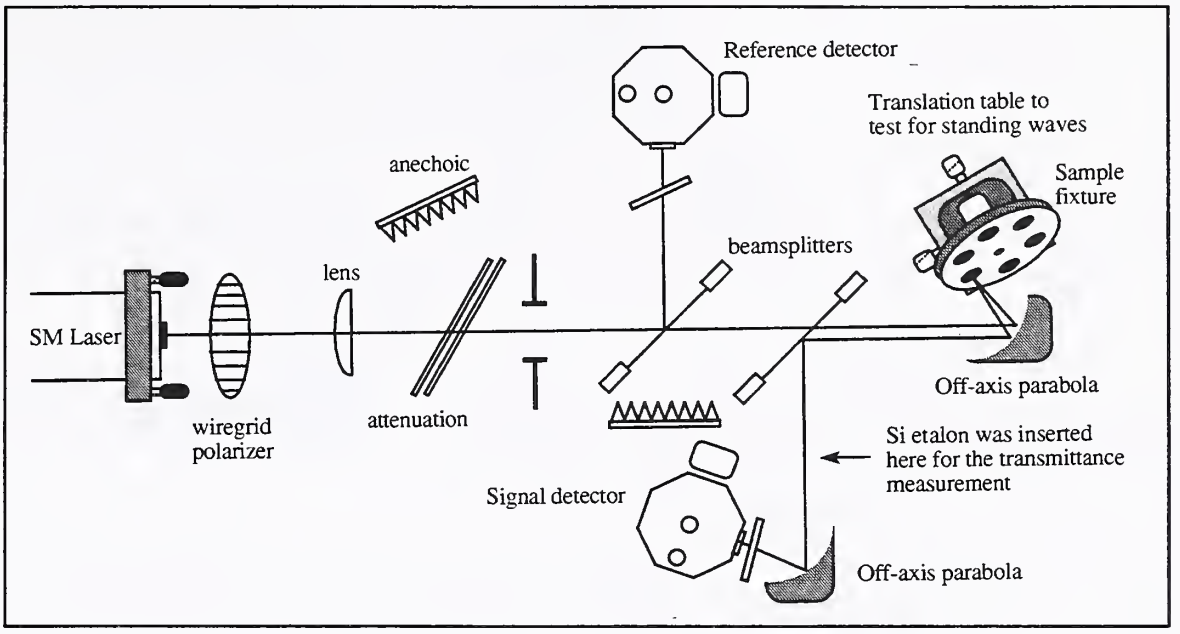

Figure 5. STL's Submillimeter-Wave Reflectometer.

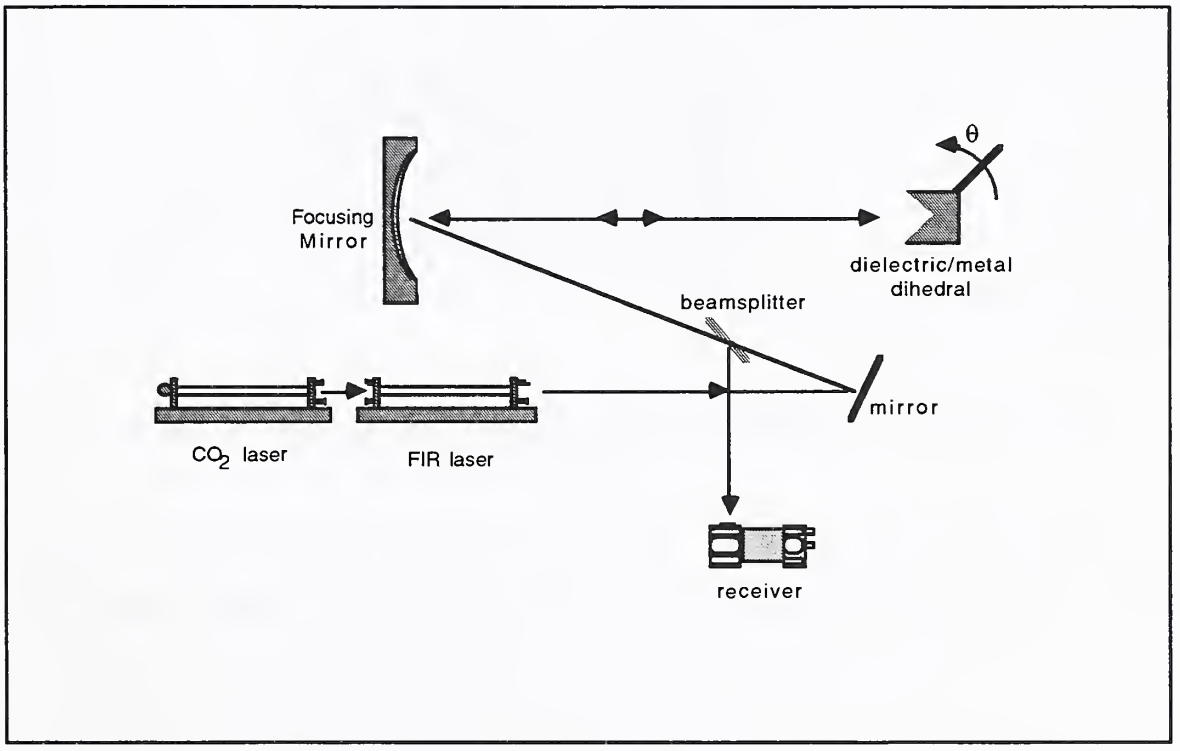

Figure 6. STL's Laser-Based Brewster's Angle Measurement System

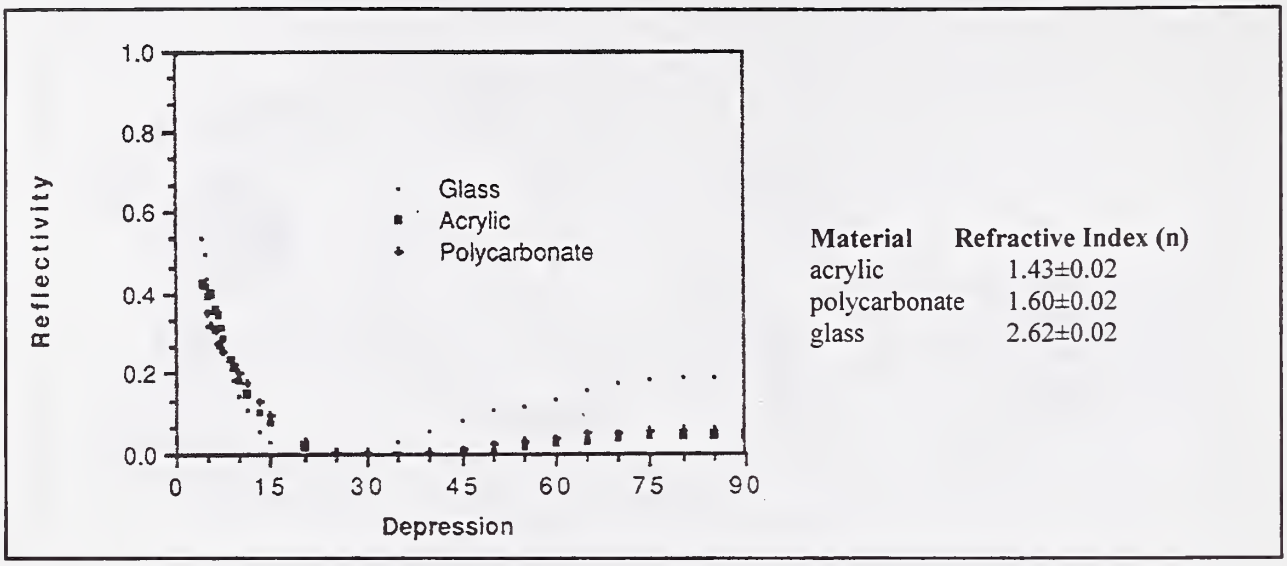

Figure 7. The measured reflectivity as a function of incident angle for three materials at 1.5 THz.

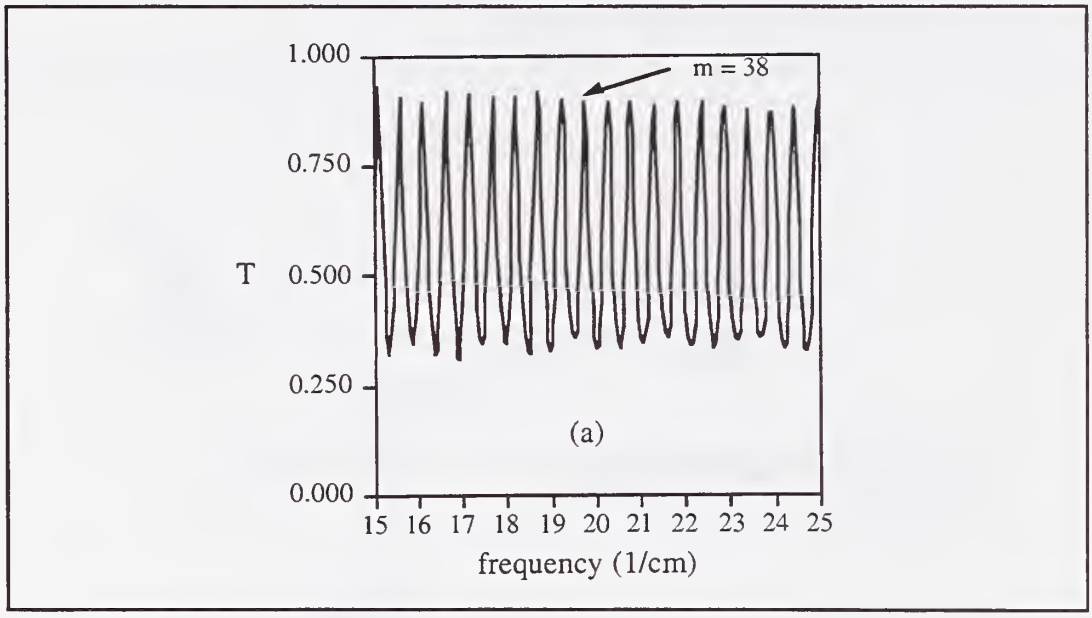

Figure 8. Locating a transmission peak in far-infrared Fourier transform spectroscopy data.

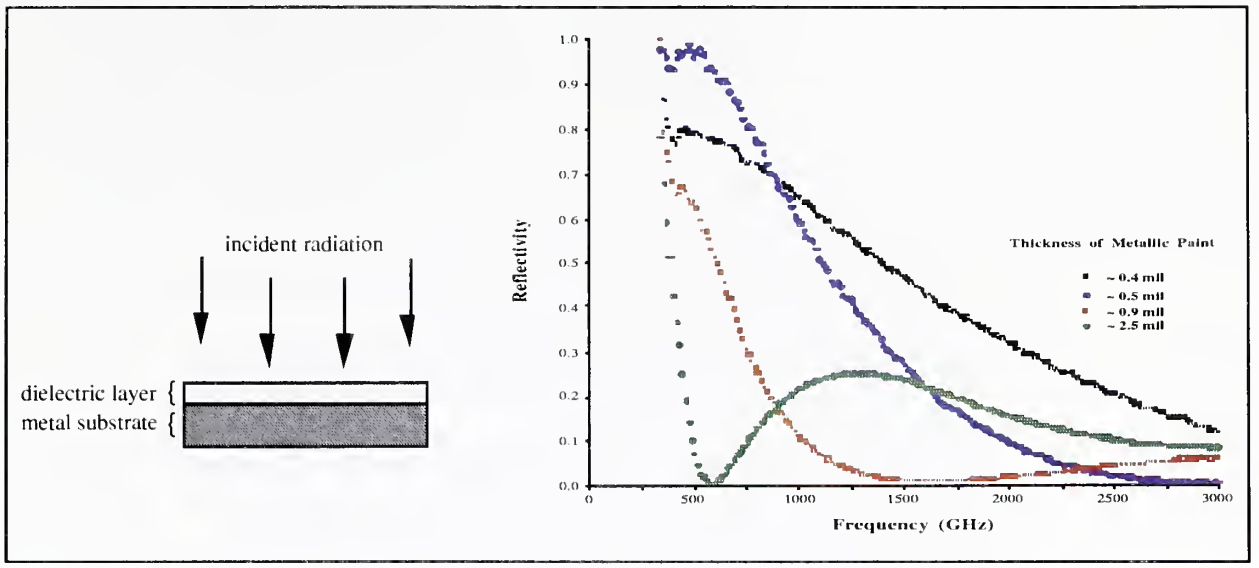

Figure 9. The reflectivity for four Dällenbach layers with a constant loading ratio.

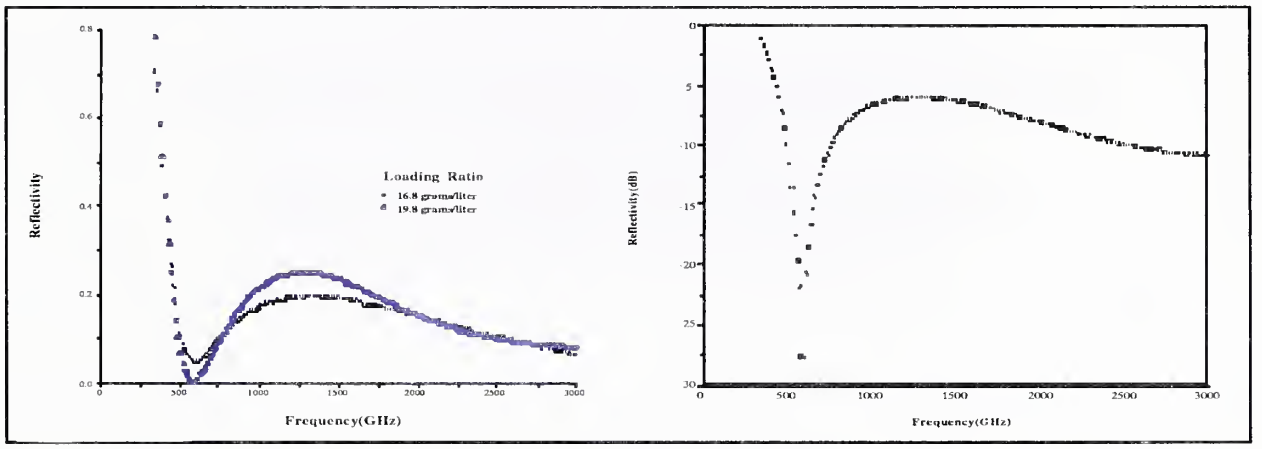

Figure 10. The reflectivity of a Dällenbach layer optimized for performance at 0.584 THz.

Planar Antennas, Power Meters, and Calibration Techniques at Terahertz Frequencies

Gabriel M. Rebeiz
Electrical Engineering/Computer Science Department
University of Michigan, Ann Arbor

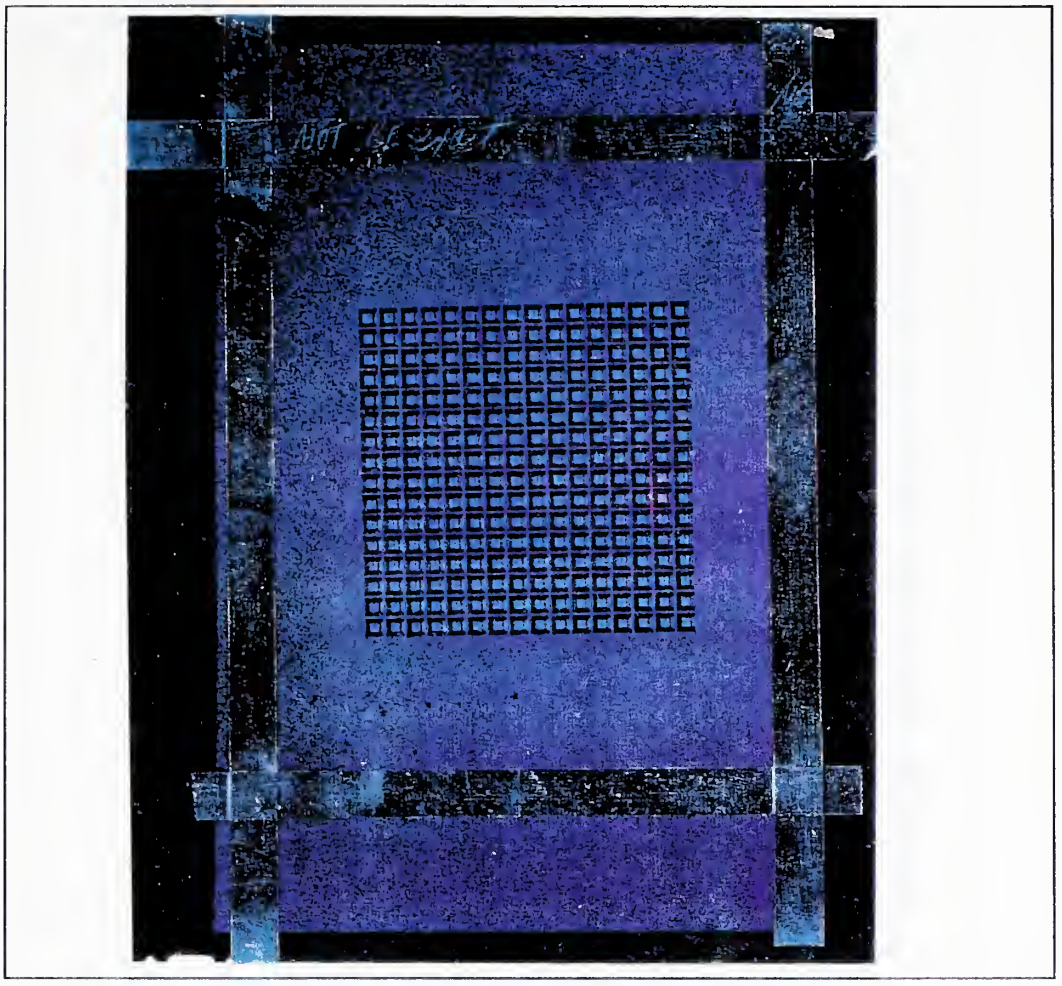

Figure 1

CSTT

OPTIMIZATION OF INTEGRATED HORN ANTENNAS

Double-Polarized Designs (-23dB isolation at 93 GHz):

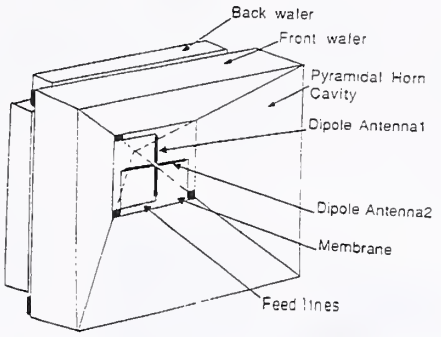

256-Element 802 GHz Imaging Array:

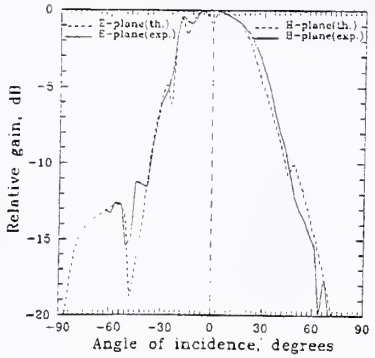

Figure 2

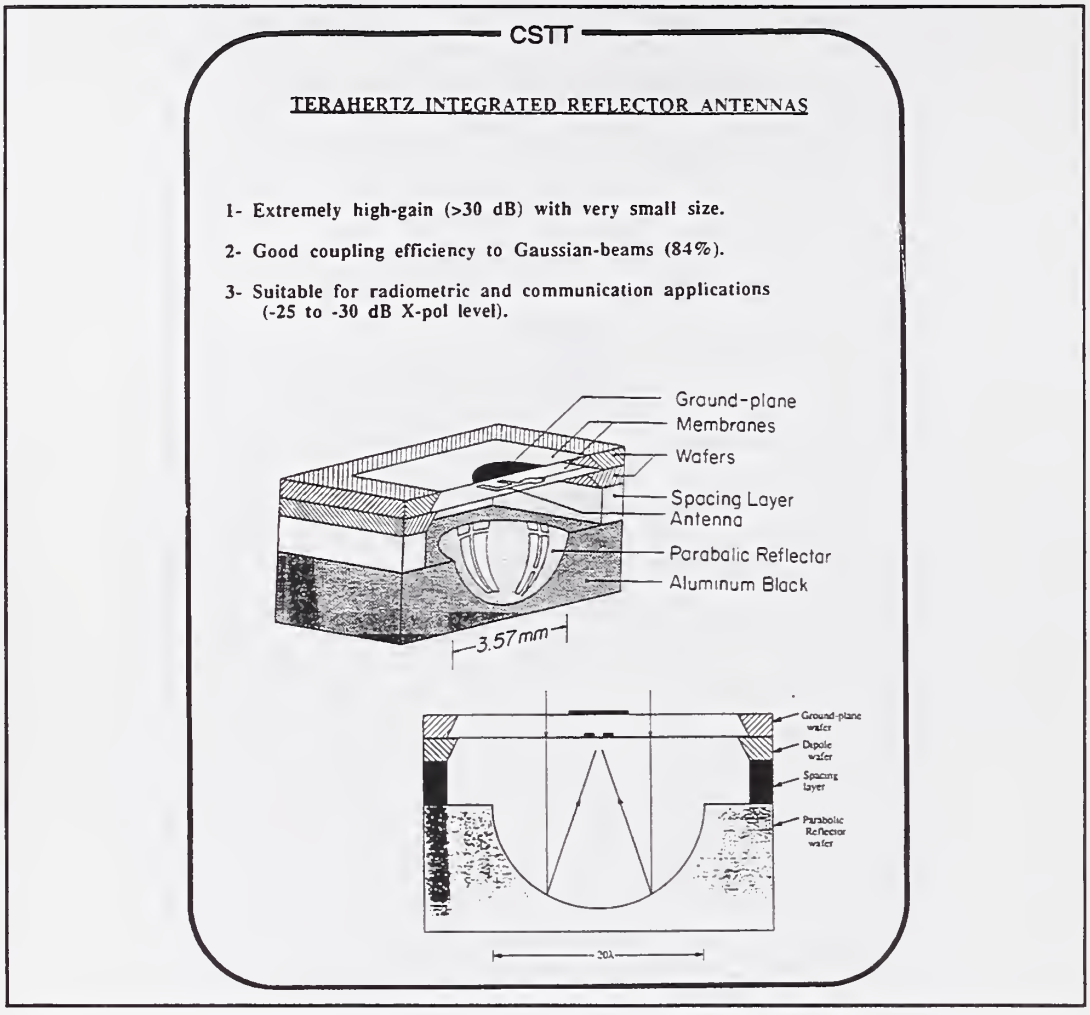
CSTT
TERAHERTZ INTEGRATED REFLECTOR ANTENNAS
1- Extremely high-gain (>30 dB) with very small size.
2- Good coupling efficiency to Gaussian-beams (84%).
3- Suitable for radiometric and communication applications (-25 to -30 dB X-pol level).
Ground-plane
Membranes
Wafers
Spacing Layer
Antenna
Parabolic Reflector
Aluminum Black
3.57mm
Ground-plane wafer
Dipole wafer
Spacing layer
Parabolic Reflector wafer
2λ

Figure 3

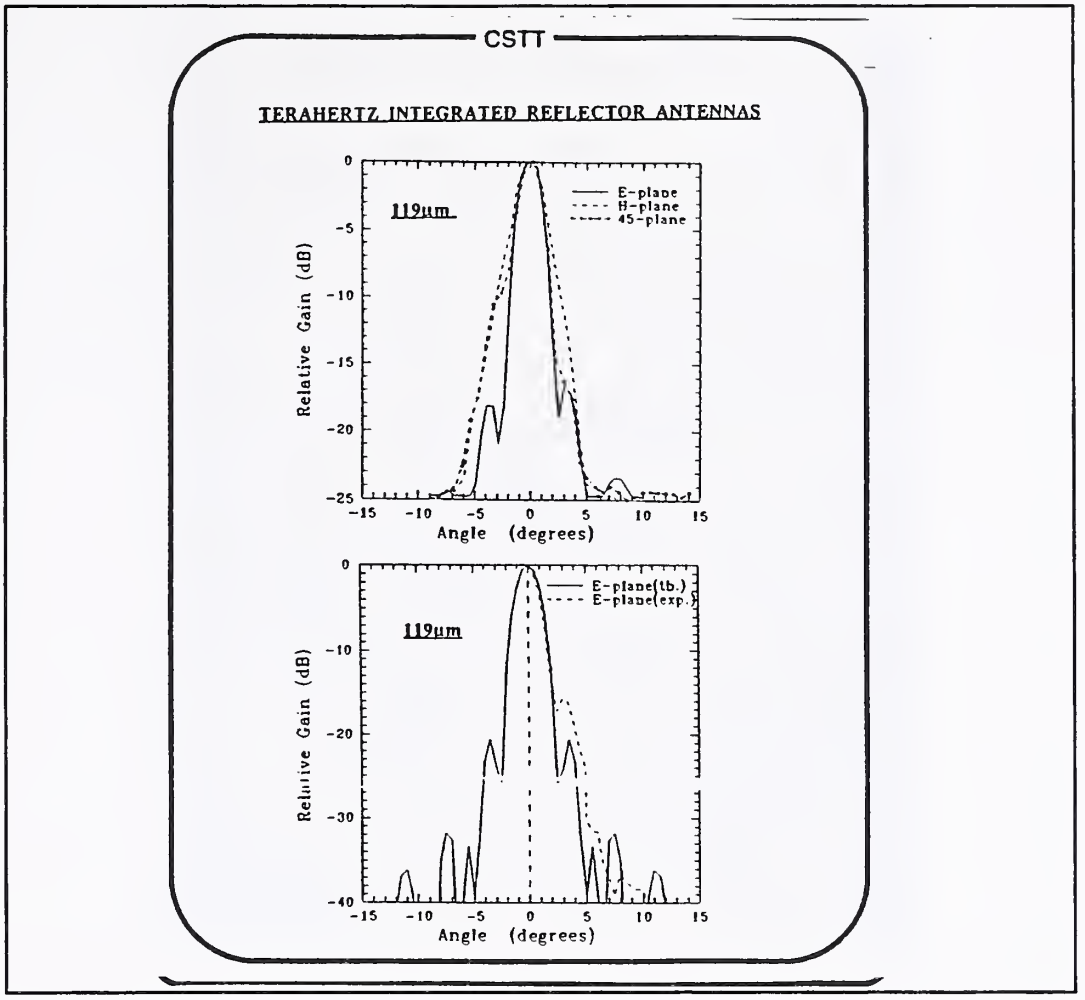
CSTT
TERAHERTZ INTEGRATED REFLECTOR ANTENNAS
119μm
E-plane
H-plane
45-plane
Relative Gain (dB)
Angle (degrees)
119μm
E-plane(th.)
E-plane(exp.)
Relative Gain (dB)
Angle (degrees)

Figure 4

Figure 5

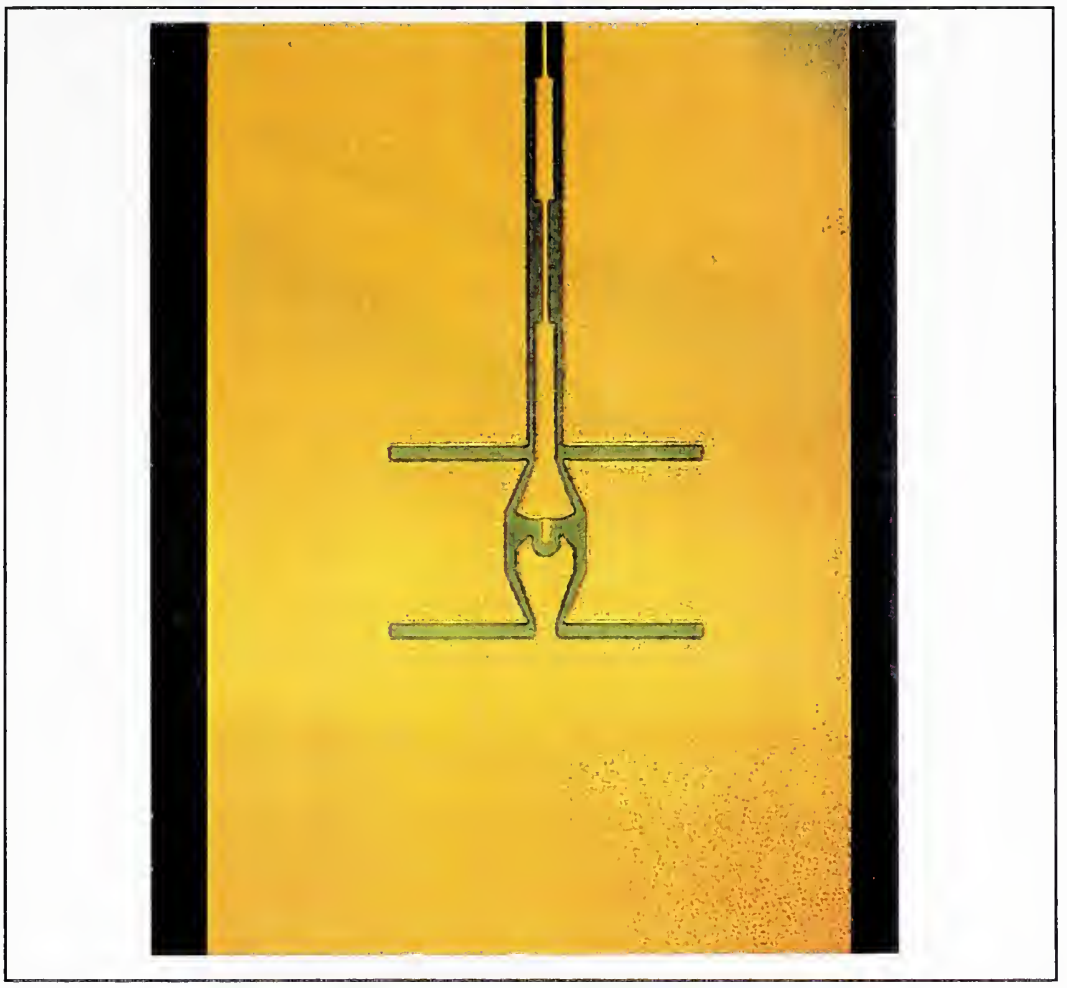

Figure 6

Figure 7

Figure 8

Antenna Gain Calibration

Two Antenna (or Three Antenna) Method:

$$Gt + Gr = 20 \log\left(\frac{4\pi R}{\lambda}\right) + 10 \log\left(\frac{Pr}{Pt}\right)$$

Problems:

- Cannot accurately measure vswr at transmit and receive ports.
- Cannot make two identical antennas.
- Standard gain (SG) antennas not yet available

Candidate for SG:

- Wideband self-complementary antennas such as log-periodic or spiral antennas.
- Z_{ant} = real = 189Ω in free space.
- Pattern is nearly same with frequency

The University of Michigan

Figure 9

Antenna Gain Calibration

Radiometric Method:

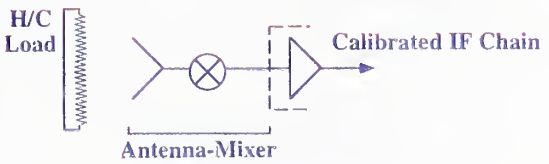

Problems:
- How good is absorber at Terahertz frequencies? (Effective temperature)
- Very hard to separate antenna performance from mixer (impedance mismatch, losses in antenna or mixer, ...)

Useful:
- Determine entire antenna-mixer performance (i.e front-end performance)
- Accuracy limited by absorber parameters

The University of Michigan

Figure 10

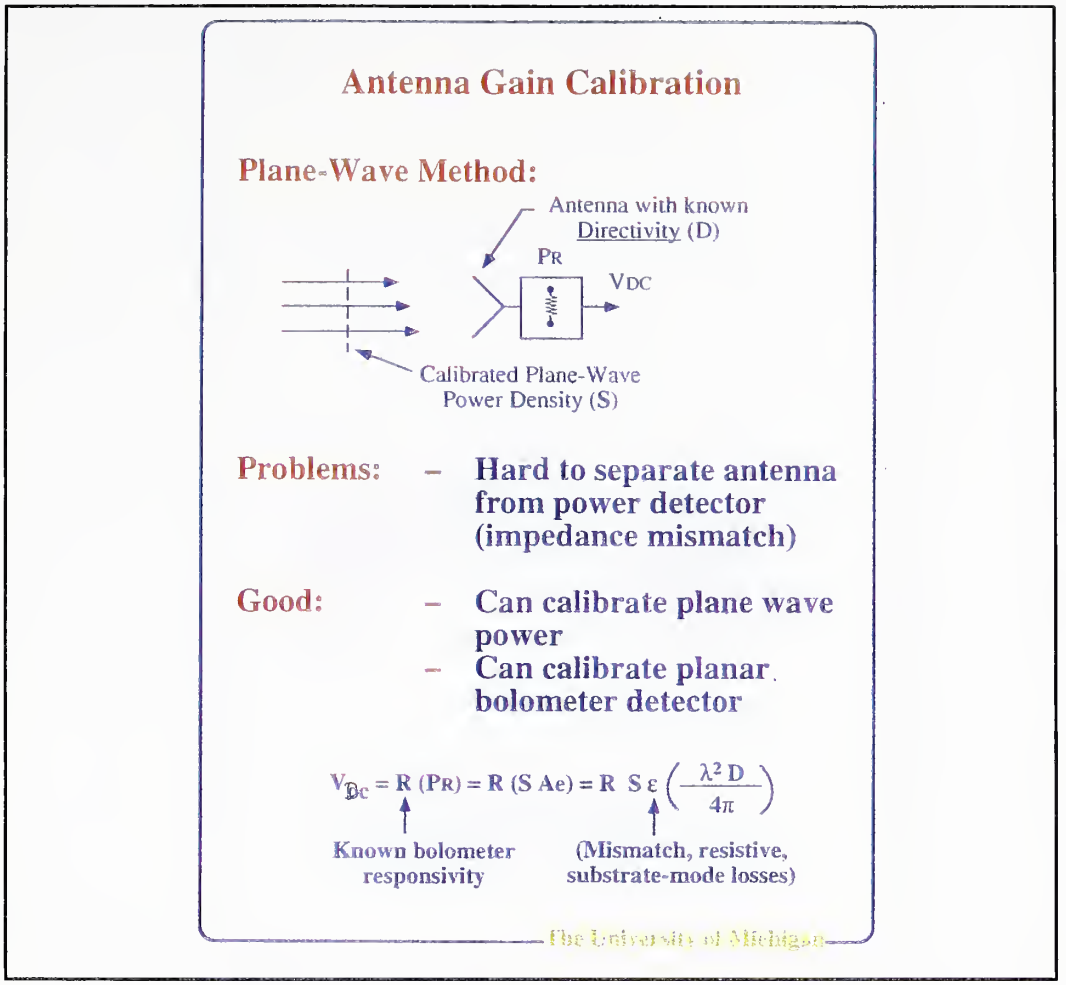
Antenna Gain Calibration
Plane-Wave Method:
Antenna with known
Directivity (D)
PR
VDC
Calibrated Plane-Wave
Power Density (S)
Problems:
– Hard to separate antenna from power detector (impedance mismatch)
Good:
– Can calibrate plane wave power
– Can calibrate planar bolometer detector
VDC = R (PR) = R (S Ae) = R S ε (λ² D / 4π)
Known bolometer responsivity
(Mismatch, resistive, substrate-mode losses)
The University of Michigan

Figure 11

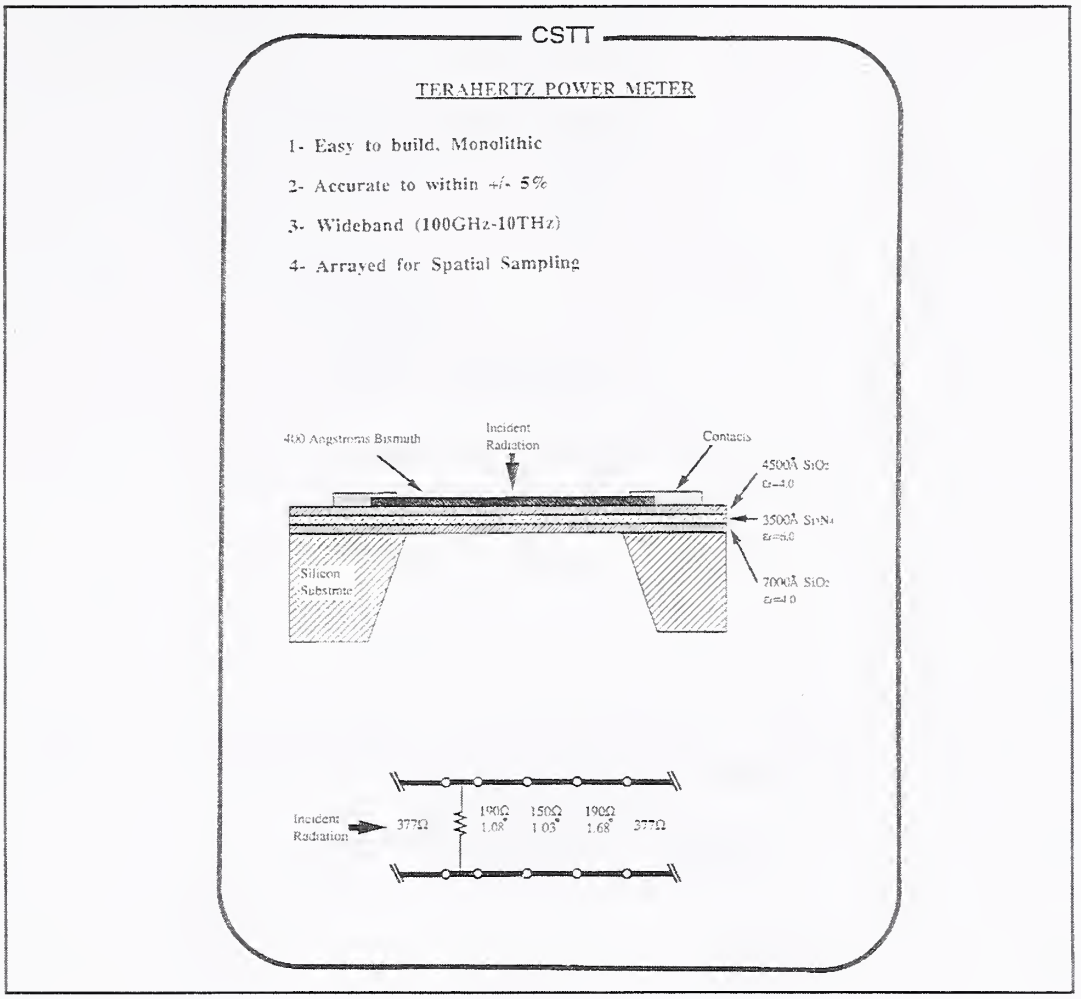
CSTT
TERAHERTZ POWER METER
1- Easy to build, Monolithic
2- Accurate to within +/- 5%
3- Wideband (100GHz-10THz)
4- Arrayed for Spatial Sampling
400 Angstroms Bismuth
Incident Radiation
Contacts
4500Å SiO2
εr=4.0
3500Å Si3N4
εr=8.0
7000Å SiO2
εr=4.0
Silicon Substrate
Incident Radiation
377Ω
190Ω
1.08°
150Ω
1.03°
190Ω
1.68°
377Ω

Figure 12

Optoelectronic Measurement Techniques

Harold Fetterman
Electrical Engineering Department
University of California, Los Angeles

OUTLINE

- **Picosecond Measurements**
  - A) Devices
  - B) Superconductivity
- **Generation**
  - A) Picosecond
  - B) Mixing
  - C) Mode Locked Systems
- **Optical Uses and Measurement Needs**
  - A) Transmission of Signals
  - B) Communications
- **Conclusion**

Figure 1

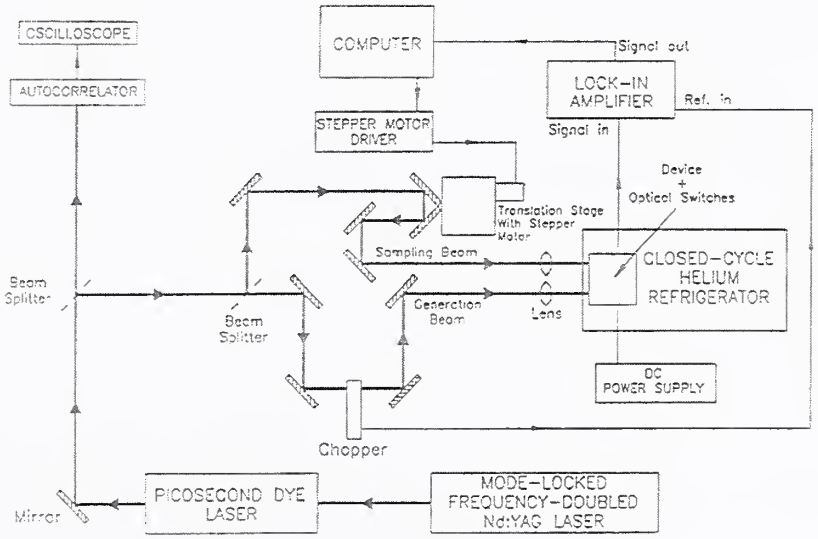

Figure 2

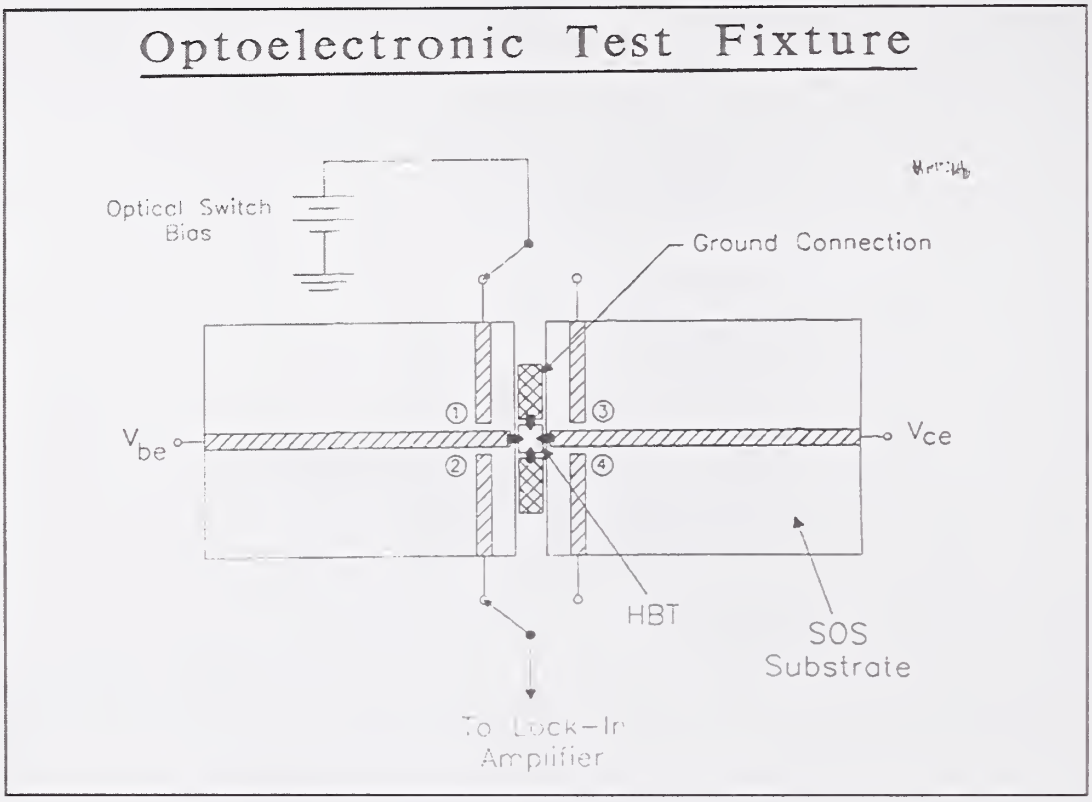
Optoelectronic Test Fixture
Optical Switch Bias
Ground Connection
V_{be}
V_{ce}
①
②
③
④
HBT
SOS Substrate
To Lock-In Amplifier

Figure 3

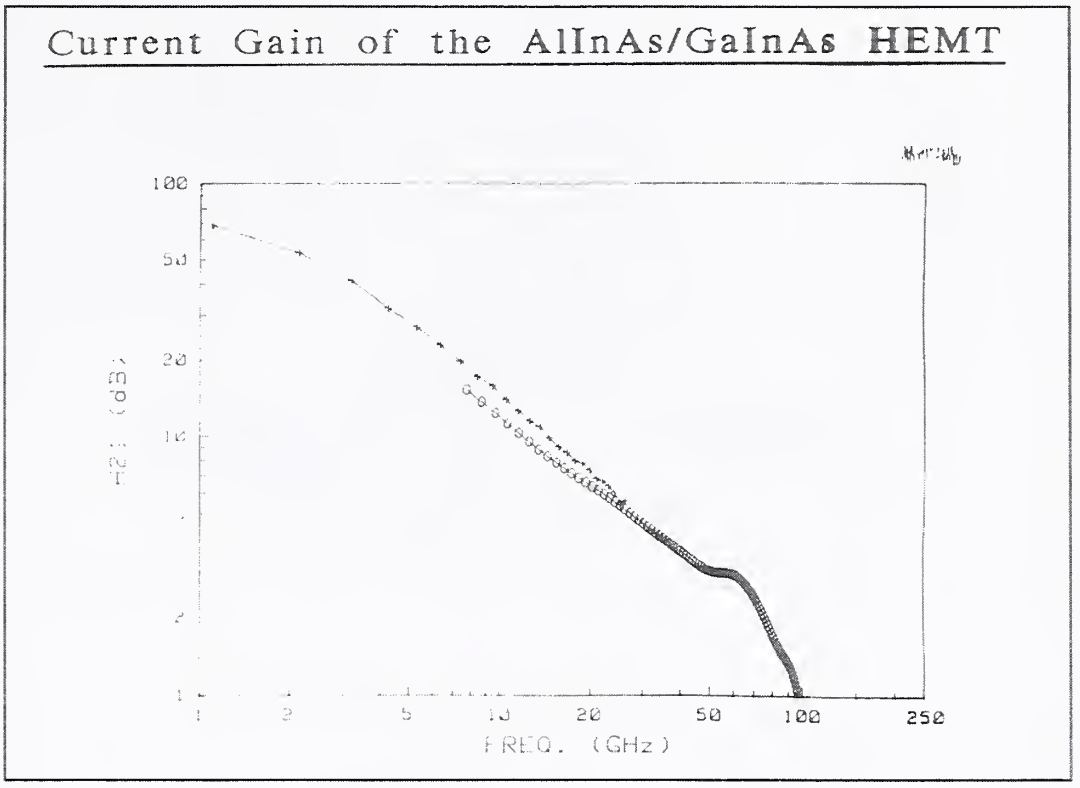

Figure 4

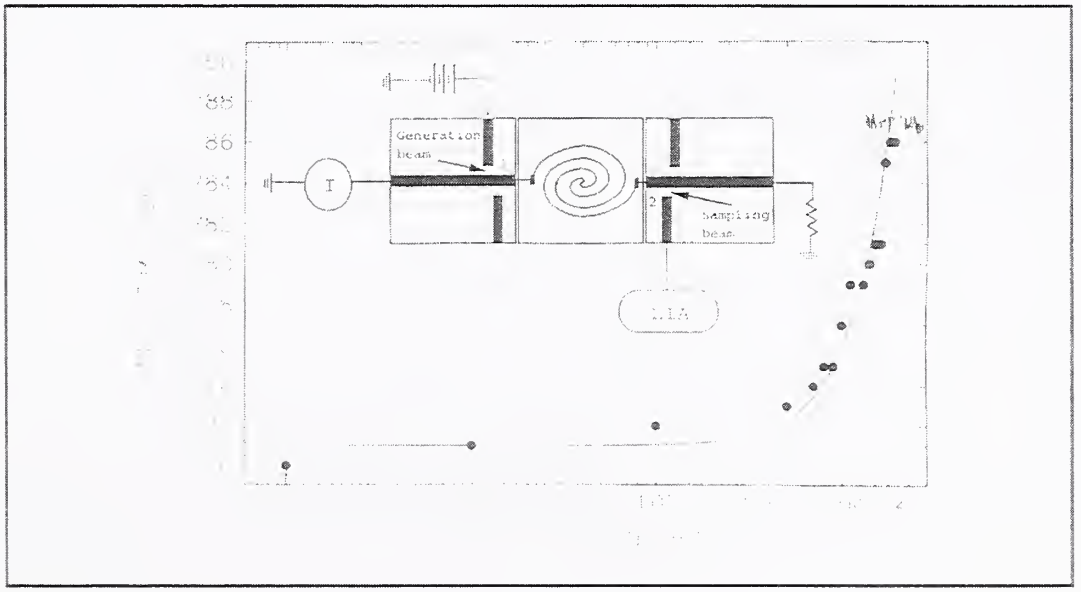

Figure 5

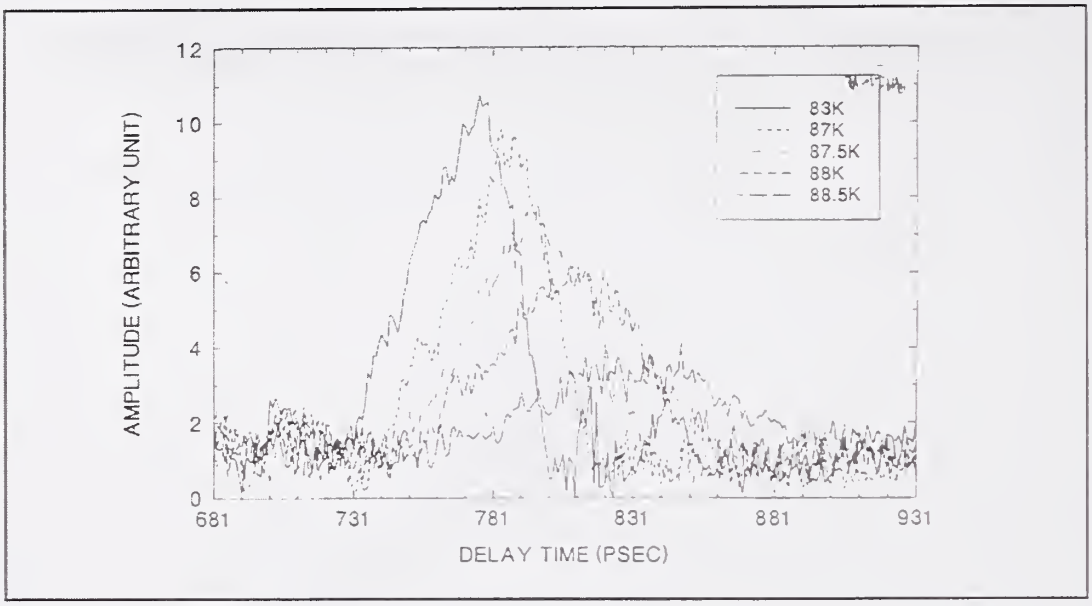

Figure 6

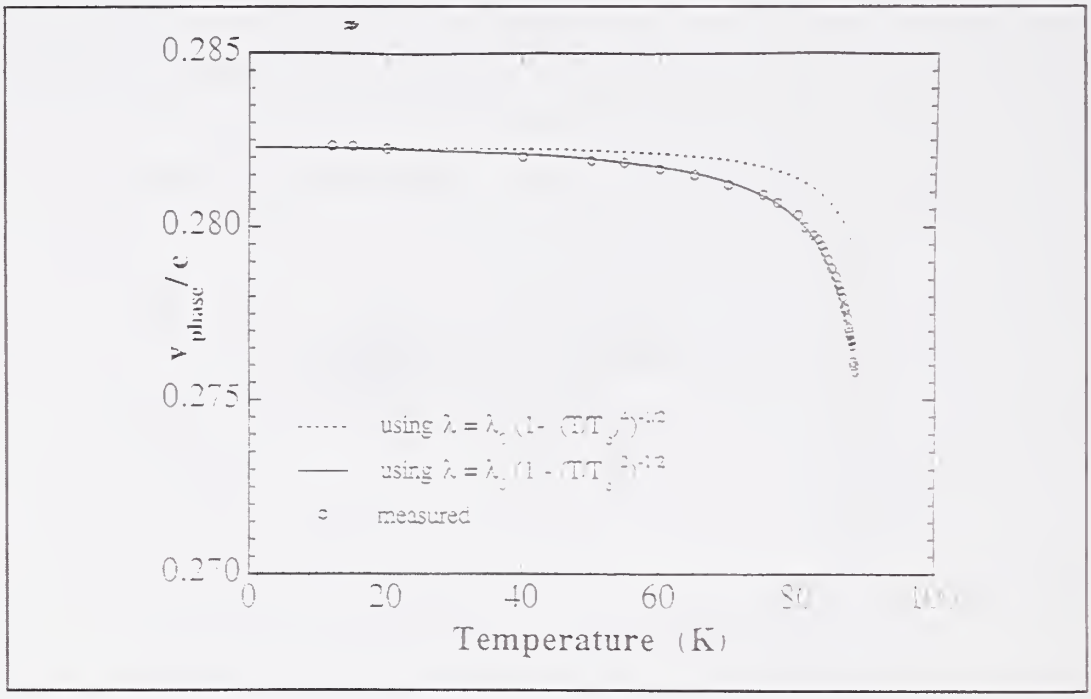

Figure 7

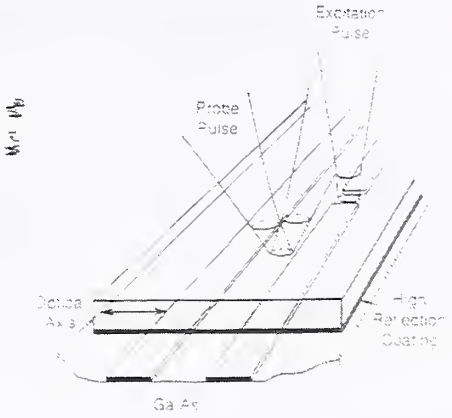

FIG. 20 A transverse superstrate-type modulator placed over coplanar transmission lines on a GaAs photoconductor. The excitation pulse passes through a region in the dielectric crystal with no HR coating, while the probing pulses are reflected back to the sampling crystal. (Figure courtesy of K. Meyer, University of Rochester.)

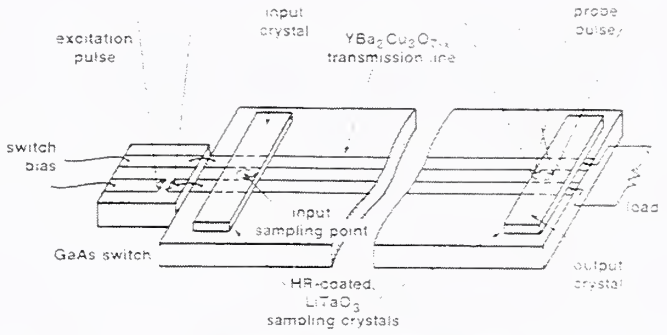

FIG. 21 The [illegible] electro-optic sampling of electrical signals on a superconducting transmission line. A photoconductive switch provides the input signal, which is then measured by two optical pulses at the beginning and end of the line. (Figure courtesy of D. Dykaar, [illegible])

Figure 8

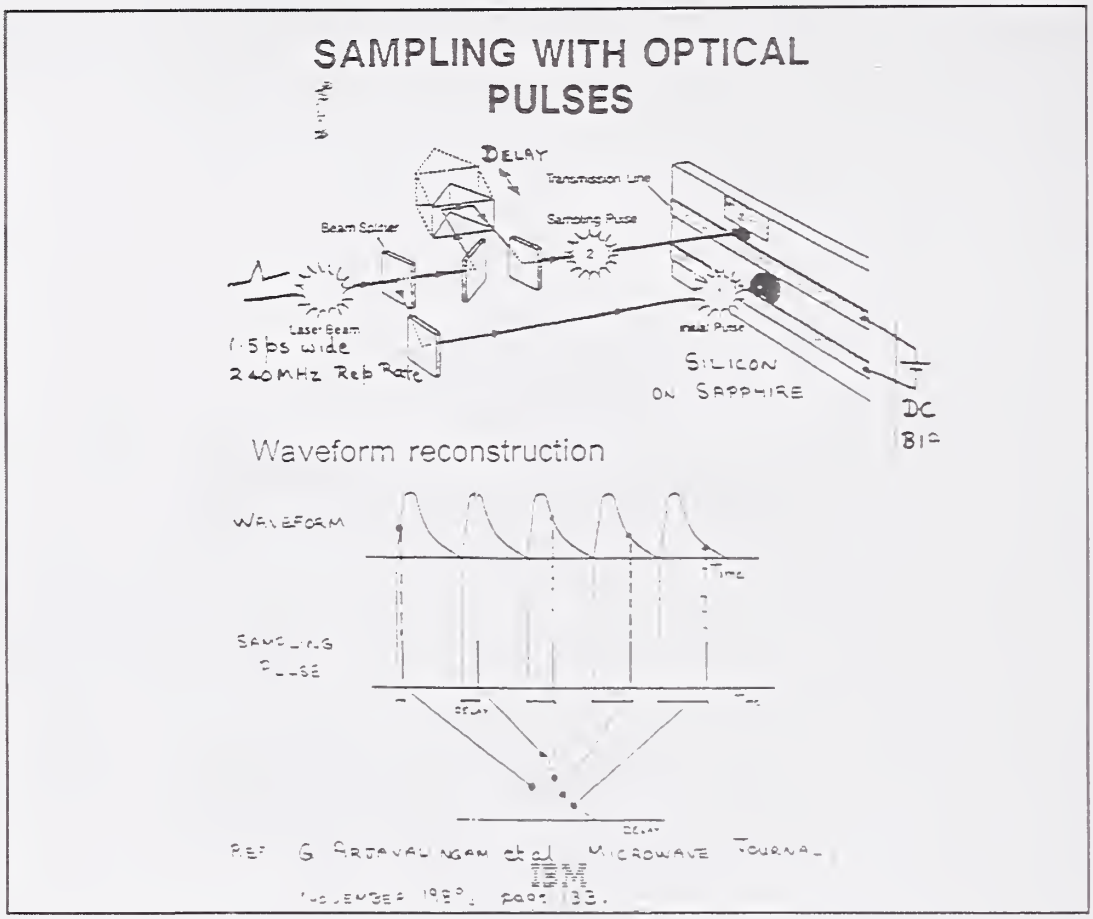
SAMPLING WITH OPTICAL PULSES
DELAY
Transmission Line
Sampling Pulse
Beam Splitter
Laser Beam
1-5 ps wide
240 MHz Rep Rate
Initial Pulse
SILICON ON SAPPHIRE
DC BIAS
Waveform reconstruction
WAVEFORM
SAMPLING PULSE
TIME
DELAY
REF G ARJAVALINGAM et al MICROWAVE JOURNAL DECEMBER 1985 page 130.
IBM

Figure 9

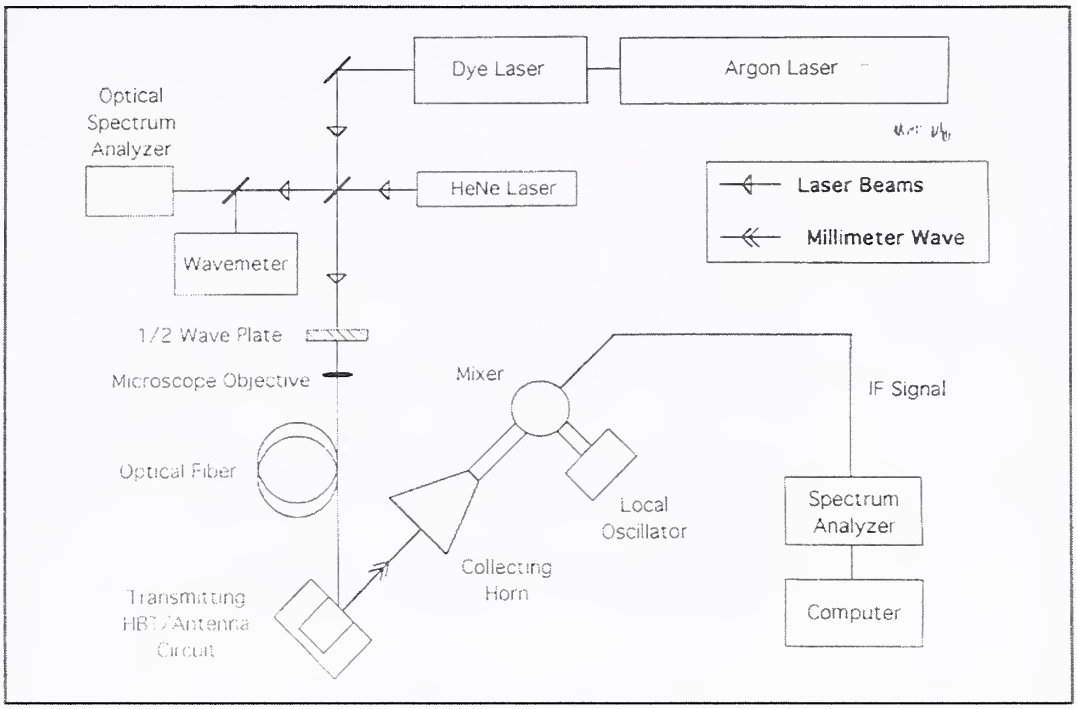
Dye Laser
Argon Laser
Optical Spectrum Analyzer
HeNe Laser
Laser Beams
Millimeter Wave
Wavemeter
1/2 Wave Plate
Microscope Objective
Mixer
IF Signal
Optical Fiber
Local Oscillator
Spectrum Analyzer
Collecting Horn
Transmitting HBT/Antenna Circuit
Computer

Figure 10

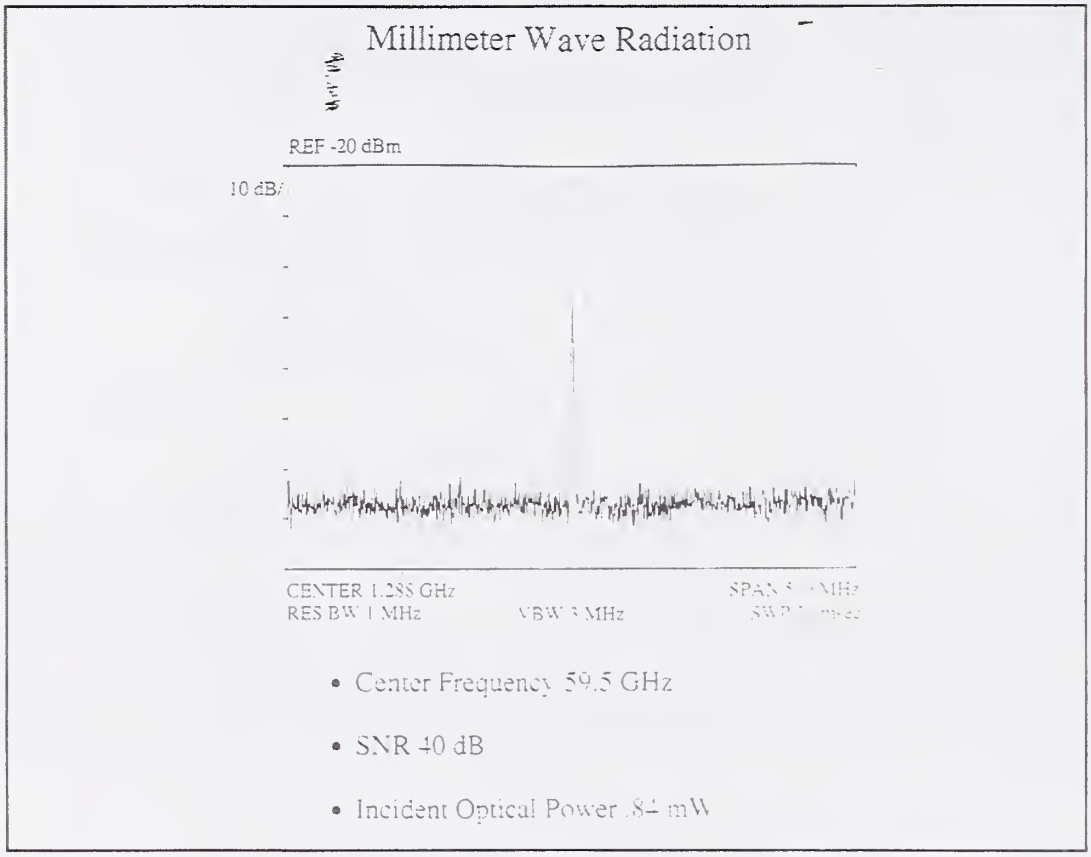
Millimeter Wave Radiation
REF -20 dBm
10 dB/
CENTER 1.288 GHz
RES BW 1 MHz
VBW 3 MHz
• Center Frequency 59.5 GHz
• SNR 40 dB
• Incident Optical Power .84 mW

Figure 11

65.12 GHz Passively Mode Locked Two Section Quantum Well Laser Diode

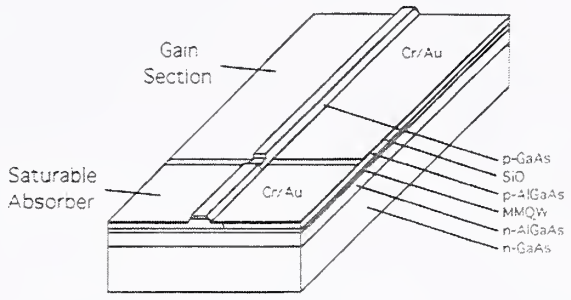

- Laser mode locked by reverse biasing saturable absorber causing a decrease in absorption recovery time.

- Output Parameters:

  Pulse Width: <2.5 psec

  Power: 2-4 milliwatts

  Wavelength: 830 nm

Figure 12

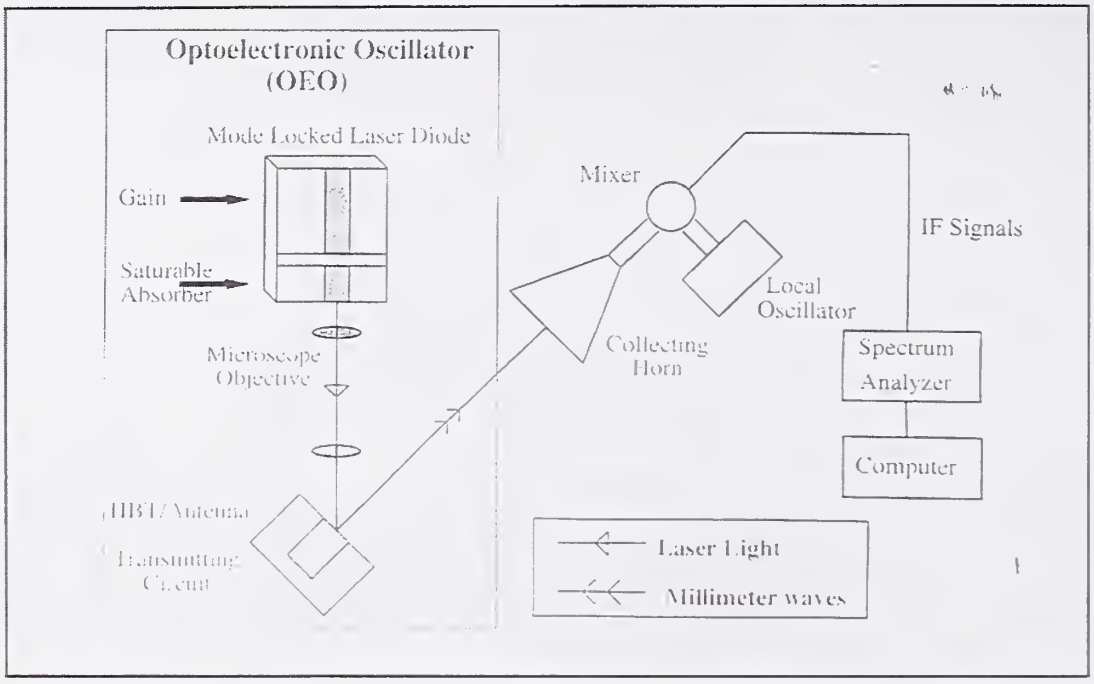
Optoelectronic Oscillator
(OEO)
Mode Locked Laser Diode
Gain
Saturable
Absorber
Microscope
Objective
HBT Antenna
Transmitting
Circuit
Mixer
IF Signals
Local
Oscillator
Collecting
Horn
Spectrum
Analyzer
Computer
Laser Light
Millimeter waves

Figure 13

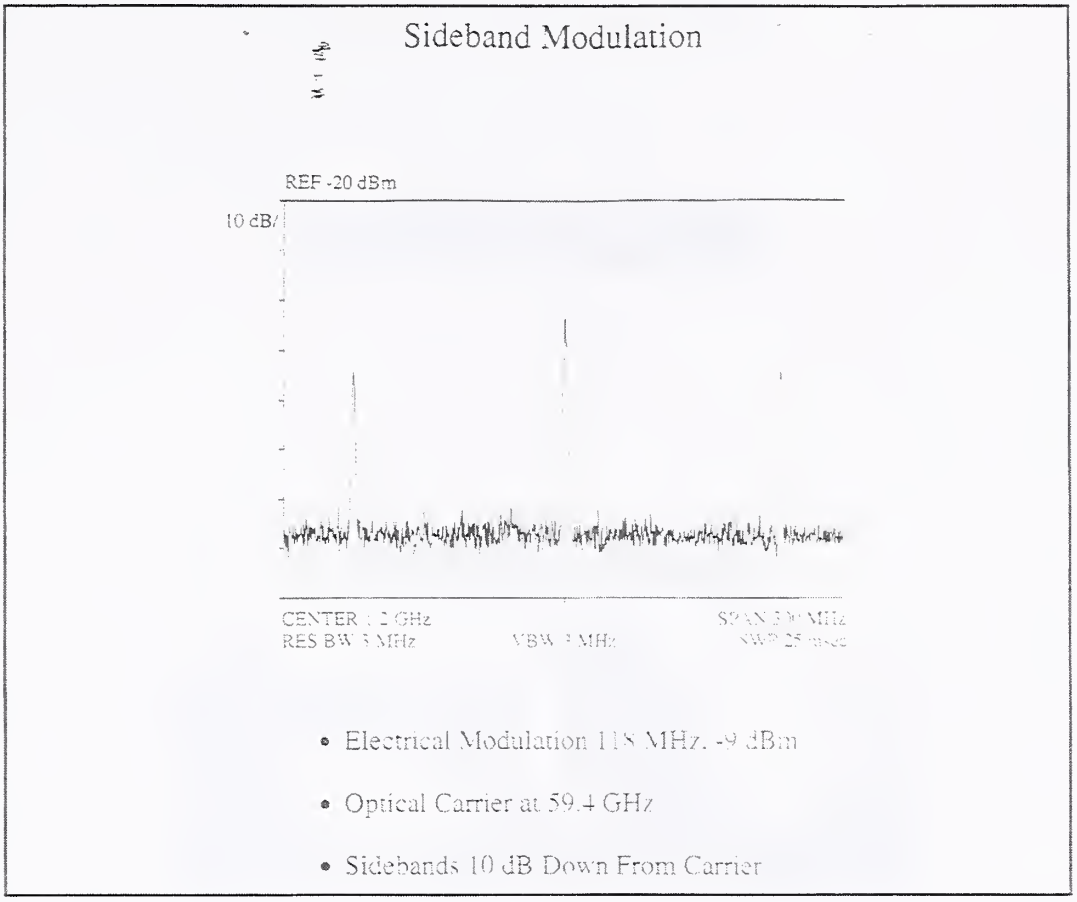
Sideband Modulation
REF -20 dBm
10 dB/
CENTER
RES BW
VBW
SPAN
• Electrical Modulation 118 MHz, -9 dBm
• Optical Carrier at 59.4 GHz
• Sidebands 10 dB Down From Carrier

Figure 14

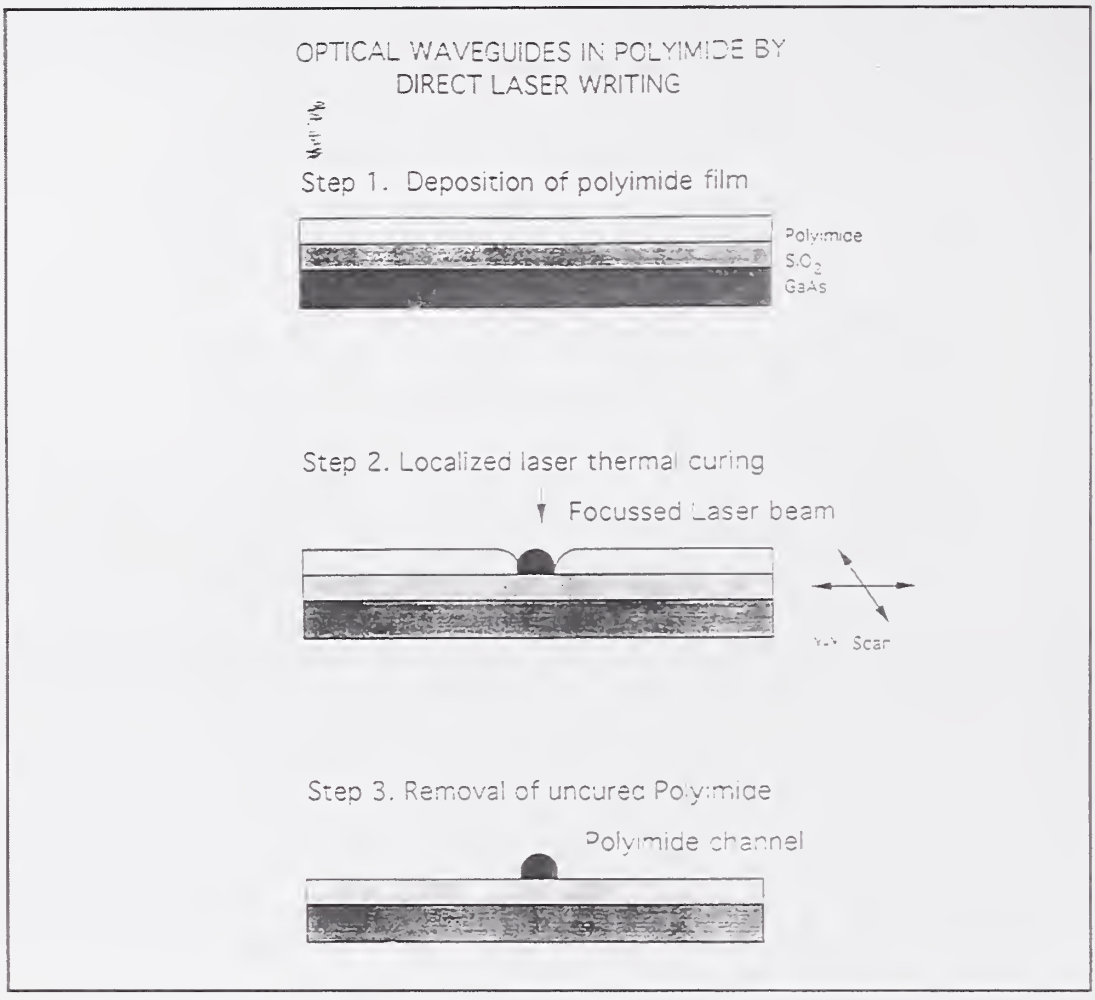
OPTICAL WAVEGUIDES IN POLYIMIDE BY
DIRECT LASER WRITING
Step 1. Deposition of polyimide film
Polyimide
SiO_2
GaAs
Step 2. Localized laser thermal curing
Focussed Laser beam
Scan
Step 3. Removal of uncured Polyimide
Polyimide channel

Figure 15

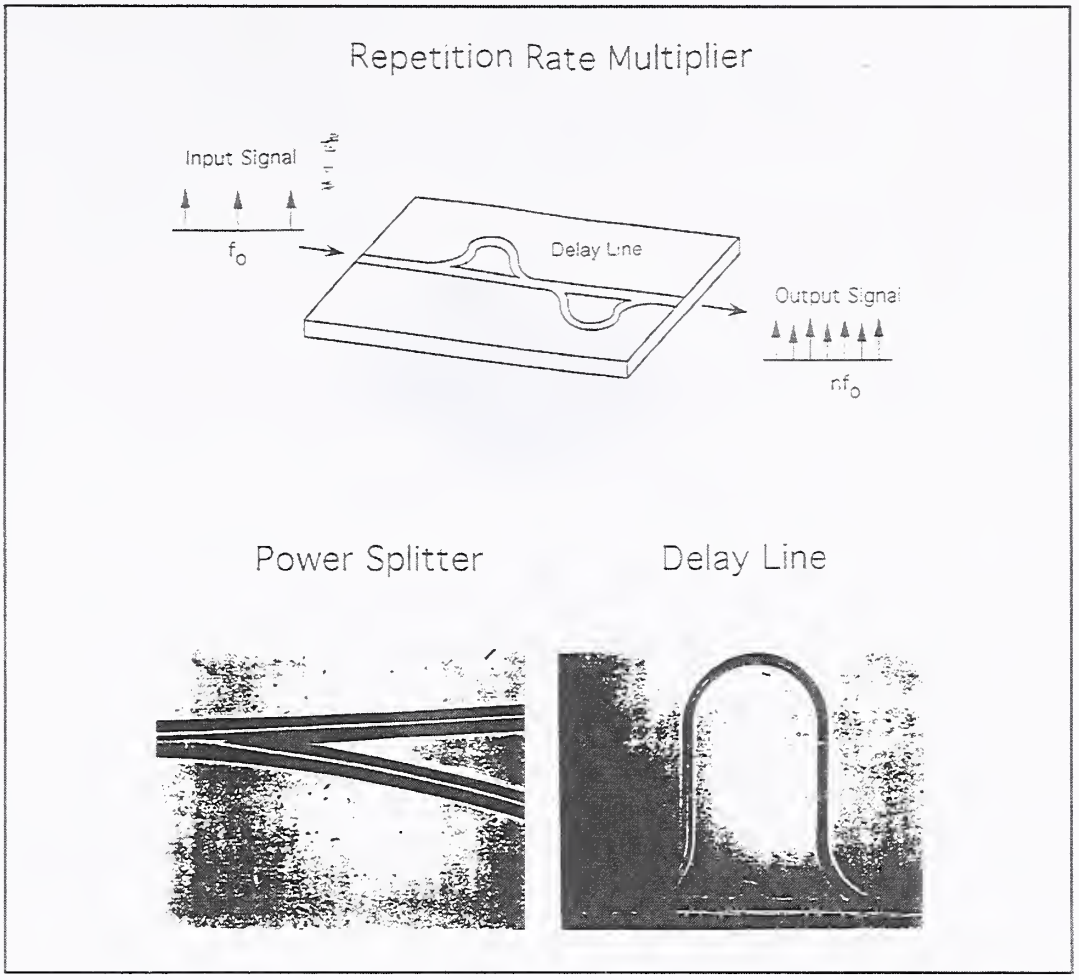
Repetition Rate Multiplier
Input Signal
f_o
Delay Line
Output Signal
nf_o
Power Splitter
Delay Line

Figure 16

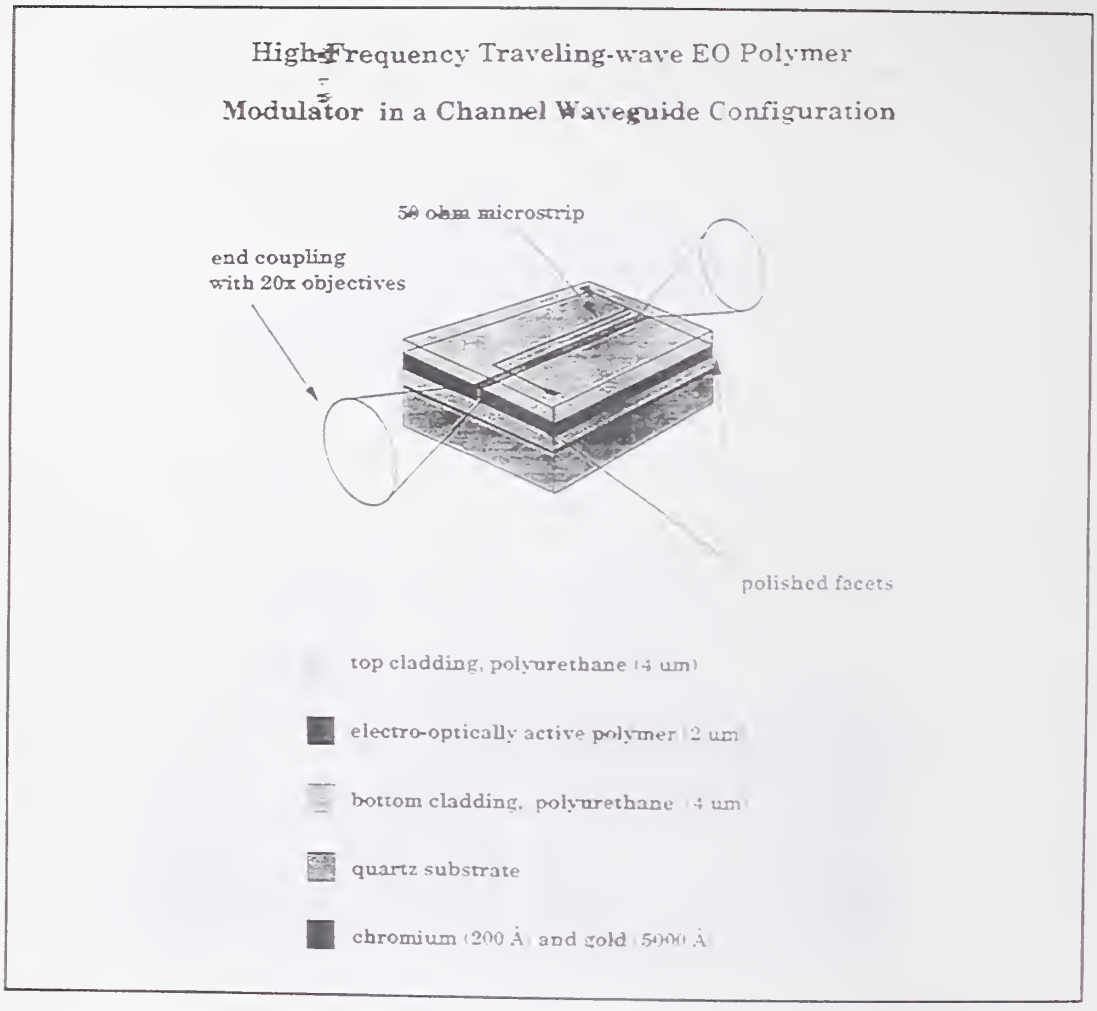
High-Frequency Traveling-wave EO Polymer
Modulator in a Channel Waveguide Configuration
50 ohm microstrip
end coupling
with 20x objectives
polished facets
top cladding, polyurethane (4 um)
electro-optically active polymer (2 um)
bottom cladding, polyurethane (4 um)
quartz substrate
chromium (200 Å) and gold (5000 Å)

Figure 17

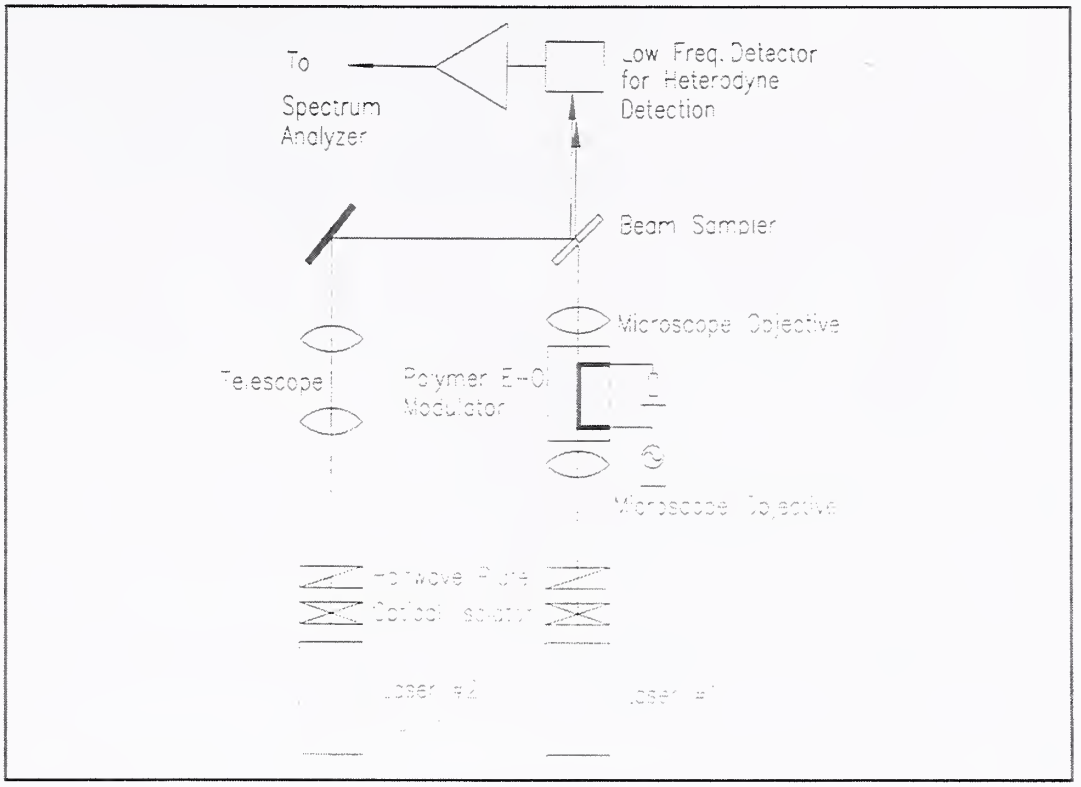

Figure 18

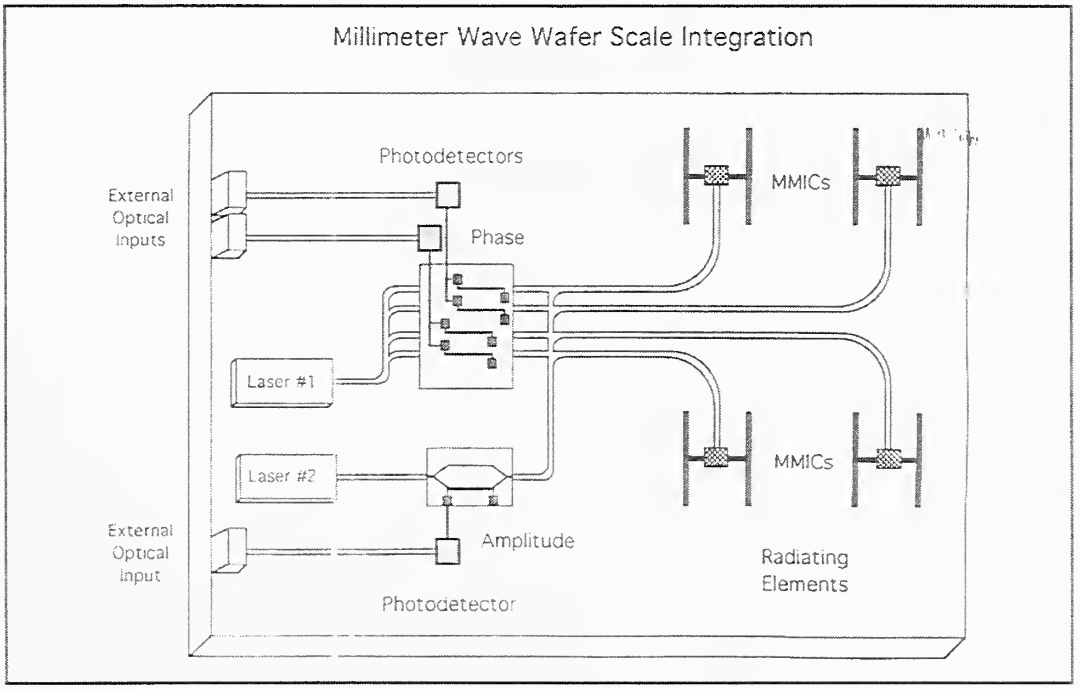

Figure 19

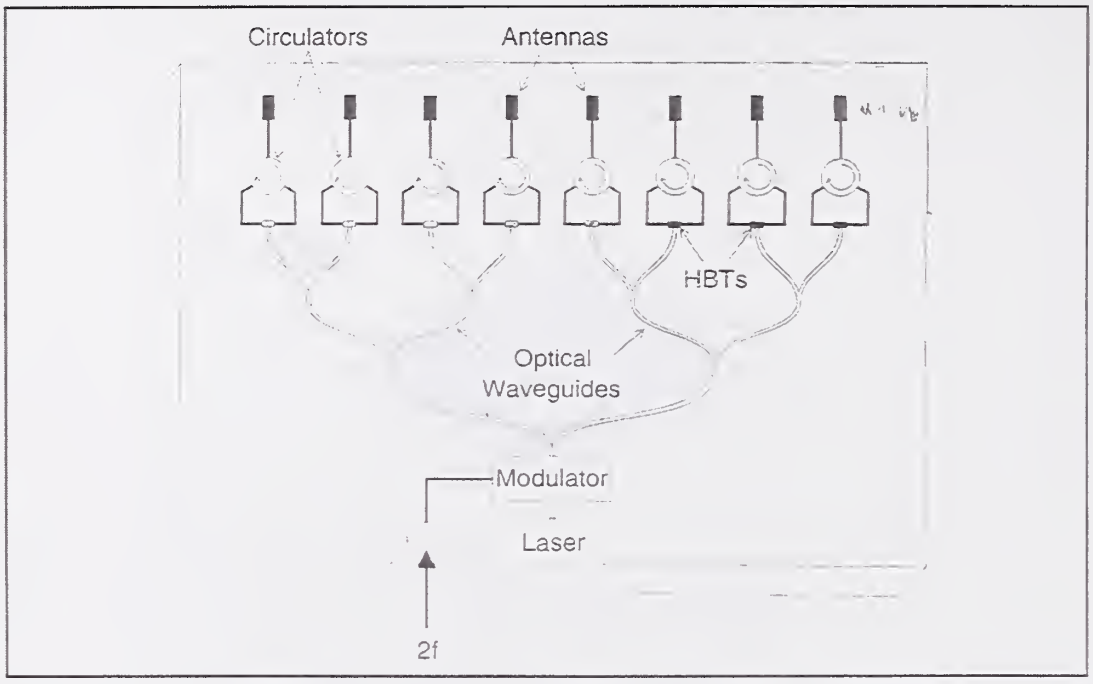

Figure 20

CONCLUSION

- **New Technology for Testing**
  - A) Requires Standards
  - B) Reproducibility
- **Optoelectronic Sources**
  - A) Frequency Measurements
  - B) Power Levels
- **New Application Areas**
  - A) Communication Bandwidths
  - B) Carrier Concepts

Figure 21

Round Table Discussion

MILLITECH

Millimeter and submm components through systems

Frequency range 30–700 GHz plus a few cube corner mixers

Sales ~$18M/yr

Major Volume Applications:

- Imaging Systems
  - Aircraft Landing
  - Contraband Detection
- Short Range Radar
  - Auto Collision Avoidance
  - Earth Moving Equipment in Post.

Submm Systems All in Small Numbers:

- SWAS Receiver System
  - 492 and 557 GHz Receiver at 150K
  - Mixers, Optics, L.O., if Strip
- SWAS Antenna Test System
  - Near Field Scanner From NSI
  - Millitech Provides Source, Multi. Channel

Figure 1

- Vector Network Analyzed Extenders
  - 120–500 GHz
  - Various Applications All Government Funded
  - Semiconductor Device Properties
  - Trans. Line Studies
  - Radar Cross Section Model
- Most Customers Buy Components:
  - Mixers (Fund. and Harmonic)
  - Detectors
  - Sources and Frequency Multipliers.
    - Gunns and Swept Sources
    - x2, x3, x4 Multipliers
  - Multipliers >200 GHz, sell ~30/yr.

Figure 2

What NIST Could Offer To Industry

- Calibration of Power Standards Must Address VSWR Problems
- Characterize Absorbers for Radiometer Calibration, Antenna Measurements
- Wave Guide Standards Dimensions Above 325 GHz Flanges
- Quasi-Optics and Antennas Standard Gain Horns, Low Gain Probes for Near Field Scanning

Figure 3